DISSERTATION

Ex vivo investigation of mechanisms to prevent oxidatively induced alterations in axonal mitochondria in murine nervous system models

Ex-vivo-Untersuchung von Mechanismen zur Prävention oxidativ induzierter Veränderungen in axonalen Mitochondrien in Nervensystem-Modellen von Mäusen

zur Erlangung des akademischen Grades
Medical Doctor-Doctor of Philosophy (MD/PhD)

vorgelegt der Medizinischen Fakultät
Charité- Universitätsmedizin Berlin

von

Rebecca Ludwig (geb. Ulshöfer)

Erstbetreuung: Prof. Dr. rer. nat Carmen Infante Duarte

Datum der Promotion: 29.11.2024

Table of contents

List of figures

List of abbreviations

aCSF	Artificial cerebrospinal fluid
ATP	Adenosine triphosphate
Ca^{2+}	Calcium ion
CFP	Cyan fluorescence protein
CNS	Central nervous system
CO_2	Carbon dioxide
DHODH	Dihydroorotate dehydrogenase
DMSO	dimethyl sulfoxide
DMT	Disease-modyfing treatment
DPSS	diode-pumped solid-state
EAE	Experimental autoimmune encephalitis
FADH	Flavin adenine dinucleotide
H^+	Proton
H_2O	Water
HEPES	4-(2-hydroxyethyl)-1-piperazineethane-sulfonic acid
K^+	Potassium ion
MAM	Mitochondrial associated membrane
MCU	Mitochondrial calcium uniporter
mHCX	Mitochondrial proton-calcium-exchanger
Miro1	Mitochondrial Rho-GTPase 1
mitoCFP mice	Tg(Thy1-CFP/COX8A)S2Lich/J mice
MMP	Mitochondrial membrane potential
mNCX	Mitochondrial sodium-calcium-exchanger
mPTP	Mitochondrial permeability transition pore
MS	Multiple sclerosis
Na^+	Sodium ion
Na^+/K^+-ATPase	Sodium-potassium-ATPase

NADH	N-adenine dinucleotide
NaV	Voltage gated sodium channels
NCX	Sodium-calcium-exchanger
O_2	Oxygen
PNS	Peripheral nervous system
PPMS	Primary progressive MS
ROI	Region of interest
ROS	Reactive oxygen species
RRMS	Relapsing remitting MS
Ru360	Ruthenium 360
SD	Standard deviation
SEM	Standard error of mean
SPMS	Secondary progressive MS
TNF	Teriflunomide
TTX	Tetrodotoxin

Abstract

Mitochondrial alterations are known to play a key role in the early stages of multiple sclerosis (MS) and happen as a result of oxidative stress. These alterations are believed to promote neuronal damage, thereby causing neuronal loss and leading to increasing disabilities.

Here, I summarize three of our studies that aimed to investigate possible mechanisms underlying oxidative-stress-induced mitochondrial alterations. In the first study we investigated the influence of blocking voltage-gated axonal sodium channels and mitochondrial calcium uniporters on mitochondrial alterations as downstream effects of oxidative stress. This was investigated using explanted murine spinal roots as an ex vivo model of the peripheral nervous system. In the second study and using the same model, we evaluated the effects of teriflunomide, an approved disease-modifying treatment for MS, on oxidatively caused mitochondrial alterations. In the third study we explored the effects of teriflunomide on oxidative stress-induced mitochondrial alterations in acute hippocampal slices, which represent an ex vivo model of the central nervous system.

In summary, we have proved that ion channel inhibitors and teriflunomide are beneficial in terms of preventing oxidative-stress-induced mitochondrial alterations. Moreover, we have contributed to the understanding of neurodegenerative pathomechanisms in an oxidative paradigm, which might help in the future development of anti-neurodegenerative drugs.

Zusammenfassung

Mitochondriale Veränderungen spielen bereits in frühen Stadien der Multiplen Sklerose (MS) eine entscheidende Rolle und treten als Folge von oxidativem Stress auf. Diese Veränderungen fördern neuronale Schäden, verursachen so den Untergang von Neuronen und führen zu zunehmenden Behinderungen.

Hier fasse ich drei Studien zusammen, deren Ziel es war, mögliche Mechanismen zu untersuchen, die den, durch oxidativen Stress ausgelösten, mitochondrialen Veränderungen zugrunde liegen. In der ersten Studie haben wir den Einfluss der

Blockade von spannungsgesteuerten axonalen Natriumkanälen und mitochondrialen Kalziumuniportern auf mitochondriale Veränderungen als nachgeschaltete Effekte von oxidativem Stress in Spinalnerven als einem ex vivo Model des peripheren Nervensystems untersucht. In der zweiten Studie haben wir die Auswirkungen von Teriflunomid, einem zugelassenen, krankheitsmodifizierenden Medikament zur Behandlung der Multiple Sklerose, auf oxidativ verursachte mitochondriale Veränderungen im selben Modell untersucht. In der dritten Studie haben wir die Auswirkungen von Teriflunomid auf die durch oxidativen Stress hervorgerufenen mitochondrialen Veränderungen in akuten Hippocampusschnitten als einem ex vivo Model des zentralen Nervensystems untersucht.

Zusammenfassend haben wir nachgewiesen, dass Ionenkanalinhibitoren und Teriflunomid die durch oxidativen Stress induzierten, mitochondrialen Veränderungen verhindern können. Darüber hinaus haben wir das Wissen über neurodegenerative Pathomechanismen in einem oxidativen Paradigma erweitert. Dies kann dazu beitragen, in Zukunft anti-neurodegenerative Medikamente zu entwickeln.

1 Introduction

1.1 Multiple Sclerosis: epidemiology and current treatment options

Multiple sclerosis (MS) is an autoimmune driven demyelinating and neurodegenerative disease of the central nervous system (CNS) that affects approximately 2.8 million people worldwide [1, 2] and about 200,000 people in Germany [3]. Usually, the onset of MS takes place between 20 and 50 years of age; the women-to-men ratio is about 2-3:1 [4]. It is the most prevalent cause of neurological disability in young adults [1].

Common initial clinical symptoms are paresthesia, numbness, and optic neuritis [1]. Further symptoms include weakness, bladder and bowel dysfunction, and cognitive impairment [3, 5]. According to the 2017 McDonald criteria, demonstration of lesion dissemination in time and space is essential for the diagnosis of MS [6]. 85% of the patients are diagnosed with relapsing-remitting MS (RRMS) and suffer from acute attacks that result in cerebral or spinal damage and are followed by a period of partial or total remission with few or no symptoms [7-9]. Around 10% of affected people suffer from primary progressive MS (PPMS) [7, 8]. This disease course manifests with increasing neurological impairment from the beginning of the disease [7]. About two thirds of RRMS patients develop a secondary progressive MS form (SPMS) over time [10, 11], which is characterized by the worsening of the clinical symptoms and irreversible neurological disabilities [12].

During MS relapses, corticosteroids are prescribed to reduce the severity and duration of acute inflammation [13, 14]. An alternative additional treatment is plasmapheresis [13]. Several disease-modifying treatments (DMTs) have been approved over the last years to alter the long-term outcome of MS, the first DMTs were interferons and glatiramer acetate e. Nowadays, according to the guidelines of the German Society of Neurology, multiple substances are approved for treating MS, including dimethyl fumarate and teriflunomide, sphingosine-1-receptor modulators and immune cell depleting antibodies [15]. Most of these DMTs are prescribed during RRMS, aiming to reduce new relapses and to lengthen the time for the development of SPMS [14]. For PPMS, only Ocrelizumab, a humanized monoclonal antibody targeting CD20-positive cells, has been approved [16]. SPMS can be directly targeted with a few specific DMTs, namely with Siponimod (first-line therapy) and Mitoxantrone [14, 17].

1.2 Neurodegeneration in MS: a story driven by mitochondria?

MS is driven by an incompletely understood, pathological autoimmune response leading to inflammation, demyelination, and subsequent neurodegeneration in CNS [10, 18]. Genetic, environmental, and infectious factors have been suggested to contribute to MS pathogenesis [10]. CNS invasion by peripheral immune cells largely promotes RRMS; other pathophysiological mechanisms, especially inflammation-induced neurodegeneration, are believed be present in early stages of the disease, but to dominate in progressive phases of the disease [1, 9, 19]. Thus, targeting axonal damage and the underlying neurodegenerative pathomechanisms represents a promising strategy for future treatments.

Neuroimmune alterations and neuroinflammation are not only hallmarks in PPMS and SPMS but also in other neurodegenerative diseases, e.g., Alzheimer's disease or Parkinson's disease [20, 21]. Understanding common pathophysiological processes might therefore offer translational treatment options for different neurodegenerative diseases. Throughout the last years, mitochondrial dysfunction has emerged as one possible key player in MS that contributes to axonal loss [21-25]. Mitochondrial changes happen in the early stages of the disease in neurons within an intact myelin sheath [26].

Mitochondria generate most of the cellular adenosine triphosphate (ATP) via oxidative phosphorylation and control N-adenine dinucleotide (NADH) and flavin adenine dinucleotide (FADH) production [27]. To function properly, cells depend on this "energy currency"; especially neuronal cells with their high energy demand to match repetitive action potential generation [28, 29]. Moreover, mitochondria are involved in cellular calcium (Ca^{2+}) homeostasis [30], as well as in the generation of reactive oxygen species (ROS) [31].

During a relapse of MS, activated microglia as well as CNS-invading immune cells produce inflammatory mediators such as ROS and reactive nitrogen species [32-34]. ROS can trigger mitochondrial alterations, which are considered one of the earliest signs of focal axonal degeneration [27, 35]. Impaired mitochondrial function itself leads to increased chances of electron slippage during oxidative phosphorylation and thereby to increased levels of mitochondrial ROS [36-38]. This causes a vicious cycle of ROS-induced ROS production leading to an oxidative stress situation.

1.3 Role of ion channels on mitochondrial alterations upon oxidative stress

Impaired mitochondria fail to provide enough ATP to properly maintain the activity of the sodium-potassium-ATPase (Na^+/K^+-ATPase) and thereby restore initial ion concentrations following action potentials [39-41]. The impaired function of Na^+/K^+-ATPase may lead to Na^+ accumulation in axons because Na^+ influx through axonal voltage-gated sodium channels (NaV) is preserved [39] (Figure 1).

The rise in intraaxonal Na^+ can reverse the action mode of the axonal sodium-calcium-exchanger (NCX) [39]. Usually, NCX shifts Na^+ into cells and Ca^{2+} out, but under increased intraaxonal Na^+ concentration it can work in the opposite direction to compensate for axonal Na^+ accumulation. As a result, the concentration of intraaxonal Ca^{2+} rises [39]. This whole process is schematically demonstrated in Figure 1.

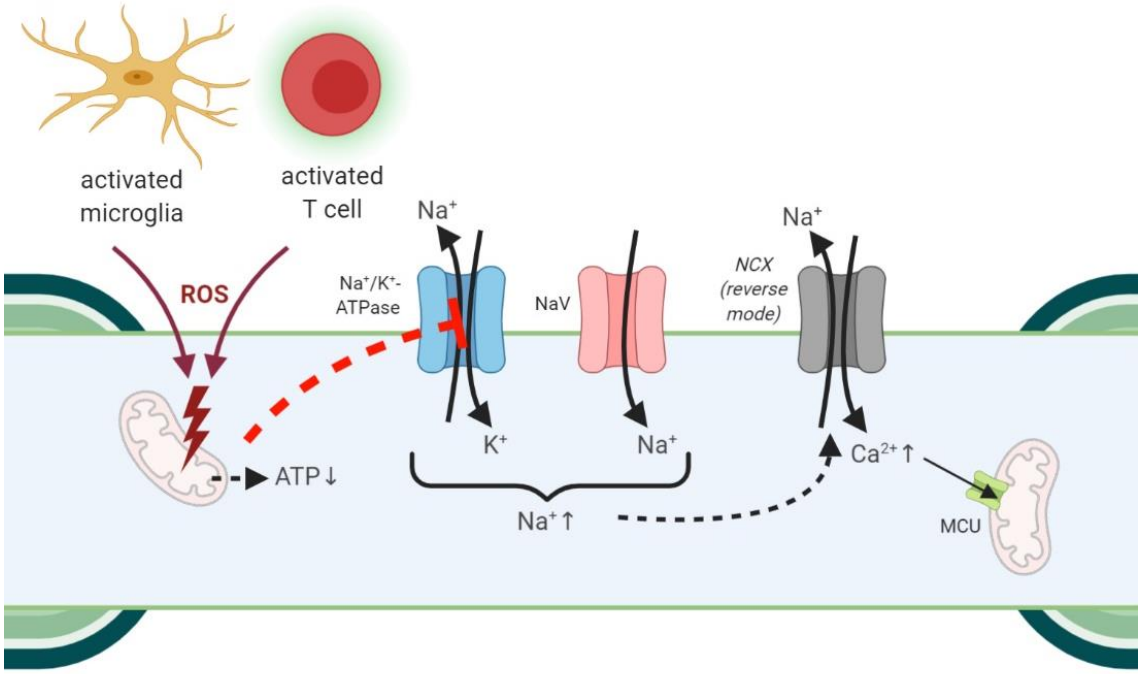

Figure 1: Schematic overview of ion alterations in axons under oxidative stress in spinal roots

ROS produced by activated immune cells cause ATP depletion and resulting dysfunction of Na+/K+-ATPase. Na+ influx into axons continues via NaV during action potentials. This leads to a rise in intraaxonal Na+ concentration. Subsequently, NCX starts working in the reverse mode, shifting Na^+ out of the axon and Ca^{2+} into the axon. A rise in intraaxonal Ca^{2+} leads to the accumulation of Ca^{2+} in mitochondria; own figure

Mitochondria serve as a buffering system for Ca^{2+} rises [30] and several mitochondrial enzymes are regulated by changes in Ca^{2+} concentration within the mitochondrial matrix [42]. Hence, a rise in Ca^{2+} concentration within mitochondria can lead to the activation of oxidative phosphorylation and thereby ATP production [42, 43]. Most Ca^{2+} diffuses into mitochondria via the mitochondrial calcium uniporter (MCU) [44]. Ca^{2+} can be released from mitochondria via the mitochondrial sodium-calcium-exchanger (mNCX), mitochondrial proton-calcium-exchanger (mHCX) and the mitochondrial permeability transition pore (mPTP) [45]. Amongst Ca^{2+} accumulation, ROS lead to the opening of the mPTP and can cause apoptosis or necrosis [46]. Variations of Na^{+} and Ca^{2+} concentration within the axon and axonal mitochondria might thereby affect the dynamics of neurodegeneration during oxidative stress. Hence, modulation of these systems emerges as a plausible target to hinder neurodegenerative processes.

Our research has developed an ex vivo model of murine ventral spinal roots to investigate oxidative-stress-induced mitochondrial alterations, namely increased mitochondrial circularity, a decrease in mitochondrial area and length, as well as a decrease in the percentage of moving mitochondria, mitochondrial track length, and track velocity [47, 48]. These alterations begin at the nodes of Ranvier [47], where ion channels, especially NaV, are abundantly present [49]. Therefore, we aimed to investigate the effect of oxidative stress on mitochondria upon inhibition of the most frequent subtypes of NaV with tetrodotoxin (TTX) and MCU with Ruthenium 360 (Ru360) [50].

1.4 Implications of dihydroorotate dehydrogenase on oxidative-stress-induced mitochondrial alterations

Dihydroorotate dehydrogenase (DHODH) is an essential mitochondrial enzyme in de novo pyrimidine synthesis and its inhibition reduces the proliferation of activated T and B cells and thereby inflammation [51]. The compound teriflunomide (TFN; Aubagio; Genzyme, Cambridge, MA, USA) is an approved, once-daily administered, oral treatment for RRMS [52]. It is the active metabolite of Leflunomide [53] and inhibits selectively and reversibly the mitochondrial enzyme DHODH [53, 54]. However, it is not known whether and how TFN affects mitochondria itself.

Therefore, we aimed to investigate whether observed neuroprotective effects of TFN also involve mitochondrial protection. We investigated the effects of TFN on oxidatively

stressed mitochondria in both CNS and peripheral nervous system (PNS) using murine acute hippocampal slices (60) and spinal root explants, respectively [55].

1.5 Importance and aims of the MD PhD thesis

Oxidative stress and mitochondrial alterations are known to play a role in MS and are a suspected link between neuroinflammatory and neurodegenerative parts of the disease [35]. At present, the number of therapeutic approaches for the prevention and treatment of neurodegenerative parts of MS is very limited. Therefore, specific pathomechanisms causing neuronal death need to be identified to develop new therapeutic strategies. My work aimed to investigate molecular pathways underlying oxidative stress-induced mitochondrial alterations in ex vivo models of both a peripheral and central nervous system.

My dissertation encompasses three pre-clinical studies. While Study 1 represents my primary research project, Study 2 and Study 3 are complementary projects conducted by Dr. Bimala Malla in the context of her doctoral thesis, to which I have contributed as co-author.

1. In Study 1, we examined how axonal Na^+ and mitochondrial Ca^{2+} channels are involved in oxidative-stress-induced mitochondrial alterations in the ex vivo model of murine spinal roots. Besides mitochondrial morphology and motility parameters, we also studied mitochondrial membrane potential.
2. In Study 2, we tested the effects of TFN on mitochondrial parameters (morphology and motility) in the ex vivo model of murine spinal roots in an oxidative stress environment.
3. Study 3 evaluated the effects of TFN on neuronal mitochondria undergoing oxidative stress in acute hippocampal brain slices. Besides mitochondrial morphology and motility, we also investigated oxygen partial pressure, local field potential, and neuronal ATP content.

Our research has provided a better insight into molecular mechanisms underlying mitochondrial alterations upon oxidative stress as well as their implication in drug effects. It also has contributed to fundamental knowledge about the involvement of changes in ion concentration, namely Na^+ and Ca^{2+}, in mitochondrial alterations due to oxidative stress. These findings might lead to the development of new treatments for progressive MS.

Mitochondrial dysfunction is also known to take place in other neurodegenerative diseases including Alzheimer's disease, Parkinson's disease, Huntington's disease, and Amyotrophic Lateral Sclerosis [31]. Thus, results from our research may be applied in other fields of neurodegenerative research.

In conclusion, we have shown that mitochondrial impairment due to oxidative stress and alterations in ion fluxes occurs in myelinated neurons. Accordingly, axonal damage may initiate during the early stages of MS. Our research may help to develop drugs targeting early pathological mechanisms in neurodegenerative disease and slowing down disease progression substantially.

2 Methods

This chapter describes schematically the methods that were applied by myself in this MD/PhD thesis. Detailed descriptions of all the methods are included in the Material & Methods sections of the studies included in this thesis.

2.1 Animals

The studies were performed in strict accordance with the Directive 2010/63/EU of the European Communities Council and of the European Parliament of 22 September 2010. All experimental procedures were approved by the local authority on animal experiments in Berlin (Landesamt für Gesundheit und Soziales Berlin). The mice were housed and maintained in a temperature-controlled environment on a 12 h light-dark cycle.

For the investigation of ion channel implication in oxidatively induced mitochondrial alterations in ventral spinal roots, we used C57BL/6 mice of both sexes that were 8 to 10 weeks old. We used relatively young mice to rule out age-related alterations of mitochondrial function.

For the investigation of TFN effects on mitochondria in ventral spinal roots, we used C57BL/6 mice at least 3 weeks old.

For Study 3, using acute hippocampal slices, we used 10 days old, transgenic Tg(Thy1-CFP/COX8A)S2Lich/J mice (mitoCFP mice) that express cyan fluorescence protein (CFP) in neuronal mitochondria.

2.2 Spinal root extraction

For Study 1 and Study 2, we explanted murine ventral spinal roots as described by Bros et al. as a model of the PNS [48]. Briefly, we anesthetized the mice deeply with isoflurane before performing cervical dislocation. After exposing the spinal cord, we explanted it together with the adherent ventral spinal roots and kept it in freshly mixed artificial cerebrospinal fluid (aCSF) saturated with carbogen (95% oxygen (O_2), 5% carbon dioxide (CO_2)) and adjusted to a pH-level of 7.3-7.4.

Finally, we separated lumbar ventral spinal roots from the spinal cord and placed them in constantly carbogenated aCSF in a submerged incubation chamber (Brain Slice Keeper-BSK6-6, Scientific Systems Design Inc., Ontario Canada), facilitating division into different experimental groups.

We first incubated the spinal roots with 300 nM MitoTracker® Orange CM-H_2 CTMRos (Life Technologies, Darmstadt, Germany) for 30 min. MitoTracker® Orange is a fluorescent dye to label mitochondria selectively, that is only entering a fluorescent state when diffusing into an actively respiring cell [56]. Moreover, the oxidation status of a cell can be measured with the reduced form of this dye [56, 57]. After the incubation time, the roots were washed with aCSF to minimize background fluorescence. Then, ventral spinal roots were randomly assigned to the experimental groups.

2.3 Acute hippocampal slices

Acute hippocampal slices were used as a model of CNS, following a modified protocol from Nitsch et al. [58]. Briefly, mice were decapitated, brains were removed and were cut to 400 µm thick brain slices using a vibratome. Brain slices were kept in freshly prepared, pH-adjusted, continuously carbogenated 4-(2-hydroxyethyl)-1-piperazineethane-sulfonic acid (HEPES) -aCSF. The whole procedure was performed in temperatures between 34 and 37 °C. Slices were randomly assigned to the experimental groups.

2.4 Solutions and treatments

In all studies, one chamber of the Brain Slice Keeper, that we used to administer different treatments, was accorded to one experimental group.

To induce oxidative stress, we used hydrogen peroxide (H_2O_2) that was purchased at a 30% concentration (w/w in water (H_2O)) and contained a stabilizer. Roots were incubated for 30 min with H_2O_2 in a concentration of 100 µM for Study 1, 50 µM for Study 2, and 100 or 200 µM, depending on the experiment, for Study 3. In all studies, we applied H_2O_2 together with the solvent of the evaluated drugs to eliminate confounding effects of the solvent itself.

In Study 1, TTX was dissolved in aCSF. aCSF served as a negative control in TTX experiments. For Ru360, dimethyl sulfoxide (DMSO) was the vehicle and correspondingly, we used DMSO as a negative control for Ru360 experiments. We applied TTX in concentrations of 1 nM and 1 µM and Ru360 in concentrations of 5, 10, and 20 µM. After the treatment, spinal roots or acute brain slices were again washed with fresh aCSF.

In Study 2, we applied TFN at concentrations of 1 µM, 5 µM and 50 µM along with H_2O_2 for 30 min. Since TFN was dissolved in DMSO, DMSO served as a negative control in Study 2.
In Study 3, we treated acute brain slices with 50 µM TFN+H_2O_2 and 50 µM TFN alone. DMSO again served as a negative control. We chose the higher concentration of TFN due to the higher thickness of acute hippocampal slices compared to spinal roots.

2.5 Laser scanning confocal and two-photon microscopy

For Study 1 and Study 2, spinal roots were immobilized with a custom-built nylon net on a glass cover slip to minimize the impact of xy shift on our motility analysis. We then put the cover slip in an imaging chamber containing carbogenated aCSF.
For our studies, we used inverted laser scanning confocal microscopes. TTX experiments in Study 1 and all experiments in Study 2 were performed using an LSM7 10 microscope (Carl Zeiss, Jena, Germany). Ru360 experiments in Study 1 were performed using a Nikon Scanning Confocal A1Rsi+ (Minato, Japan).
In spinal root experiments (Study 1 and Study 2), MitoTracker® Orange was excited at 561 nm with a diode-pumped solid-state (DPSS) laser. Visualization of mitochondria was performed through a 60x (Nikon Scanning Confocal A1Rsi+) or 100x (LSM 710, Carl Zeiss) oil immersion objective. After setting a sharp image, we identified three regions of interest (ROI). ROIs lay in axons with intact myelin sheath in both adjacent directions to clearly visible nodes of Ranvier. They had to be at least 2 mm away from the end of the roots. We recorded a time-lapse (60 s duration, 2 s/frame) for each ROI. We minimized exposure time and laser power to reduce photobleaching and phototoxicity. To reduce measurement bias, we rotated the imaging order of treatment groups in each experiment. We used the first frame of every time-lapse video to assess mitochondrial morphology with a semi-automated analysis tool of the Volocity®6.3 software (Perkin Elmer, Rodgau, Germany).
For the evaluation of changes in mitochondrial morphology, we analyzed the following parameters:

1) shape factor ($4\pi X$ [Area/Perimeter^2]): This is a measure of circularity ranging from 0 to 1, where 1 signifies a perfectly circular object
2) length (µm)
3) area (µm^2) of an individual mitochondrion

In Study 1 and Study 2, we tracked mitochondria manually using Volocity®6.3 software (Perkin Elmer, Rodgau, Germany) to assess motility. We used a manual approach because a former study of our laboratory has shown that automated tracking tools underestimate track length and overestimate track velocity [62]. As in our previous studies, any mitochondrion with a displacement of ≥1 µm was considered motile [47, 59]. For experiments with Ru360 and TFN, motile mitochondria were further analyzed for the following parameters:

1) track length (µm), the measure of the real distance traveled by a mitochondrion
2) velocity (µm/s)

Imaging experiments in Study 3 were performed using a two-photon Laser Scanning Microscope. Due to the increased imaging depth of this imaging technique, we were able to investigate not only the superficial but also deeper layers of the acute hippocampal slices [63].

2.6 Analysis of mitochondrial membrane potential

In Study 1, we also assessed mitochondrial membrane potential (MMP), an indirect method to assess mitochondrial integrity and their ability to produce ATP. Together with the proton gradient, MMP forms the transmembrane potential which is the driving force in ATP production during oxidative phosphorylation [64]. We used JC-1 in the experiments of Study 1. This dye accumulates preferably in negatively charged mitochondria, thus with intact MMP [65]. If enough dye accumulates inside mitochondria, the dye aggregates and those aggregates emit another fluorescence (590 nm, red spectrum) than the non-aggregated dye (529 nm, green spectrum) [65]. Red-green ratio normalized to the control group was considered a measure for MMP [66].

2.7 ATP assay

In Study 3, we performed an ATP assay using the Abcam ATP assay kit (Abcam, ab83355) following the manufacturer's protocol. Briefly, we homogenized the tissue in ATP assay buffer sitting on ice. Then, we centrifuged at 4 °C at 13,000×g for 5 min. We collected the supernatant in a new tube and deproteinized it with perchloric acid. ATP standard samples in the range of 0-1 nmol as well as the samples were then incubated with reaction-mix for 30 min.

We performed a fluorometric detection at 535/587 nm in a plate reader (GloMax®-Multi Detection System, Promega Corporation, Madison, WI, USA). We subtracted the sample background in each slice, multiplied with the dilution factor as proposed by the manufacturer and then calculated the ATP concentration [55].

2.8 Statistical analysis

The data were analyzed using different versions of Prism software (GraphPad, San Diego, USA; Study 1 and Study 2: Prism 5.01 software, Study 3: Prism 8 Software). First, all datasets were subjected to the D'Agostino and Pearson omnibus K-squared normality test and the Shapiro-Wilk test for Gaussian distribution. All data fitting the criteria for normal distribution were subsequently analyzed using either t-test (comparison of two groups) or a one-way analysis of variance (ANOVA; comparison of more than two groups)) with Bonferroni's post hoc test. Comparisons between two groups of non-parametric data were performed by the Mann-Whitney U test, comparisons between more than two groups of non-parametric data were analyzed with the Kruskal-Wallis test for non-parametric data followed by Dunn's post hoc multiple comparisons test.

All data of Study 1 are shown in mean± standard error of mean [60] [10]. All data of Study 2 and 3 are given in mean ± standard deviation [61]. The data of these studies are shown as Tukey boxplots. In Tukey boxplots, the central line denotes the median, and the lower and upper boundaries denote the 1^{st} and 3^{rd} quartile. The whiskers denote the data except the outliers presented as individual dots. Outliers were not included in the analysis.

p values ≤ 0.05 were considered significant. The significance of the data was further depicted as $*$ implying $p \leq 0.05$, $**$ implying $p \leq 0.01$, $***$ implying $p \leq 0.001$, and $****$ implying $p \leq 0.0001$.

3 Results

This chapter contains key results published in the studies that are included in this thesis.

3.1 Study 1: Preventing Axonal Sodium Overload or Mitochondrial Calcium Uptake Protects Axonal Mitochondria from Oxidative Stress-Induced Alterations

In consistence with our previous publications [47, 59], incubation with 100 µM H_2O_2 led to a decrease in mitochondrial length (Fig. 2c). Interestingly, we observed an increase in mitochondrial shape factor in TTX experiments upon oxidative stress, while in Ru360 experiments 100 µM H_2O_2 did not alter mitochondrial shape factor (Fig. 2b). In TTX experiments, we observed an increase in mitochondrial area under oxidative stress, while in Ru360 experiments, we saw a decrease in mitochondrial area (Fig. 2d).
Inhibition of axonal Na^+ influx by 100 nM TTX prevented oxidatively induced alterations in mitochondrial morphology (Fig. 2b-d). 1 µM TTX led to no change in mitochondrial circularity and even reinforced oxidatively induced decrease in mitochondrial length and increase in mitochondrial area (Fig. 2b-d).

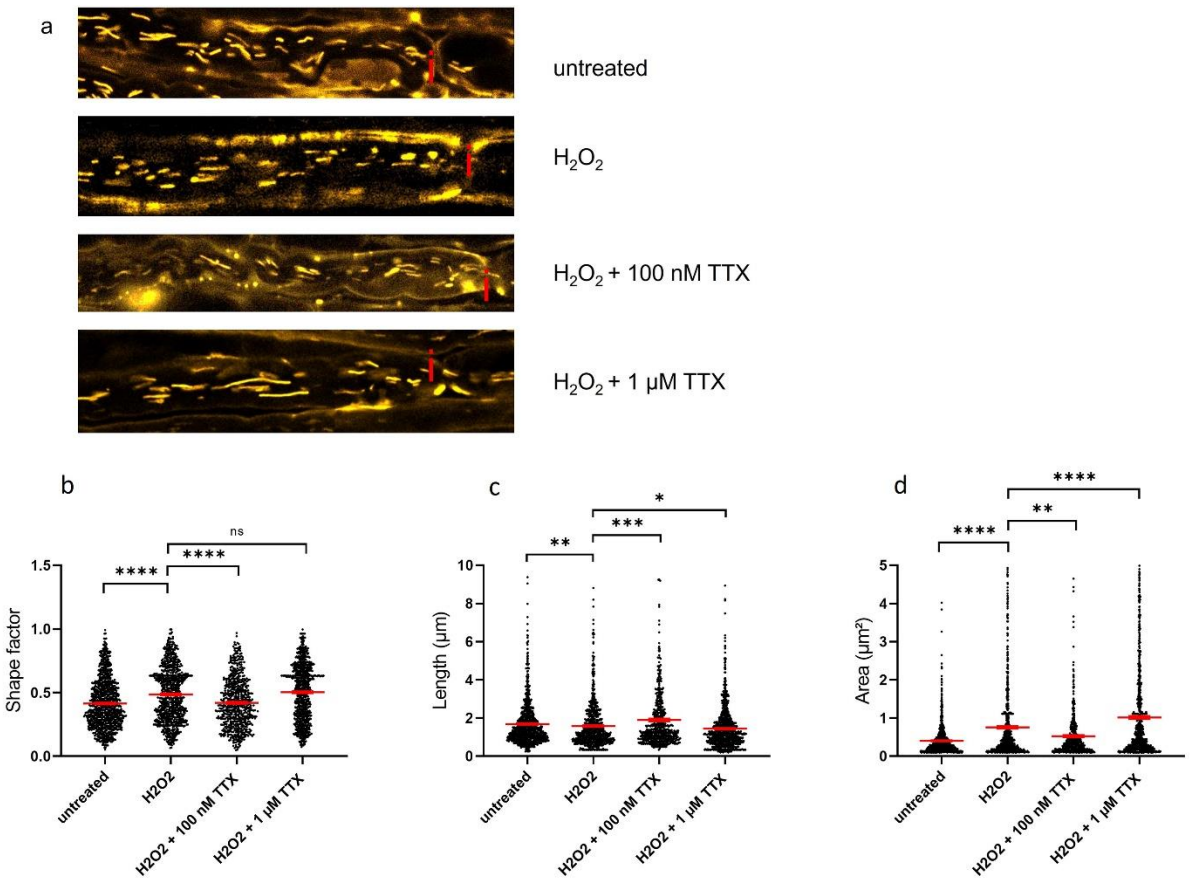

Figure 2: Effects of TTX on oxidatively induced mitochondrial motility alterations in spinal roots

Representative images of TTX experiments, the "i" depicts the node of Ranvier (a), quantification of morphological alterations, shape factor, mitochondrial length and area in TTX experiments (b-d), red lines depicting the mean and SEM, $*$ implying $p \leq 0.05$, $**$ implying $p \leq 0.01$, $***$ implying $p \leq 0.001$, and $****$ implying $p \leq 0.0001$; from [50]

By inhibiting mitochondrial Ca^{2+} uptake, we could not prevent oxidatively caused changes in mitochondrial area (Fig. 3c). Only at the smallest concentration of 5 µM, Ru360 prevented the H_2O_2-induced increase in shape factor while 20 µM Ru360 even increased the mitochondrial circularity (Fig.3a). With 10 µM Ru360, we prevented oxidatively caused reduction of mitochondrial length, 20 µM Ru360 even pronounced the decrease in length (Fig. 3b).

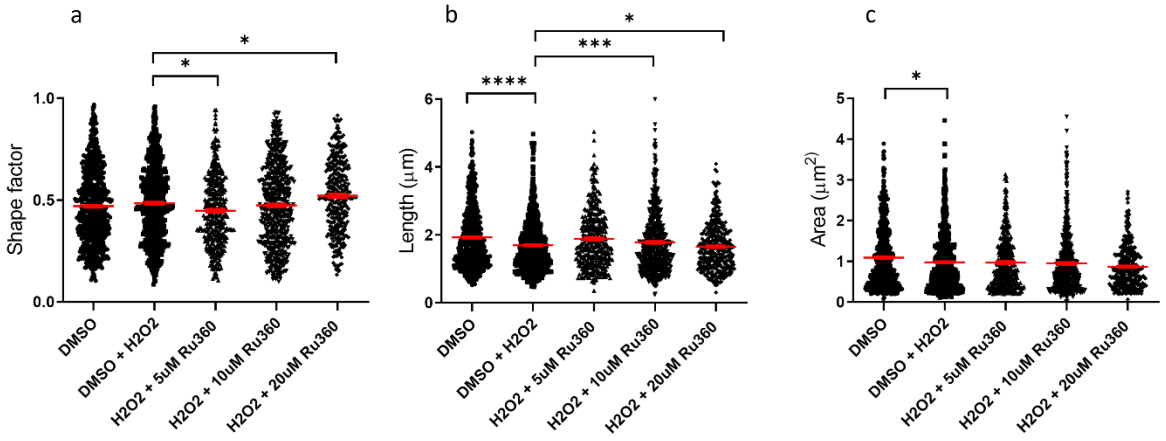

Figure 3: Effects of Ru360 on oxidatively induced mitochondrial morphology alterations in spinal roots

Quantification of morphological alterations, shape factor, mitochondrial length and area in TTX experiments (a-c), red lines depicting the mean and SEM; ∗ implying $p \leq 0.05$, ∗∗ implying $p \leq 0.01$, ∗∗∗ implying $p \leq 0.001$, and ∗∗∗∗ implying $p \leq 0.0001$; modified after [50]

100 µM H_2O_2 caused a decrease in the percentage of moving mitochondria in both TTX and Ru360 experiments. In Ru360 experiments, we further analyzed mitochondrial track length and mitochondrial velocity and observed a decrease under oxidative stress for both parameters.

With 1 µM TTX, we could prevent oxidatively induced loss of mitochondrial motility, but the percentage of motile mitochondria was still lower than in untreated spinal roots (data not shown). With 10 and 20 µM Ru360 we could prevent all oxidatively induced alterations in mitochondrial motility, while 5 µM Ru360 only prevented H_2O_2-induced decrease in mitochondrial track length (Fig. 4a-c). Importantly, with 10 µM Ru360, we observed similar motility results as in the negative control group (Fig. 4a-c).

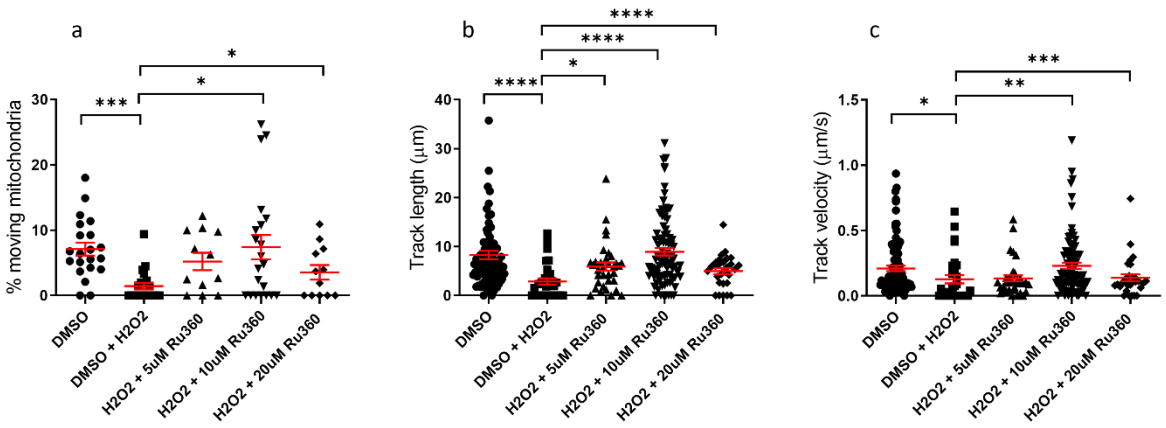

Figure 4: Effects of Ru360 on oxidatively induced mitochondrial motility alterations in spinal roots

Quantification of oxidatively induced alterations of percentage of motile mitochondria, mitochondrial track length and mitochondrial track velocity in Ru360 experiments, red lines depicting the mean and SEM, ∗ implying $p \leq 0.05$, ∗∗ implying $p \leq 0.01$, ∗∗∗ implying $p \leq 0.001$, and ∗∗∗∗ implying $p \leq 0.0001$; modified after [50]

Under oxidative stress, we discovered a reduction of JC-1 red/green ratio (Fig. 5a, b). This signifies a reduction of mitochondrial membrane potential as a measure of mitochondrial functionality. Both 1 µM TTX and 10 µM Ru360 prevented the oxidative stress-induced loss of mitochondrial membrane potential (Fig. 5a, b).

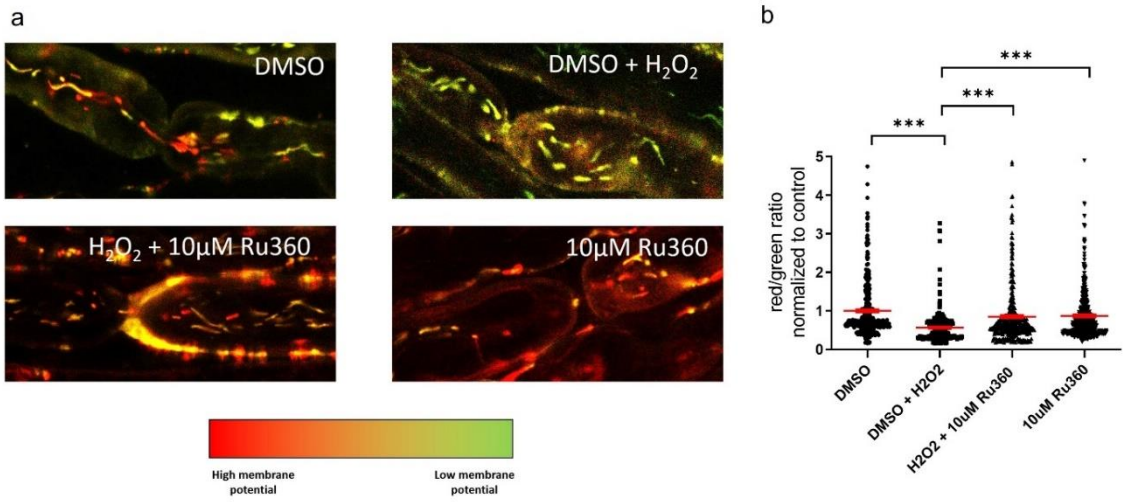

Figure 5: Effects of Ru360 on oxidatively induced alterations of mitochondrial membrane potential in spinal roots

Representative confocal images of mitochondrial membrane quantification with JC-1 in Ru360 experiments (a), green meaning low and red meaning high mitochondrial potential; quantification of red/green ratio normalized to the negative control (b), red lines depicting the mean and SEM; ∗ implying $p \leq 0.05$, ∗∗ implying $p \leq 0.01$, ∗∗∗ implying $p \leq 0.001$, and ∗∗∗∗ implying $p \leq 0.0001$, from [50]

3.2 Study 2: Teriflunomide preserves peripheral nerve mitochondria from oxidative stress-mediated alterations

Study 2 is also part of Dr. Bimala Malla's doctoral thesis.

In spinal roots, the concentration of both 1 µM TFN or 50 µM TFN prevented oxidative stress-induced decrease in mitochondrial length and area (data not shown). However, 5 µM TFN did not prevent oxidatively induced mitochondrial alterations (data not shown). Only at a concentration of 1 µM, TFN prevented the oxidatively caused increase of mitochondrial circularity (data not shown). Application of TFN alone resulted in a decrease of shape factor and mitochondrial length but did not affect mitochondrial area (data not shown).

Only 1 µM TFN prevented an oxidatively induced decrease in mitochondrial motility (Fig. 6). Incubation with TFN alone caused only a decrease of mitochondrial velocity (data not shown).

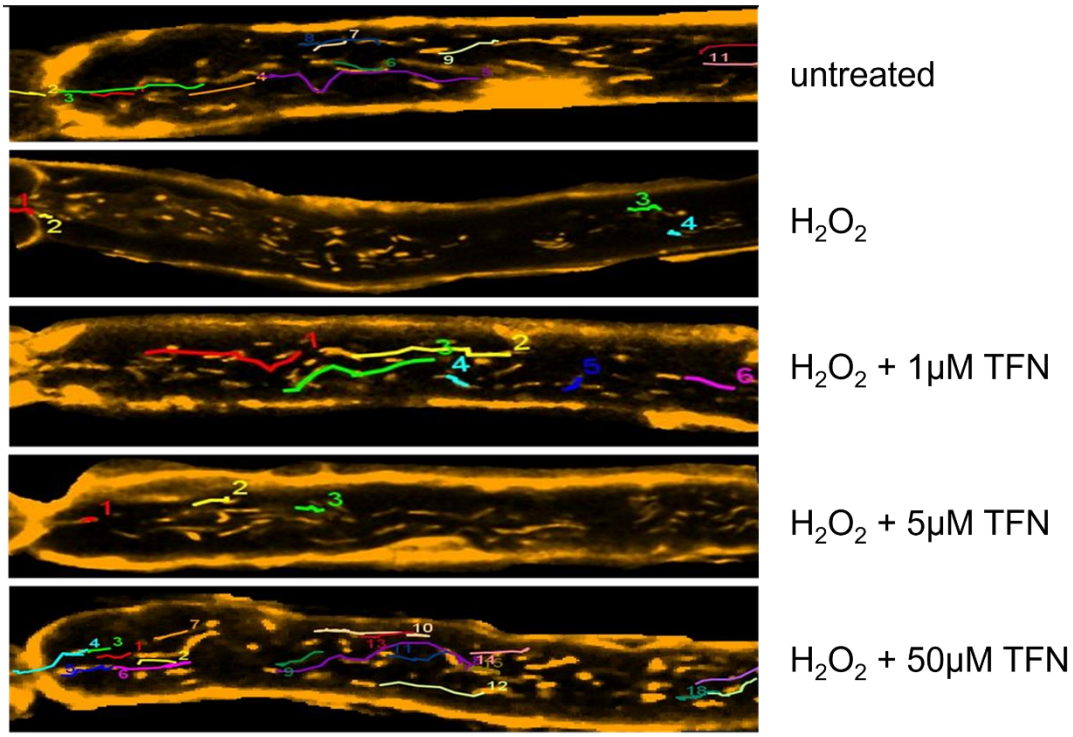

Figures 6: Effects of TFN on oxidatively induced mitochondrial motility alterations in spinal roots

Representative images of mitochondrial motility in TFN experiments, each colored track represents the track one mitochondrion has covered throughout the observed time period of 60 s; modified after [59]

With H_2O_2, we observed an increase in the fluorescence intensity of MitoTracker Orange® CMTMRos, depicting a high oxidation status. 1 µM TFN, but not 5 µM TFN or 50 µM TFN prevented this increase in ROS (data not shown).

3.3 Study 3: Teriflunomide Preserves Neuronal Activity and Protects Mitochondria in Brain Slices Exposed to Oxidative Stress

Study 3 is also part of Dr. Bimala Malla's doctoral thesis.

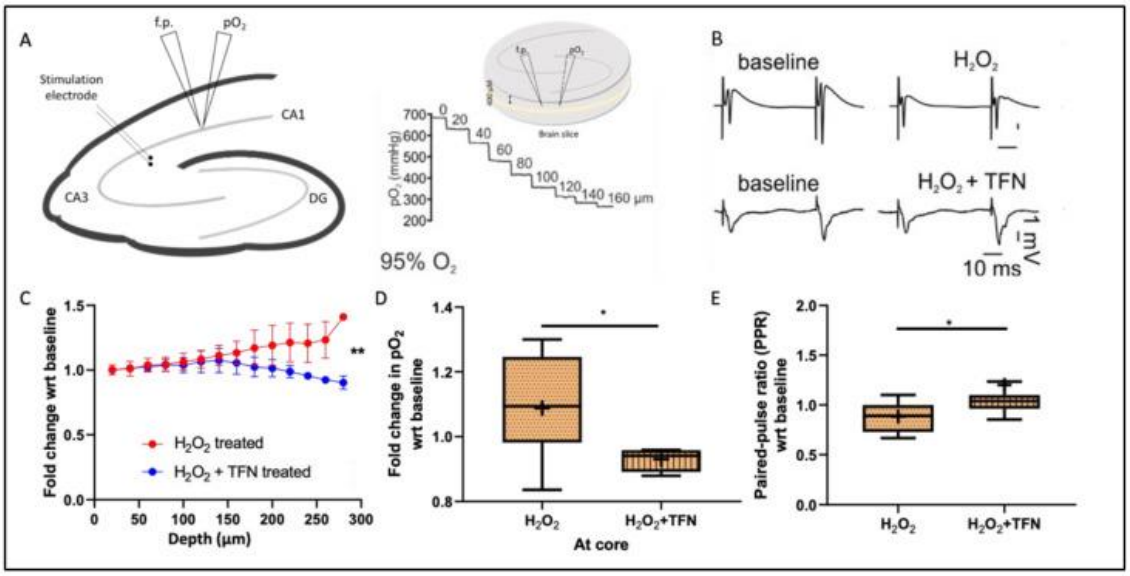

Figure 7: Schematic overview of electrophysiology recordings and effects of TFN on oxidatively induced alterations of electrophysiological parameters in acute hippocampal slices

(A), representative population spike in a paired-pulse at baseline, with H_2O_2 and H_2O_2 + TFN treatment (B); fold change compared to the baseline in the pO_2 at tissue depth in the interval of 20 µm (C); fold change compared to the baseline in pO_2 at the core (D); the paired-pulse ratio (PPR) compared to the respective baseline recording of PS2 and PS1(E). Graphs are shown in Tukey boxplots. Inside the box, '+' marks the mean, the box covers the 25th to the 75th quartile, the whiskers show the minimum and the maximum of the data; ∗ implying $p \leq 0.05$, ∗∗ implying $p \leq 0.01$, ∗∗∗ implying $p \leq 0.001$, and ∗∗∗∗ implying $p \leq 0.0001$; from [62]

In Study 3, incubation with H_2O_2 led to a decrease in neuronal oxygen consumption in acute hippocampal slices (Fig. 7C). Moreover, oxidative stress resulted in a depression of synaptic transmission (Fig. 7E). 50 µM TFN prevented oxidative stress-induced reduction of oxygen consumption as an indirect measure of cellular metabolism (Fig. 7C, D). Reduction of ATP levels upon oxidative stress could, however, not be prevented by 50 µM TFN in acute hippocampal slices (data not shown).

In acute hippocampal slices, oxidative stress induced by 100 µM H_2O_2 led to a decrease in mitochondrial length, area (Fig. 8C, D), and displacement (data not shown). This is consistent with our data on spinal roots from previous work [47]. Unlike our findings in spinal roots, oxidative stress in acute hippocampal slices led to an increase in mitochondrial speed (data not shown). 50 µM TFN prevented oxidatively induced reduction in mitochondrial area, but not in mitochondrial length (Fig. 8C, D). 50 µM TFN

caused a reduction in mitochondrial displacement, but increased mitochondrial speed compared to oxidatively stress slices (data now shown).

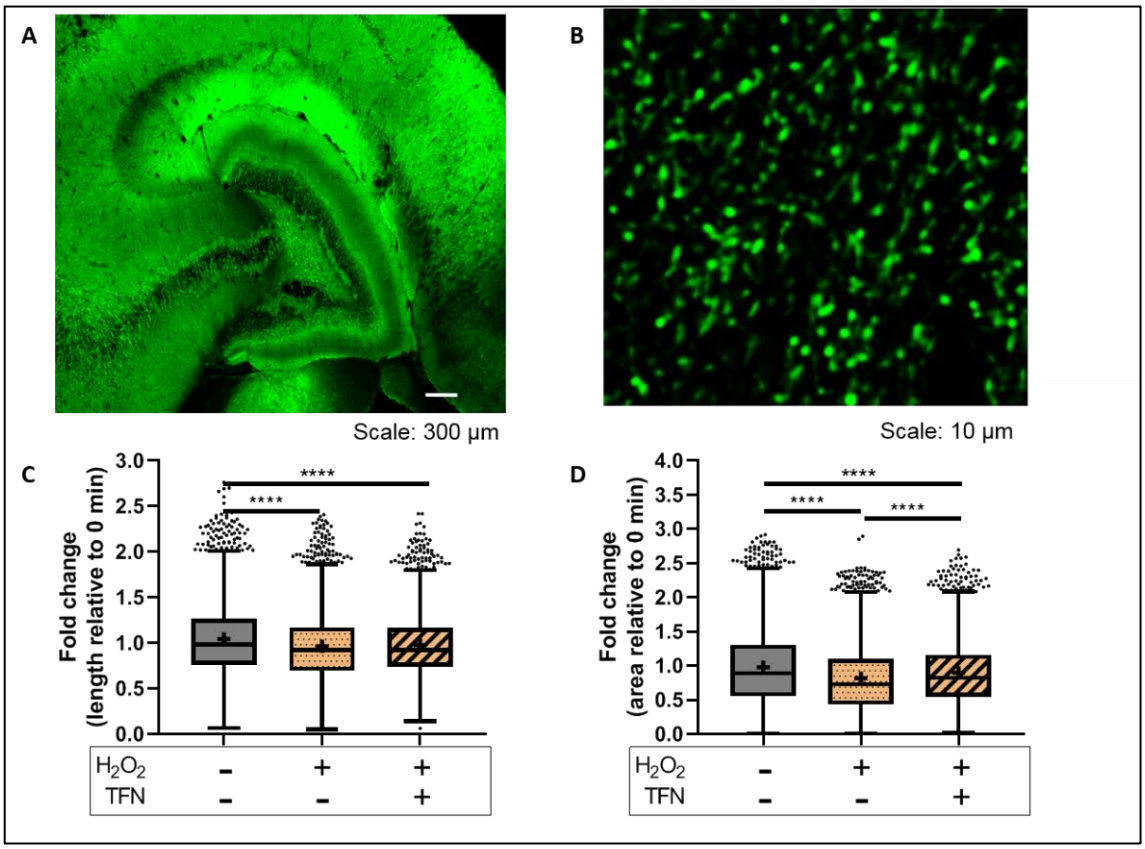

Figure 8: Effects of TFN on oxidatively induced mitochondrial morphology alterations in acute hippocampal slices

(A) represents an overview image of the acute hippocampal slice, mitochondrial fluorescence is shown in green; (B) is a representative two-photon microscope image with larger magnification; quantification of fold change in mitochondrial length (C) and mitochondrial area (D) compared to timepoint 0 of the same slice. Graphs are shown in Tukey boxplots. Inside the box, '+' marks the mean, the box covers the 25th to the 75th quartile, the whiskers show the minimum and the maximum of the data; ∗ implying $p \leq 0.05$, ∗∗ implying $p \leq 0.01$, ∗∗∗ implying $p \leq 0.001$, and ∗∗∗∗ implying $p \leq 0.0001$; from [62]

4 Discussion

4.1 Short summary of results

This thesis presents two models to evaluate drug effects on oxidatively stressed neuronal mitochondria in PNS and CNS. We have shown that pharmacological inhibitors of NaV and MCU could prevent mitochondrial alterations in the PNS model and added thereby to the understanding of neurodegenerative pathomechanisms and their possible prevention. We have also shown that TFN can exert beneficial effects on neuronal mitochondrial dynamics and functionality.

4.2 Interpretation of results, embedding the results into the current state of research and strengths and weaknesses of the included studies

The spinal root model used in Studies 1 and 2 was used to screen for mitochondrial alterations upon therapeutic intervention and ion channel inhibition, respectively. We have shown that this model is a suited model for investigating the morphology and motility of axonal mitochondria [48]. One advantage of this model lies in the relatively simple preparation and analysis of mitochondrial dynamics due to the parallel arrangement of axons. It also preserves cytoarchitecture and the thinness of the spinal roots ensures high availability of administered drugs [48].

We have also tested the effects of TFN in acute hippocampal slices as a model of the CNS. Acute hippocampal brain slices are more similar to the in vivo situation; however, they represent a more complex and more difficult-to-handle ex vivo model for monitoring drug effects on neuronal mitochondria.

Spinal roots and acute hippocampal slices show differences in tissue thickness. Therefore, we adjusted the applied concentrations of reagents. However, we have observed a decrease in mitochondrial length and motile mitochondria in both models, independently of the used H_2O_2 concentration. The concentrations used in our experiments are high when compared to physiological, steady-state intracellular concentrations that range from 1 to 100 nM approximately when H_2O_2 is working as a signaling molecule [63]. However, there is a 100 to 500-fold difference between the intracellular and extracellular space and, during inflammation, plasma H_2O_2 levels were shown to rise to higher concentrations (µM range) [64]. Moreover, others have shown that H_2O_2 concentration decreases quickly over time due to its high reactivity [65, 66].

In both ex vivo models, oxidative stress led to a decrease in mitochondrial length [50, 59, 62]. This might be caused by oxidatively induced mitochondrial fission, which is a cellular mechanism to clear out damaged parts of mitochondria [67-69].

Blocking NaV with 100 nM TTX prevented the decrease in mitochondrial length due to oxidative stress (Fig. 2C). We have demonstrated in Study 1 that MCU-inhibition with 10 µM Ru360 prevented oxidative stress-induced reduction of mitochondrial length (Fig 3b). This might be related to the Ca^{2+}-controlled regulation of proteins involved in mitochondrial fission (e.g. dynamin-related protein 1) [70].

Our data in Study 1 confirm the non-linear effects of alterations in Na^{+} and Ca^{2+} concentrations on mitochondrial morphology, motility, and functionality [71]. Changes in Ca^{2+} concentration may have both stimulating (e.g., increase in mitochondrial ATP production [72]) and detrimental effects (e.g. opening of mPTP upon excessive Ca^{2+} concentrations [73]). In addition, ROS regulate the transcription of enzymes and enzyme activity by oxidizing cellular structures [32, 74, 75] and some of these mechanisms might take place in our models. ROS, regulate the activity of MCU and NaV [76, 77], thereby also influencing ional concentrations within axons and mitochondria, making it even more challenging to predict how ional concentrations alter, especially in subcellular compartments. Furthermore, with Ru360 we did not block either a reverse action model of mNCX that has been described to occur in metabolically inhibited cells, or mitochondria-associated membranes (MAMs) with the endoplasmatic reticulum that also serve to exchange Ca^{2+} between organelles [46]. MAMs also take part in mitochondrial fusion and fission processes [78]. Thus, we did not modulate all possible ways by which Ca^{2+} may enter mitochondria.

Oxidative stress led to a decrease in the percentage of moving mitochondria in Study 1. Both 1 µM TTX and 10 µM Ru360 could prevent this oxidatively caused motility decrease (Fig. 4). Again, Ca^{2+} concentrations are known to play a role in regulating mitochondrial motility, e.g., via mitochondrial Rho-GTPase 1 (Miro1), a protein linking mitochondria to motor proteins with the help of other connector proteins [79]. Miro1 is a protein on the outer mitochondrial membrane, consisting of two GTPase parts on the N-terminal part and EF-hand domains working as Ca^{2+} sensors on the cytoplasmic side [80]. Miro1 usually promotes anterograde mitochondrial transport [81], but upon rising Ca^{2+} levels a conformational shift takes place and mitochondrial transport is halted [82, 83]. TTX may prevent the oxidative-stress-induced decrease in motility by hindering intraaxonal Ca^{2+} rise. MCU itself seems to play a role in regulating mitochondrial movement and is thereby

one possible answer to the question of how Ru360 prevents oxidatively induced decrease in mitochondrial motility [84]. Also, it has been assumed that there is an interaction between MCU and Miro1 and that Ca^{2+} influx via MCU may lead to the same conformational changes of Miro1 mentioned above, resulting in decreased mitochondrial motility [85]. Since Ru360 blocks this Ca^{2+} influx, this might be another explanation for its motility-preserving effects.

In Study 1, we have shown that oxidative stress decreases mitochondrial membrane potential (Fig. 5), indicating a loss in mitochondrial capacity to produce ATP. Furthermore, in Study 3 we have directly measured ATP levels and have been able to show a reduction under oxidative stress. Thus, we have shown that oxidative stress reduces mitochondrial capacity to properly provide ATP.

In Study 1, 1 µM TTX prevented the decrease in mitochondrial membrane potential under simultaneous exposition to H_2O_2 (data not shown). 1 µM TTX alone induced mitochondrial hyperpolarization [86, 87]. One explanation for this observation could be reduced Na^+ influx and subsequent reduced activity of the ATP-dependent Na^+/K^+-ATPase, which leads to an intraaxonal increase of ATP. It has been described that elevated ATP levels may lead to a reverse action mode of complex V, consuming cellular ATP content [49]. 10 µM Ru360 also protected mitochondria against oxidative stress-induced reduction in mitochondrial membrane potential (Fig. 5a, b). TFN, however, could not prevent the oxidatively caused reduction in ATP levels in acute hippocampal slices (data not shown).

We did not succeed in the establishment of a protocol to directly measure intraaxonal and intramitochondrial Ca^{2+} concentrations in Study 1, neither with Fluo-4 and stimulation with Ionomycin [88] nor with a genetic mice model for Ca^{2+} staining in central neurons (CerTNL-15 mice) [89]. We suppose that spinal roots, which are not part of the CNS, may not express the fluorescent marker.

Regarding the effects of TFN, we have shown that the drug directly influences mitochondrial dynamics. The exact mechanisms remain incompletely understood and partially contradictive: Some have discovered that TFN alters intracellular Ca^{2+} concentrations via store-operated calcium entry [90], while others state that TFN does not influence neuronal Ca^{2+} concentrations [91].

A limitation of the studies is the quantity of experimental conditions that can be compared at once. This results from the size of the used incubation chamber and the restricted time window, in which spinal roots and acute hippocampal slices are viable and suited for imaging. In addition, the time window in which experiments can be conducted is limited

to 3-4 hours, since afterward, spinal roots and acute hippocampal slices undergo irreversible damage.
Moreover, we lack direct measurement of Ca^{2+} concentrations to detect protective and detrimental levels.

4.3 Implications for practice and/or future research

The next step could be the investigation of the effect of ion channel inhibition in the CNS model. We will also include already established methods of assessing neuronal parameters such as ATP content, oxygen consumption, and electrophysiology.
Mitochondrial morphology and motility change under oxidative stress, thus, proteins associated with fusion and fission as well as mitochondrial transport could be affected and show altered expression patterns. To investigate this, PCR analysis of altered protein expression patterns could be established. Candidates for investigation could be proteins associated with mitochondrial fusion (e.g. mitofusin 1 or 2, dynamin-related GTPases, optic atrophy1), fission (e.g. dynamin related protein 1), movement (e.g. kinesin, dynein), and immobility (e.g. syntaphilin) [69].
The model of acute hippocampal slices can be used to monitor mitochondrial alterations of the CNS. However, this model cannot provide insights into the long term effects of drugs due to the limited period (4-6 h) to image the slices [92]. Therefore, we have established a model of chronic hippocampal brain slices in our group [93]. We have evaluated the effects of Fingolimod and Siponimod on mitochondria in chronic slice culture (paper in preparation).
The spinal roots model, as well as the acute and chronic hippocampal slice model, offer ways to reduce animal experiments, a part of the 3 “R’s” (refinement, replacement and reduction), as first described by Russell and Burch in the 1950s [94].
Finally, as the next step in pre-clinical trials, verification of observed mechanisms could be performed in an in vivo model of MS. Several animal models exist to mimic different aspects of MS. The most used model is experimental autoimmune encephalomyelitis (EAE). Classically, mice are injected with an antigen (e.g., proteolipid protein, myelin basic protein, etc.) in emulsion with complete Freund’s adjuvant, as well as pertussis toxin in glycol buffer [95]. Alternatively, one can perform a transfer of lymphocytes that were activated with these antigens in vitro [95]. The different forms of EAE (relapsing vs. chronic) can be induced by choosing different mice strains [96]. Predominantly, EAE

models represent the autoimmune part of MS [97]. Other models include demyelination caused by viral infection or toxin-induced demyelination [98, 99].

Other groups, e.g., Kerschensteiner et al., have developed models to monitor mitochondria in vivo in the spinal column [100]. In combination with murine MS models, this might be a suited model to test the effects of ion channel inhibitors and already developed drugs on mitochondria.

Neurodegenerative diseases are on the rise, partly because the world's population is getting older and neurodegenerative diseases are often age-related [101]. New drugs for the treatment of neurodegenerative diseases and a better understanding of underlying pathomechanisms are therefore urgently needed [102]. Since development of new drugs is cost- and time-intensive, repurposing of already developed and approved drugs is a valid alternative [103]. We have investigated effects of blocking axonal Na^+ influx and mitochondrial Ca^{2+} uptake which are known to be key features in neurodegenerative disorders [104, 105]. Understanding the implication of ional alterations in neurodegeneration may be an essential step towards developing targeted drugs against neuronal death. Moreover, we have added important knowledge to understanding the effects of TFN.

5 Conclusions

The overall aims of our studies were the identification of neurodegenerative pathomechanisms and the evaluation of potential interventions for the targeted treatment of neuronal loss. We have proved ion channel inhibitors and TFN to be beneficial in terms of preventing oxidative stress-induced mitochondrial alterations.

With Study 1 of this thesis, we have shown that our PNS model is suited to monitor alterations in Na^+ and Ca^{2+} concentrations that we had hypothesized to happen downstream of oxidative insult on neurons. We have also demonstrated that inhibition of both NaV and MCU might prevent oxidatively induced mitochondrial alterations.

In Study 2 and Study 3, we have shown conclusively that prevention of oxidatively induced mitochondrial alterations might be one possible mechanism by which TFN protects neuronal cells from degeneration. Moreover, TFN exerts its neuroprotective effects in our CNS model via the prevention of a reduction in oxygen metabolism and neuronal activity as well as its effects on mitochondrial dynamics.

Reference list

1. Thompson AJ, Baranzini SE, Geurts J, Hemmer B, Ciccarelli O. Multiple sclerosis. Lancet (London, England). 2018;391(10130):1622-36.
2. Kobelt G, Thompson A, Berg J, Gannedahl M, Eriksson J. New insights into the burden and costs of multiple sclerosis in Europe. Multiple sclerosis (Houndmills, Basingstoke, England). 2017;23(8):1123-36.
3. Flachenecker P, Kobelt G, Berg J, Capsa D, Gannedahl M. New insights into the burden and costs of multiple sclerosis in Europe: Results for Germany. Multiple Sclerosis Journal. 2017;23(2_suppl):78-90.
4. Walton C, King R, Rechtman L, Kaye W, Leray E, Marrie RA, Robertson N, La Rocca N, Uitdehaag B, van der Mei I, Wallin M, Helme A, Angood Napier C, Rijke N, Baneke P. Rising prevalence of multiple sclerosis worldwide: Insights from the Atlas of MS, third edition. Multiple sclerosis (Houndmills, Basingstoke, England). 2020;26(14):1816-21.
5. Gelfand JM. Chapter 12 - Multiple sclerosis: diagnosis, differential diagnosis, and clinical presentation. In: Goodin DS, editor. Handbook of clinical neurology. 122: Elsevier; 2014. p. 269-90.
6. Thompson AJ, Banwell BL, Barkhof F, Carroll WM, Coetzee T, Comi G, Correale J, Fazekas F, Filippi M, Freedman MS, Fujihara K, Galetta SL, Hartung HP, Kappos L, Lublin FD, Marrie RA, Miller AE, Miller DH, Montalban X, Mowry EM, Sorensen PS, Tintoré M, Traboulsee AL, Trojano M, Uitdehaag BMJ, Vukusic S, Waubant E, Weinshenker BG, Reingold SC, Cohen JA. Diagnosis of multiple sclerosis: 2017 revisions of the McDonald criteria. The Lancet Neurology. 2018;17(2):162-73.
7. Lublin FD, Reingold SC, Cohen JA, Cutter GR, Sørensen PS, Thompson AJ, Wolinsky JS, Balcer LJ, Banwell B, Barkhof F, Bebo B, Jr., Calabresi PA, Clanet M, Comi G, Fox RJ, Freedman MS, Goodman AD, Inglese M, Kappos L, Kieseier BC, Lincoln JA, Lubetzki C, Miller AE, Montalban X, O'Connor PW, Petkau J, Pozzilli C, Rudick RA, Sormani MP, Stüve O, Waubant E, Polman CH. Defining the clinical course of multiple sclerosis: the 2013 revisions. Neurology. 2014;83(3):278-86.
8. Klineova S, Lublin FD. Clinical Course of Multiple Sclerosis. Cold Spring Harbor perspectives in medicine. 2018;8(9).
9. Weiner HL. A shift from adaptive to innate immunity: a potential mechanism of disease progression in multiple sclerosis. Journal of neurology. 2008;255 Suppl 1:3-11.
10. Ghasemi N, Razavi S, Nikzad E. Multiple Sclerosis: Pathogenesis, Symptoms, Diagnoses and Cell-Based Therapy. Cell J. 2017;19(1):1-10.
11. Kister I, Bacon TE, Chamot E, Salter AR, Cutter GR, Kalina JT, Herbert J. Natural history of multiple sclerosis symptoms. International journal of MS care. 2013;15(3):146-58.
12. Oh J, Alikhani K, Bruno T, Devonshire V, Giacomini PS, Giuliani F, Nakhaipour HR, Schecter R, Larochelle C. Diagnosis and management of secondary-progressive multiple sclerosis: time for change. Neurodegenerative disease management. 2019;9(6):301-17.
13. Berkovich RR. Acute Multiple Sclerosis Relapse. Continuum (Minneapolis, Minn). 2016;22(3):799-814.
14. Hauser SL, Cree BAC. Treatment of Multiple Sclerosis: A Review. The American journal of medicine. 2020;133(12):1380-90.e2.
15. Neurologie DGf. Diagnose und Therapie der Multiplen Sklerose, Neuromyelitis-optica-Spektrum-Erkrankungen und MOG-IgG-assoziierten Erkrankungen 2023, March

31 [Available from: https://dgn.org/leitlinie/diagnose-und-therapie-der-multiplen-sklerose-neuromyelitis-optica-spektrum-erkrankungen-und-mog-igg-assoziierten-erkrankungen.
16. Montalban X, Hauser SL, Kappos L, Arnold DL, Bar-Or A, Comi G, de Seze J, Giovannoni G, Hartung HP, Hemmer B, Lublin F, Rammohan KW, Selmaj K, Traboulsee A, Sauter A, Masterman D, Fontoura P, Belachew S, Garren H, Mairon N, Chin P, Wolinsky JS. Ocrelizumab versus Placebo in Primary Progressive Multiple Sclerosis. The New England journal of medicine. 2017;376(3):209-20.
17. Kappos L, Bar-Or A, Cree BAC, Fox RJ, Giovannoni G, Gold R, Vermersch P, Arnold DL, Arnould S, Scherz T, Wolf C, Wallström E, Dahlke F. Siponimod versus placebo in secondary progressive multiple sclerosis (EXPAND): a double-blind, randomised, phase 3 study. Lancet (London, England). 2018;391(10127):1263-73.
18. Wan ECK. Cellular and Molecular Mechanisms in the Pathogenesis of Multiple Sclerosis. Cells. 2020;9(10):2223.
19. Salapa HE, Lee S, Shin Y, Levin MC. Contribution of the Degeneration of the Neuro-Axonal Unit to the Pathogenesis of Multiple Sclerosis. Brain sciences. 2017;7(6).
20. Stephenson J, Nutma E, van der Valk P, Amor S. Inflammation in CNS neurodegenerative diseases. Immunology. 2018;154(2):204-19.
21. Butler R, Bradford D, Rodgers KE. Analysis of shared underlying mechanism in neurodegenerative disease. Frontiers in aging neuroscience. 2022;14:1006089.
22. Mahad D, Ziabreva I, Lassmann H, Turnbull D. Mitochondrial defects in acute multiple sclerosis lesions. Brain : a journal of neurology. 2008;131(Pt 7):1722-35.
23. Su KG, Banker G, Bourdette D, Forte M. Axonal degeneration in multiple sclerosis: The mitochondrial hypothesis. Current Neurology and Neuroscience Reports. 2009;9(5):411-7.
24. Witte ME, Mahad DJ, Lassmann H, van Horssen J. Mitochondrial dysfunction contributes to neurodegeneration in multiple sclerosis. Trends in molecular medicine. 2014;20(3):179-87.
25. Patergnani S, Fossati V, Bonora M, Giorgi C, Marchi S, Missiroli S, Rusielewicz T, Wieckowski MR, Pinton P. Mitochondria in Multiple Sclerosis: Molecular Mechanisms of Pathogenesis. International review of cell and molecular biology. 2017;328:49-103.
26. Su K, Bourdette D, Forte M. Mitochondrial dysfunction and neurodegeneration in multiple sclerosis. Frontiers in physiology. 2013;4:169.
27. Barcelos IP, Troxell RM, Graves JS. Mitochondrial Dysfunction and Multiple Sclerosis. Biology. 2019;8(2).
28. Zhu XH, Qiao H, Du F, Xiong Q, Liu X, Zhang X, Ugurbil K, Chen W. Quantitative imaging of energy expenditure in human brain. NeuroImage. 2012;60(4):2107-17.
29. Kann O, Kovács R. Mitochondria and neuronal activity. American journal of physiology Cell physiology. 2007;292(2):C641-57.
30. Rossi A, Pizzo P, Filadi R. Calcium, mitochondria and cell metabolism: A functional triangle in bioenergetics. Biochimica et Biophysica Acta (BBA) - Molecular Cell Research. 2019;1866(7):1068-78.
31. Stowe DF, Camara AK. Mitochondrial reactive oxygen species production in excitable cells: modulators of mitochondrial and cell function. Antioxidants & redox signaling. 2009;11(6):1373-414.
32. Ohl K, Tenbrock K, Kipp M. Oxidative stress in multiple sclerosis: Central and peripheral mode of action. Experimental neurology. 2016;277:58-67.
33. Signorile A, Ferretta A, Ruggieri M, Paolicelli D, Lattanzio P, Trojano M, De Rasmo D. Mitochondria, Oxidative Stress, cAMP Signalling and Apoptosis: A Crossroads in Lymphocytes of Multiple Sclerosis, a Possible Role of Nutraceutics. Antioxidants. 2021;10(1):21.

34. Mossakowski AA, Pohlan J, Bremer D, Lindquist R, Millward JM, Bock M, Pollok K, Mothes R, Viohl L, Radbruch M, Gerhard J, Bellmann-Strobl J, Behrens J, Infante-Duarte C, Mähler A, Boschmann M, Rinnenthal JL, Füchtemeier M, Herz J, Pache FC, Bardua M, Priller J, Hauser AE, Paul F, Niesner R, Radbruch H. Tracking CNS and systemic sources of oxidative stress during the course of chronic neuroinflammation. Acta neuropathologica. 2015;130(6):799-814.
35. Nikić I, Merkler D, Sorbara C, Brinkoetter M, Kreutzfeldt M, Bareyre FM, Brück W, Bishop D, Misgeld T, Kerschensteiner M. A reversible form of axon damage in experimental autoimmune encephalomyelitis and multiple sclerosis. Nature medicine. 2011;17(4):495-9.
36. Kozin MS, Kulakova OG, Favorova OO. Involvement of Mitochondria in Neurodegeneration in Multiple Sclerosis. Biochemistry Biokhimiia. 2018;83(7):813-30.
37. Wilson DF. Oxidative phosphorylation: regulation and role in cellular and tissue metabolism. The Journal of Physiology. 2017;595(23):7023-38.
38. Federico A, Cardaioli E, Da Pozzo P, Formichi P, Gallus GN, Radi E. Mitochondria, oxidative stress and neurodegeneration. Journal of the Neurological Sciences. 2012;322(1):254-62.
39. Persson A-K, Kim I, Zhao P, Estacion M, Black JA, Waxman SG. Sodium Channels Contribute to Degeneration of Dorsal Root Ganglion Neurites Induced by Mitochondrial Dysfunction in an In Vitro Model of Axonal Injury. The Journal of Neuroscience. 2013;33(49):19250.
40. Dutta R, McDonough J, Yin X, Peterson J, Chang A, Torres T, Gudz T, Macklin WB, Lewis DA, Fox RJ, Rudick R, Mirnics K, Trapp BD. Mitochondrial dysfunction as a cause of axonal degeneration in multiple sclerosis patients. Annals of neurology. 2006;59(3):478-89.
41. Soane L, Kahraman S, Kristian T, Fiskum G. Mechanisms of impaired mitochondrial energy metabolism in acute and chronic neurodegenerative disorders. Journal of neuroscience research. 2007;85(15):3407-15.
42. Denton RM. Regulation of mitochondrial dehydrogenases by calcium ions. Biochimica et biophysica acta. 2009;1787(11):1309-16.
43. Walters GC, Usachev YM. Mitochondrial calcium cycling in neuronal function and neurodegeneration. Frontiers in cell and developmental biology. 2023;11:1094356.
44. De Stefani D, Patron M, Rizzuto R. Structure and function of the mitochondrial calcium uniporter complex. Biochimica et Biophysica Acta (BBA) - Molecular Cell Research. 2015;1853(9):2006-11.
45. Jung H, Kim SY, Canbakis Cecen FS, Cho Y, Kwon SK. Dysfunction of Mitochondrial Ca(2+) Regulatory Machineries in Brain Aging and Neurodegenerative Diseases. Frontiers in cell and developmental biology. 2020;8:599792.
46. Giorgi C, Marchi S, Pinton P. The machineries, regulation and cellular functions of mitochondrial calcium. Nature reviews Molecular cell biology. 2018;19(11):713-30.
47. Bros H, Millward JM, Paul F, Niesner R, Infante-Duarte C. Oxidative damage to mitochondria at the nodes of Ranvier precedes axon degeneration in ex vivo transected axons. Experimental neurology. 2014;261:127-35.
48. Bros H, Niesner R, Infante-Duarte C. An ex vivo model for studying mitochondrial trafficking in neurons. Methods in molecular biology (Clifton, NJ). 2015;1264:465-72.
49. Wang J, Ou SW, Wang YJ. Distribution and function of voltage-gated sodium channels in the nervous system. Channels (Austin, Tex). 2017;11(6):534-54.
50. Ulshöfer R, Bros H, Hauser AE, Niesner RA, Paul F, Malla B, Infante-Duarte C. Preventing Axonal Sodium Overload or Mitochondrial Calcium Uptake Protects Axonal

Mitochondria from Oxidative Stress-Induced Alterations. Oxidative medicine and cellular longevity. 2022;2022:6125711.
51. Bar-Or A, Pachner A, Menguy-Vacheron F, Kaplan J, Wiendl H. Teriflunomide and its mechanism of action in multiple sclerosis. Drugs. 2014;74(6):659-74.
52. Miller AE. An updated review of teriflunomide's use in multiple sclerosis. Neurodegenerative disease management. 2021;11(5):387-409.
53. Claussen MC, Korn T. Immune mechanisms of new therapeutic strategies in MS: teriflunomide. Clinical immunology (Orlando, Fla). 2012;142(1):49-56.
54. Wiese MD, Rowland A, Polasek TM, Sorich MJ, O'Doherty C. Pharmacokinetic evaluation of teriflunomide for the treatment of multiple sclerosis. Expert opinion on drug metabolism & toxicology. 2013;9(8):1025-35.
55. Malla B, Niesner R, Hauser A, Infante-Duarte C. Imaging and analysis of neuronal mitochondria in murine acute brain slices. Journal of neuroscience methods. 2022;372:109558.
56. Cottet-Rousselle C, Ronot X, Leverve X, Mayol J-F. Cytometric assessment of mitochondria using fluorescent probes. Cytometry Part A. 2011;79A(6):405-25.
57. Kweon SM, Kim HJ, Lee ZW, Kim SJ, Kim SI, Paik SG, Ha KS. Real-time measurement of intracellular reactive oxygen species using Mito tracker orange (CMH2TMRos). Bioscience reports. 2001;21(3):341-52.
58. Nitsch R, Pohl EE, Smorodchenko A, Infante-Duarte C, Aktas O, Zipp F. Direct impact of T cells on neurons revealed by two-photon microscopy in living brain tissue. The Journal of neuroscience : the official journal of the Society for Neuroscience. 2004;24(10):2458-64.
59. Malla B, Cotten S, Ulshoefer R, Paul F, Hauser AE, Niesner R, Bros H, Infante-Duarte C. Teriflunomide preserves peripheral nerve mitochondria from oxidative stress-mediated alterations. Ther Adv Chronic Dis. 2020;11:2040622320944773-.
60. Ghasemi N, Razavi S, Nikzad E. Multiple Sclerosis: Pathogenesis, Symptoms, Diagnoses and Cell-Based Therapy. Cell journal. 2017;19(1):1-10.
61. Gupta R, Tekade M, Vasdev N, Gupta T, Pawar B, Bansal KK, Tekade RK. Chapter 13 - Mechanism of drug-induced neurotoxicity and its management. In: Tekade R, editor. Essentials of Pharmatoxicology in Drug Research. 1: Academic Press; 2023. p. 317-41.
62. Malla B, Liotta A, Bros H, Ulshöfer R, Paul F, Hauser AE, Niesner R, Infante-Duarte C. Teriflunomide Preserves Neuronal Activity and Protects Mitochondria in Brain Slices Exposed to Oxidative Stress. International journal of molecular sciences. 2022;23(3).
63. Sies H, Jones DP. Reactive oxygen species (ROS) as pleiotropic physiological signalling agents. Nature Reviews Molecular Cell Biology. 2020;21(7):363-83.
64. Forman HJ, Bernardo A, Davies KJA. What is the concentration of hydrogen peroxide in blood and plasma? Archives of Biochemistry and Biophysics. 2016;603:48-53.
65. Iwakami S, Misu H, Takeda T, Sugimori M, Matsugo S, Kaneko S, Takamura T. Concentration-dependent dual effects of hydrogen peroxide on insulin signal transduction in H4IIEC hepatocytes. PloS one. 2011;6(11):e27401.
66. Gülden M, Jess A, Kammann J, Maser E, Seibert H. Cytotoxic potency of H2O2 in cell cultures: impact of cell concentration and exposure time. Free radical biology & medicine. 2010;49(8):1298-305.
67. Carinci M, Vezzani B, Patergnani S, Ludewig P, Lessmann K, Magnus T, Casetta I, Pugliatti M, Pinton P, Giorgi C. Different Roles of Mitochondria in Cell Death and Inflammation: Focusing on Mitochondrial Quality Control in Ischemic Stroke and Reperfusion. Biomedicines. 2021;9(2).

68. Chan DC. Mitochondrial Dynamics and Its Involvement in Disease. Annual review of pathology. 2020;15:235-59.
69. Ni HM, Williams JA, Ding WX. Mitochondrial dynamics and mitochondrial quality control. Redox biology. 2015;4:6-13.
70. Palmer CS, Osellame LD, Stojanovski D, Ryan MT. The regulation of mitochondrial morphology: Intricate mechanisms and dynamic machinery. Cellular Signalling. 2011;23(10):1534-45.
71. Bagur R, Hajnóczky G. Intracellular Ca(2+) Sensing: Its Role in Calcium Homeostasis and Signaling. Molecular cell. 2017;66(6):780-8.
72. Griffiths EJ, Rutter GA. Mitochondrial calcium as a key regulator of mitochondrial ATP production in mammalian cells. Biochimica et biophysica acta. 2009;1787(11):1324-33.
73. Peng TI, Jou MJ. Oxidative stress caused by mitochondrial calcium overload. Annals of the New York Academy of Sciences. 2010;1201:183-8.
74. Camara AK, Lesnefsky EJ, Stowe DF. Potential therapeutic benefits of strategies directed to mitochondria. Antioxidants & redox signaling. 2010;13(3):279-347.
75. Kumar A, Ratan RR. Oxidative Stress and Huntington's Disease: The Good, The Bad, and The Ugly. Journal of Huntington's disease. 2016;5(3):217-37.
76. Nemani N, Shanmughapriya S, Madesh M. Molecular regulation of MCU: Implications in physiology and disease. Cell calcium. 2018;74:86-93.
77. Patel R, Sesti F. Oxidation of ion channels in the aging nervous system. Brain research. 2016;1639:174-85.
78. Krols M, van Isterdael G, Asselbergh B, Kremer A, Lippens S, Timmerman V, Janssens S. Mitochondria-associated membranes as hubs for neurodegeneration. Acta neuropathologica. 2016;131(4):505-23.
79. Mishra P, Chan DC. Metabolic regulation of mitochondrial dynamics. The Journal of cell biology. 2016;212(4):379-87.
80. Fransson S, Ruusala A, Aspenström P. The atypical Rho GTPases Miro-1 and Miro-2 have essential roles in mitochondrial trafficking. Biochemical and biophysical research communications. 2006;344(2):500-10.
81. Glater EE, Megeath LJ, Stowers RS, Schwarz TL. Axonal transport of mitochondria requires milton to recruit kinesin heavy chain and is light chain independent. Journal of Cell Biology. 2006;173(4):545-57.
82. MacAskill AF, Rinholm JE, Twelvetrees AE, Arancibia-Carcamo IL, Muir J, Fransson A, Aspenstrom P, Attwell D, Kittler JT. Miro1 Is a Calcium Sensor for Glutamate Receptor-Dependent Localization of Mitochondria at Synapses. Neuron. 2009;61(4):541-55.
83. Wang X, Schwarz TL. The Mechanism of Ca2+-Dependent Regulation of Kinesin-Mediated Mitochondrial Motility. Cell. 2009;136(1):163-74.
84. Chang KT, Niescier RF, Min K-T. Mitochondrial matrix Ca²⁺ as an intrinsic signal regulating mitochondrial motility in axons. Proceedings of the National Academy of Sciences. 2011;108(37):15456-61.
85. Niescier R, Chang K, Min K-T. Miro, MCU, and calcium: bridging our understanding of mitochondrial movement in axons. Frontiers in Cellular Neuroscience. 2013;7.
86. Forkink M, Manjeri GR, Liemburg-Apers DC, Nibbeling E, Blanchard M, Wojtala A, Smeitink JAM, Wieckowski MR, Willems PHGM, Koopman WJH. Mitochondrial hyperpolarization during chronic complex I inhibition is sustained by low activity of complex II, III, IV and V. Biochimica et Biophysica Acta (BBA) - Bioenergetics. 2014;1837(8):1247-56.

87. Abramov AY, Smulders-Srinivasan TK, Kirby DM, Acin-Perez R, Enriquez JA, Lightowlers RN, Duchen MR, Turnbull DM. Mechanism of neurodegeneration of neurons with mitochondrial DNA mutations. Brain : a journal of neurology. 2010;133(Pt 3):797-807.
88. Bouron A. Phyto and endocannabinoids exert complex actions on calcium and zinc signaling in mouse cortical neurons. Biochemical pharmacology. 2018;152:244-51.
89. Radbruch H, Bremer D, Mothes R, Günther R, Rinnenthal JL, Pohlan J, Ulbricht C, Hauser AE, Niesner R. Intravital FRET: Probing Cellular and Tissue Function in Vivo. International journal of molecular sciences [Internet]. 2015; 16(5):[11713-27 pp.].
90. Rahman S, Rahman T. Unveiling some FDA-approved drugs as inhibitors of the store-operated Ca2+ entry pathway. Scientific Reports. 2017;7(1):12881.
91. Mothes R, Ulbricht C, Leben R, Günther R, Hauser AE, Radbruch H, Niesner R. Teriflunomide Does Not Change Dynamics of Nadph Oxidase Activation and Neuronal Dysfunction During Neuroinflammation. Frontiers in Molecular Biosciences. 2020;7.
92. Lein PJ, Barnhart CD, Pessah IN. Acute hippocampal slice preparation and hippocampal slice cultures. Methods in molecular biology (Clifton, NJ). 2011;758:115-34.
93. Anderhalten L, Silva RV, Morr A, Wang S, Smorodchenko A, Saatz J, Traub H, Mueller S, Boehm-Sturm P, Rodriguez-Sillke Y, Kunkel D, Hahndorf J, Paul F, Taupitz M, Sack I, Infante-Duarte C. Different Impact of Gadopentetate and Gadobutrol on Inflammation-Promoted Retention and Toxicity of Gadolinium Within the Mouse Brain. Investigative radiology. 2022;57(10):677-88.
94. Russell WMS, Burch RL. The principles of humane experimental technique: Methuen; 1959.
95. Miller SD, Karpus WJ. Experimental autoimmune encephalomyelitis in the mouse. Current protocols in immunology. 2007;Chapter 15:15.1.1-.1.8.
96. Constantinescu CS, Farooqi N, O'Brien K, Gran B. Experimental autoimmune encephalomyelitis (EAE) as a model for multiple sclerosis (MS). British journal of pharmacology. 2011;164(4):1079-106.
97. Glatigny S, Bettelli E. Experimental Autoimmune Encephalomyelitis (EAE) as Animal Models of Multiple Sclerosis (MS). Cold Spring Harbor perspectives in medicine. 2018;8(11).
98. Procaccini C, De Rosa V, Pucino V, Formisano L, Matarese G. Animal models of Multiple Sclerosis. European journal of pharmacology. 2015;759:182-91.
99. Gerhauser I, Hansmann F, Ciurkiewicz M, Löscher W, Beineke A. Facets of Theiler's Murine Encephalomyelitis Virus-Induced Diseases: An Update. International journal of molecular sciences. 2019;20(2).
100. Misgeld T, Kerschensteiner M, Bareyre FM, Burgess RW, Lichtman JW. Imaging axonal transport of mitochondria in vivo. Nature methods. 2007;4(7):559-61.
101. Heemels MT. Neurodegenerative diseases. Nature. 2016;539(7628):179.
102. Durães F, Pinto M, Sousa E. Old Drugs as New Treatments for Neurodegenerative Diseases. Pharmaceuticals. 2018;11(2):44.
103. Doan TL, Pollastri M, Walters MA, Georg GI. Chapter 23 - The Future of Drug Repositioning: Old Drugs, New Opportunities. In: Macor JE, editor. Annual Reports in Medicinal Chemistry. 46: Academic Press; 2011. p. 385-401.
104. Bagheri S, Haddadi R, Saki S, Kourosh-Arami M, Komaki A. The effect of sodium channels on neurological/neuronal disorders: A systematic review. International Journal of Developmental Neuroscience. 2021;81(8):669-85.
105. Bezprozvanny I. Calcium hypothesis of neurodegeneration - An update. Biochemical and biophysical research communications. 2019;520(4):667-9.

Statutory Declaration

“I, Rebecca Ludwig (geb. Ulshöfer), by personally signing this document in lieu of an oath, hereby affirm that I prepared the submitted dissertation on the topic “Ex vivo investigation of mechanisms to prevent oxidatively induced alterations in axonal mitochondria in murine nervous system models” (Ex-vivo-Untersuchung von Mechanismen zur Prävention oxidativ induzierter Veränderungen in axonalen Mitochondrien in Nervensystem-Modellen von Mäusen), independently and without the support of third parties, and that I used no other sources and aids than those stated.
All parts which are based on the publications or presentations of other authors, either in letter or in spirit, are specified as such in accordance with the citing guidelines. The sections on methodology (in particular regarding practical work, laboratory regulations, statistical processing) and results (in particular regarding figures, charts and tables) are exclusively my responsibility.

Furthermore, I declare that I have correctly marked all of the data, the analyses, and the conclusions generated from data obtained in collaboration with other persons, and that I have correctly marked my own contribution and the contributions of other persons (cf. declaration of contribution). I have correctly marked all texts or parts of texts that were generated in collaboration with other persons.

My contributions to any publications to this dissertation correspond to those stated in the below joint declaration made together with the supervisor. All publications created within the scope of the dissertation comply with the guidelines of the ICMJE (International Committee of Medical Journal Editors; http://www.icmje.org) on authorship. In addition, I declare that I shall comply with the regulations of Charité-Universitätsmedizin Berlin on ensuring good scientific practice.

I declare that I have not yet submitted this dissertation in identical or similar form to another Faculty.

The significance of this statutory declaration and the consequences of a false statutory declaration under criminal law (Sections 156, 161 of the German Criminal Code) are known to me.”

Date Signature

Declaration of your own contribution to the publications

Rebecca Ludwig (geb. Ulshöfer) contributed the following to the below listed publications:

Publication 1: **Ulshöfer R**, Bros H, Hauser AE, Niesner RA, Paul F, Malla B, Infante-Duarte C. **Preventing Axonal Sodium Overload or Mitochondrial Calcium Uptake Protects Axonal Mitochondria from Oxidative Stress-Induced Alterations.** Oxid Med Cell Longev. 2022 May 24. (Impact factor: 7.310)
Contribution: Rebecca Ludwig (geb. Ulshöfer) designed the study under supervision of BM and CID and performed all the experiments, image analysis and statistical analysis except the morphology and motility experiments with TTX which were done by BM. She created all the figures and tables, only figures 1 and 2 (and related tables) contained data from experiments performed by BM. Additionally, she interpreted the data, wrote the manuscript in agreement with all co-authors, and responded to the reviewers' comments during the revision process.

Publication 2: Malla B, Liotta A, Bros H, **Ulshöfer R**, Paul F, Hauser AE, Niesner R, Infante-Duarte C. **Teriflunomide Preserves Neuronal Activity and Protects Mitochondria in Brain Slices Exposed to Oxidative Stress.** Int J Mol Sci. 2022 Jan 28. (Impact factor: 5.314)
Contribution: Rebecca Ludwig (geb. Ulshöfer) established the ATP assay in acute hippocampal slices and the related statistical analysis together with BM and thereby specifically contributed to Figure 4. She was involved in interpretation of all the given data and in the writing and revision process of the publication.

Publication 3: Malla B, Cotten S, **Ulshoefer R**, Paul F, Hauser AE, Niesner R, Bros H, Infante-Duarte C. **Teriflunomide preserves peripheral nerve mitochondria from oxidative stress-mediated alterations.** Ther Adv Chronic Dis. 2020 Aug 11. (Impact factor: 4.970)
Contribution: Rebecca Ludwig (geb. Ulshöfer) was involved in analysis and interpretation of results in figure 1-4 (mitochondrial morphology and motility). She created figure 4. Moreover, she was involved in the writing and revision process of the publication.

_____

Signature, date and stamp of first supervising university professor / lecturer

_____

Signature of doctoral candidate

Excerpt from Journal Summary List

Publication 1: **Ulshöfer R**, Bros H, Hauser AE, Niesner RA, Paul F, Malla B, Infante-Duarte C. **Preventing Axonal Sodium Overload or Mitochondrial Calcium Uptake Protects Axonal Mitochondria from Oxidative Stress-Induced Alterations.** Oxid Med Cell Longev. 2022 May 24. (Impact factor: 7.310)

Publication 2: Malla B, Liotta A, Bros H, **Ulshöfer R**, Paul F, Hauser AE, Niesner R, Infante-Duarte C. **Teriflunomide Preserves Neuronal Activity and Protects Mitochondria in Brain Slices Exposed to Oxidative Stress.** Int J Mol Sci. 2022 Jan 28. (Impact factor: 5.314)

Publication 3: Malla B, Cotten S, **Ulshoefer R**, Paul F, Hauser AE, Niesner R, Bros H, Infante-Duarte C. **Teriflunomide preserves peripheral nerve mitochondria from oxidative stress-mediated alterations.** Ther Adv Chronic Dis. 2020 Aug 11. (Impact factor: 4.970)

Printing copies of the publications

Journal Data Filtered By: **Selected JCR Year: 2021** Selected Editions: SCIE,SSCI
Selected Categories: **"CELL BIOLOGY"** Selected Category Scheme: WoS
Gesamtanzahl: 194 Journale

Rank	Full Journal Title	Total Cites	Journal Impact Factor	Eigenfaktor
1	NATURE REVIEWS MOLECULAR CELL BIOLOGY	66,072	113.915	0.07790
2	NATURE MEDICINE	141,857	87.241	0.23255
3	CELL	362,236	66.850	0.53397
4	CELL RESEARCH	29,215	46.297	0.04003
5	CANCER CELL	57,294	38.585	0.07359
6	Signal Transduction and Targeted Therapy	11,026	38.104	0.01781
7	Cell Discovery	5,318	38.079	0.01319
8	Cell Metabolism	61,067	31.373	0.08630
9	NATURE CELL BIOLOGY	55,078	28.213	0.06043
10	Cell Stem Cell	35,867	25.269	0.05806
11	TRENDS IN CELL BIOLOGY	20,498	21.167	0.02577
12	MOLECULAR CELL	94,258	19.328	0.13937
13	Science Translational Medicine	52,639	19.319	0.09144
14	NATURE STRUCTURAL & MOLECULAR BIOLOGY	33,999	18.361	0.04689
15	CYTOKINE & GROWTH FACTOR REVIEWS	9,002	17.660	0.00625
16	Journal of Extracellular Vesicles	11,679	17.337	0.01126
17	Cell Reports Medicine	2,183	16.988	0.00524
18	Protein & Cell	6,830	15.328	0.00937
19	TRENDS IN MOLECULAR MEDICINE	14,585	15.272	0.01381
20	EMBO JOURNAL	80,536	14.012	0.05438

Rank	Full Journal Title	Total Cites	Journal Impact Factor	Eigenfaktor
21	DEVELOPMENTAL CELL	38,913	13.417	0.05064
22	Autophagy	28,964	13.391	0.02766
23	GENES & DEVELOPMENT	64,203	12.890	0.03851
24	JOURNAL OF BIOMEDICAL SCIENCE	8,671	12.771	0.00912
25	PLANT CELL	67,319	12.085	0.02964
26	CELL DEATH AND DIFFERENTIATION	31,035	12.067	0.02639
27	Annual Review of Cell and Developmental Biology	12,402	11.902	0.00834
28	AGEING RESEARCH REVIEWS	12,789	11.788	0.01368
29	Cell Systems	8,047	11.091	0.03332
30	AGING CELL	16,926	11.005	0.01890
31	CURRENT BIOLOGY	85,124	10.900	0.10641
32	MATRIX BIOLOGY	9,415	10.447	0.00856
33	Cell Reports	91,103	9.995	0.23082
34	Cold Spring Harbor Perspectives in Biology	26,240	9.708	0.02204
35	Cell Death & Disease	52,674	9.685	0.06578
36	Science Signaling	17,426	9.517	0.02046
37	Wiley Interdisciplinary Reviews-RNA	4,502	9.349	0.00773
38	CELLULAR AND MOLECULAR LIFE SCIENCES	38,745	9.207	0.03204
39	EMBO REPORTS	21,705	9.071	0.02695
40	HLA	1,819	8.762	0.00190
41	ONCOGENE	81,646	8.756	0.05014
42	CELL PROLIFERATION	7,299	8.755	0.00706

Selected JCR Year: 2021; Selected Categories: "CELL BIOLOGY"

Rank	Full Journal Title	Total Cites	Journal Impact Factor	Eigenfaktor
43	CELLULAR & MOLECULAR BIOLOGY LETTERS	2,684	8.702	0.00250
44	CURRENT OPINION IN CELL BIOLOGY	16,077	8.386	0.01479
45	Journal of Molecular Cell Biology	3,664	8.185	0.00506
46	Stem Cell Research & Therapy	19,072	8.079	0.01980
47	JOURNAL OF CELL BIOLOGY	76,617	8.077	0.04412
48	CURRENT OPINION IN STRUCTURAL BIOLOGY	13,407	7.786	0.01689
49	HISTOPATHOLOGY	14,098	7.778	0.01493
50	AMERICAN JOURNAL OF RESPIRATORY CELL AND MOLECULAR BIOLOGY	16,259	7.748	0.01386
51	Cells	40,461	7.666	0.06054
52	Cell Communication and Signaling	6,412	7.525	0.00736
53	SEMINARS IN CELL & DEVELOPMENTAL BIOLOGY	15,850	7.499	0.01742
54	Tissue Engineering Part B-Reviews	5,132	7.376	0.00285
55	Oxidative Medicine and Cellular Longevity	37,850	7.310	0.03931
56	Stem Cell Reports	12,127	7.294	0.02370
57	Cell Death Discovery	3,965	7.109	0.00619
58	CELLULAR ONCOLOGY	3,031	7.051	0.00296
59	INFLAMMATION RESEARCH	6,771	6.986	0.00491
60	CELL BIOLOGY AND TOXICOLOGY	2,678	6.819	0.00176
61	Stem Cell Reviews and Reports	4,340	6.692	0.00391
62	JOURNAL OF CELLULAR PHYSIOLOGY	45,492	6.513	0.04482
63	International Review of Cell and Molecular Biology	3,388	6.420	0.00314

Selected JCR Year: 2021; Selected Categories: "CELL BIOLOGY"

Hindawi
Oxidative Medicine and Cellular Longevity
Volume 2022, Article ID 6125711, 13 pages
https://doi.org/10.1155/2022/6125711

Research Article

Preventing Axonal Sodium Overload or Mitochondrial Calcium Uptake Protects Axonal Mitochondria from Oxidative Stress-Induced Alterations

Rebecca Ulshöfer,[1,2,3] Helena Bros,[4] Anja Erika Hauser,[5,6] Raluca Aura Niesner,[6,7] Friedemann Paul,[1,2,3,8] Bimala Malla,[2] and Carmen Infante-Duarte[1,2,3]

[1]*Experimental and Clinical Research Center (ECRC), A Cooperation between Charité-Universitätsmedizin Berlin and Max-Delbrück-Center for Molecular Medicine, 13125 Berlin, Germany*
[2]*Charité-Universitätsmedizin Berlin, Corporate Member of Freie Universität Berlin, Humboldt Universität zu Berlin and Berlin Institute of Health, 10117 Berlin, Germany*
[3]*Max-Delbrück-Center for Molecular Medicine (MDC) in the Helmholtz Association, 13125 Berlin, Germany*
[4]*Charité-Universitätsmedizin Berlin, Institute for Medical Immunology, Augustenburger Platz 1, 13353 Berlin, Germany*
[5]*Charité-Universitätsmedizin Berlin, Medizinische Klinik mit Schwerpunkt Rheumatologie und Klinische Immunologie, Charité Platz 1, 10117 Berlin, Germany*
[6]*Deutsches Rheuma-Forschungszentrum, a Leibniz Institute, Charité Platz 1, 10117 Berlin, Germany*
[7]*Dynamic and Functional In Vivo Imaging, Veterinary Medicine, Freie Universität Berlin, Germany*
[8]*Charité-Universitätsmedizin Berlin, NeuroCure Clinical Research Center, Charité Platz 1, 10117 Berlin, Germany*

Correspondence should be addressed to Carmen Infante-Duarte; carmen.infante@charite.de

Bimala Malla and Carmen Infante-Duarte contributed equally to this work.

Received 23 June 2021; Revised 2 May 2022; Accepted 5 May 2022; Published 24 May 2022

Academic Editor: Luzia Kalyne Almeida Moreira Leal

In neuroinflammatory and neurodegenerative disorders such as multiple sclerosis, mitochondrial damage caused by oxidative stress is believed to contribute to neuroaxonal damage. Previously, we demonstrated that exposure to hydrogen peroxide (H_2O_2) alters mitochondrial morphology and motility in myelinated axons and that these changes initiate at the nodes of Ranvier, where numerous sodium channels are located. Therefore, we suggested that mitochondrial damage may lead to ATP deficit, thereby affecting the efficiency of the sodium-potassium ATPase and eventually leading to sodium overload in axons. The increased intra-axonal sodium may revert the axonal sodium-calcium exchangers and thus may lead to a pathological calcium overload in the axoplasm and mitochondria. Here, we used the explanted murine ventral spinal roots to investigate whether modulation of sodium or calcium influx may prevent mitochondrial alterations in myelinated axons during exogenous application of H_2O_2 inducing oxidative stress. For that, tetrodotoxin, an inhibitor of voltage-gated sodium ion channels, and ruthenium 360, an inhibitor of the mitochondrial calcium uniporter, were applied simultaneously with hydrogen peroxide to axons. Mitochondrial shape and motility were analyzed. We showed that inhibition of axonal sodium influx prevented oxidative stress-induced morphological changes (i.e., increase in circularity and area and decrease in length) and preserved mitochondrial membrane potential, which is crucial for ATP production. Blocking mitochondrial calcium uptake prevented decrease in mitochondrial motility and also preserved membrane potential. Our findings indicate that alterations of both mitochondrial morphology and motility in the contexts of oxidative stress can be counterbalanced by modulating intramitochondrial ion concentrations pharmacologically. Moreover, motile mitochondria show preserved membrane potentials, pointing to a dose association between mitochondrial motility and functionality.

1. Introduction

Multiple sclerosis (MS) is a chronic inflammatory disease of the central nervous system (CNS) that affects approximately 2.5 million people worldwide [1]. The pathological hallmarks of MS include inflammation, demyelination, and neurodegeneration; however, its pathogenesis and the relationship between those three aspects are not completely understood [1].

In this context, mitochondria have emerged as one of the key players that are affected by inflammation and contribute to neuroaxonal loss [2–4]. During neuroinflammatory events in MS, activated CNS-invading leukocytes, as well as microglia, are potential sources of reactive oxygen species (ROS), mainly via increased activation of nicotinamide adenine dinucleotide phosphate (NADPH) oxidases [5–8]. It is assumed that excessive ROS production may lead to oxidative stress and consequently to the inhibition of adenosine triphosphate (ATP) production. Activation of oxidative phosphorylation under pathological stress conditions may also lead to increased chances of electron slippage to oxygen and the formation of additional detrimental ROS [9–11]. In a physiological state, cells have mechanisms to cope with increased ROS production [12, 13]. However, sustained inflammation and oxidative stress may lead to irreversible damage in mitochondria and affect the survivability of the cells [14].

To investigate the impact of oxidative stress on neuroaxonal mitochondria, we have developed an ex vivo model to monitor mitochondrial alterations in murine spinal roots [15, 16]. We focused on ventral spinal roots because they consist predominantly of efferent motor axons and are thicker than dorsal roots making them easier to handle. Using this model, we previously showed that oxidative stress alters both mitochondrial morphology (increases mitochondrial circularity and decreases mitochondrial area and length) and mitochondrial motility (reduces the percentage of moving mitochondria, length of their trajectories and their velocity) [17]. We also observed that, following an oxidative insult, all these alterations consistently initiate at the nodes of Ranvier [17].

In axons, voltage-gated sodium channels (NaV) are mainly located near the nodes of Ranvier [18]. In the presence of oxidative stress, mitochondrial damage may lead to reduced ATP generation [19] and the consequent failure of the sodium-potassium-ATPase (Na^+/K^+-ATPase), leading to sodium (Na^+) accumulation inside the axons [20]. Moreover, in a degeneration paradigm using dorsal root ganglion cells, it has been demonstrated that influx of Na^+ via NaV contributes to intraneuronal Na^+ accumulation [13]. To compensate for the excess of intracellular Na^+ in the presence of a dysfunctional Na^+/K^+-ATPase, the axonal sodium-calcium exchanger (NCX) may start acting in a reverse mode, causing axonal calcium (Ca^{2+}) overload [5, 13, 20].

High cytosolic Ca^{2+} concentration directly impacts mitochondria, which in turn are part of the Ca^{2+} buffering system of cells [13, 21, 22]. Tightly regulated intracellular Ca^{2+} homeostasis is crucial because an excessive mitochondrial Ca^{2+} uptake may lead to the opening of the permeability transition pore (PTP), resulting in apoptosis [9, 14]. A mitochondrial Ca^{2+} uniporter (MCU) transports Ca^{2+} into the mitochondrial matrix [19]. It has been shown that overexpression of MCU and subsequent mitochondrial Ca^{2+} overload results in neuronal death, both *in vitro* and *in vivo* [23]. Moreover, mitochondria are linked to motor proteins via Miro-1/2, which have Ca^{2+}-sensing structures, suggesting that mitochondrial motility is also Ca^{2+}-sensitive [18]. Although during physiological state, a slight increase in mitochondrial Ca^{2+} appears to directly stimulate mitochondrial ATP production by activating Ca^{2+}-sensitive enzymes of Krebs' Cycle [21], high levels of Ca^{2+} may lead to the suppression of mitochondrial movement [20].

In neuroinflammation, the assumption that alteration of ion concentrations and neuronal damage are connected is supported by the beneficial effects of ion channel blockers reported in experimental autoimmune encephalitis (EAE), where blocking NaV or voltage-gated Ca^{2+} channels attenuates the disease course [13, 24]. Hence, we hypothesized that the abnormal activity of ion channels at the nodes of Ranvier following oxidative stress may cause the observed mitochondrial alterations [5, 13, 24].

Thus, we investigated here if preventing Na^+ overload within axons and Ca^{2+} overload within mitochondria using the NaV blocker tetrodotoxin (TTX) and the MCU inhibitor ruthenium 360 (Ru360), respectively, would protect both mitochondria and axons from oxidative-stress mediated damage.

2. Material and Methods

2.1. Ethics Statement. All experimental procedures were approved by the regional animal study committee of Berlin (Landesamt für Gesundheit und Soziales Berlin). Animal experiments were conducted in strict accordance with Directive 2010/63/EU of the European Parliament and of the European Council of 22 September 2010. Female and male mice (8-10 weeks old) were used for the experiments. The mice were housed and maintained in a temperature-controlled environment on a 12 h light-dark cycle.

2.2. Preparation and Maintenance of Ventral Spinal Roots. Ventral spinal roots were prepared as described previously [15]. Briefly, C57BL/6 mice were deeply anesthetized with isoflurane before cervical dislocation. After separating the connective tissue, the dorsal side of the spinal cord was exposed, and the vertebrae were cut laterally from rostral to caudal. The spinal cord was sectioned at the thoracic level and the ventral spinal roots were cut distal to the spinal cord. Together with the attached spinal roots, the explanted spinal cord was then placed into artificial cerebrospinal fluid (aCSF), saturated with carbogen (95% O_2 and 5% CO_2), and adjusted to a pH of 7.3-7.4. Under a dissecting microscope, the lumbar ventral roots were finally selected and separated from the spinal cord. Explanted ventral roots were maintained in aCSF, containing the following solutions: Solution I – 124 mM NaCl, 1.25 mM NaH_2PO_4, 10.0 mM Glucose, 1.8 mM $MgSO_4$, 1.6 mM $CaCl_2$, 3.00 mM KCl;

Solution II – 26.0 mM $NaHCO_3$. Both solutions were mixed immediately before use.

2.3. Induction of Oxidative Stress and Treatment Groups. All experiments were conducted in a submerged incubation chamber (Brain Slice Keeper-BSK 6 Scientific Systems Design Inc., Ontario, Canada), allowing up to five different treatment conditions and continuous carbogen perfusion of each submersion well throughout the entire process. Although the BSK 6 has 6 individual tubes to supply gas to each of the six wells, one tube had to be used to carbogenate the aCSF stock and therefore only 5 wells were available for the experiments.

To assess the effect of TTX and Ru360 on mitochondrial alterations induced by oxidative stress, we assigned spinal roots randomly to the following experimental groups: a) Negative controls of TTX experiments consisted of axons incubated with aCSF for 30 min at room temperature (RT). Negative controls of Ru360 experiments consisted of axons incubated with the corresponding solvent dimethyl sulfoxide (DMSO) at 1 μl/ml (0,001%) for 30 min at RT. This concentration corresponded to the one used to solve Ru360. DMSO does not exert an effect on investigated mitochondrial parameters (data not shown). We also refer to the negative groups as "untreated groups". b) In the oxidatively-stressed control group, ventral spinal roots were incubated with 100 μM H_2O_2 for 30 min at RT along with the corresponding vehicle (aCSF for TTX experiments, DMSO for Ru360 experiments). We also refer to this group as "positive control". c) Effects of blocking NaV channels on spinal roots were investigated by incubating the spinal roots with 100 nM or 1 μM TTX along with 100 μM H_2O_2. d) Effects of blocking mitochondrial Ca^{2+} influx were determined by incubation with 5, 10, or 20 μM Ru360 along with 100 μM H_2O_2.

2.4. Labeling of Mitochondria, Microscopy, and Analysis of Mitochondrial Dynamics (Morphology and Motility). After incubation with the treatments, transected ventral spinal roots were washed and transferred into aCSF containing 100 nM MitoTracker® Orange CMTMRos (Life Technologies, Darmstadt, Germany) dissolved in DMSO for 30 min at RT and then washed again with fresh aCSF.

Microscopy and imaging analysis of the ventral spinal roots were performed as previously described [15]. For microscopy, spinal roots were placed on a glass coverslip and transferred to an imaging chamber containing carbogenated aCSF. A custom-built nylon net was placed on top of the spinal roots to prevent them from moving during image acquisition. For all experiments, an inverted laser-scanning confocal microscope adapted for live-cell imaging was used. Experiments with Na^+ channel blockade were imaged with an LSM 710 (Carl Zeiss, Jena, Germany). Experiments with Ca^{2+} channel blockade were conducted using a Nikon Scanning Confocal A1Rsi+. MitoTracker® Orange was excited at 561 nm with a diode-pumped solid-state (DPSS) laser. Visualization of mitochondria was performed through a 100x (LSM 710, Carl Zeiss) or 60x (Nikon Scanning Confocal A1Rsi+) oil immersion objective. Regions of interest (ROI) were chosen based on the following criteria: 1) clearly visible node of Ranvier 2) well-labeled mitochondria 3) axon with intact myelin sheath and no signs of membrane disruption in regions adjacent to the selected ROI 4) areas at least 2 mm away from the end of the roots. Scrutinizing the spinal roots from the proximal to the distal end, three separate ROI were chosen. For each ROI, a time-lapse (60-second duration, 2 s/frame) with a resolution of 512x512 pixels was recorded. Exposure time and laser power were reduced to minimize photobleaching and phototoxicity.

The first frame of every time-lapse video was used to assess mitochondrial morphology with an automated analysis tool of the Volocity®6.3 software (Perkin Elmer, Rodgau, Germany). To determine the changes in mitochondrial morphology, the following parameters were analyzed: shape factor (4πX [Area/Perimeter^2]), a measure of circularity ranging from 0 to 1, in which "1" indicates a perfect circle, length (μm) and area (μm^2) of an individual mitochondrion. To assess motility, mitochondria were tracked manually using Volocity®6.3 software (Perkin Elmer, Rodgau, Germany). Any mitochondrion with a displacement of $\geq$1 μm was considered "mobile". For experiments with Ru360, mobile mitochondria were further analyzed for track length (μm), the measure of the real distance traveled by a mitochondrion, and velocity (μm/s).

Under physiological and pathological conditions, mitochondrial populations display high heterogeneity within one cell due to their adaption to different energetic states. Thus, to minimize selection bias, large amounts of mitochondria in different axons of several experiments were analyzed and matched.

2.5. Assessment of Mitochondrial Membrane Potential. To determine mitochondrial membrane potential, spinal roots were stained with 20 μg/ml 5,5′,6,6′-tetrachloro-1,1′,3,3′-tetraethylbenzimidazolylcarbocyanine iodide (JC-1; Life Technologies, Darmstadt, Germany) in aCSF at RT for 1 h. JC-1 accumulates in mitochondria with intact membrane potential and negative charge. Sufficient accumulation due to unaltered mitochondrial membrane potential leads to the formation of J aggregates and a shift in emitted fluorescence from green (529 nm) to red (590 nm) [25]. To minimize background noise, roots were washed with fresh aCSF before imaging. JC-1 was excited with dual illumination with argon (514 nm) and DPSS (561 nm) lasers.

Red/green fluorescence ratio of JC-1 stained mitochondria determined at a Nikon Scanning Confocal A1Rsi+microscope was used for the analysis of mitochondrial membrane potential. Results of the red/green fluorescence ratio of individual mitochondrion were normalized to the average red/green fluorescence ratio of the untreated group as established by others [26].

2.6. Statistical Analysis. Acquired data were analyzed with Prism 8 Software (GraphPad, CA, USA). All datasets were first subjected to D'Agostino and Pearson omnibus K2 normality test and Shapiro-Wilk normality test for Gaussian distribution. Data fitting the criteria for normal distribution were subsequently analyzed using a one-way ANOVA with

Bonferroni's post hoc test. Data following a non-parametric distribution were analyzed using a Kruskal-Wallis test followed by a Dunn's post hoc multiple comparisons test. p values ≤ 0.05 were considered significant. The significance of the data was further depicted as $*$ implying $p \leq 0.05$, $**$ implying $p \leq 0.01$, $***$ implying $p \leq 0.001$, and $****$ implying $p \leq 0.0001$. All data are shown in mean ± SEM.

3. Results

3.1. Blocking Axonal Na^+ Influx Prevents Oxidative Stress-Induced Morphological Changes in Mitochondria. To investigate the effect of Na^+ channel blockade on mitochondrial morphology, the explanted ventral spinal roots were treated with 100 μM H_2O_2 alone, or 100 μM H_2O_2 along with different concentrations of TTX (100 nM or 1 μM). Explants were then imaged using a confocal microscope (Figure 1(a)). Shape factor (Figure 1(b)), mitochondrial length (Figure 1(c)), and mitochondrial area (Figure 1(d)) were analyzed.

During oxidative stress, mitochondrial shape factor (untreated: 0.4148 ± 0.0060; H_2O_2: 0.4854 ± 0.0074) and area (untreated: 0.4043 ± 0.0124 μm^2; H_2O_2: 0.7557 ± 0.0335 μm^2) increased while mitochondrial length decreased (untreated: 1.684 ± 0.0375 μm; H_2O_2: 1.5800 ± 0.0431 μm; Figures 1(b) and 1(c)). All observed morphological changes induced by oxidative stress were prevented with 100 nM of TTX (shape factor = 0.4202 ± 0.0079; length = 1.8990 ± 0.0702 μm; area = 0.5247 ± 0.0268 μm^2; Figures 1(b)–1(d)). In contrast, 1 μM of TTX did not affect the H_2O_2-induced increase in shape factor (0.5030 ± 0.0072; Figure 1(b)), but significantly reduced length (1.4400 ± 0.0362 μm, Figure 1(c)) and increased mitochondrial area in comparison to oxidative stress conditions (1.0150 ± 0.0377 μm^2; Figure 1(d)).

3.2. Blocking Axonal Na^+ Influx Prevents Oxidative Stress-Induced Changes of Mitochondria Motility. Next, we performed time-lapse imaging and analyzed mitochondrial motility parameters under the above-mentioned experimental conditions (Figure 2(a)). We analyzed the percentage of manually tracked motile mitochondria (Figure 2(b)). The untreated group with aCSF alone showed an average percentage of motile mitochondria of about 16% (15.890 ± 1.395%), while in the presence of 100 μM H_2O_2 only around 5% (5.044 ± 1.228%) of mitochondria were motile (Figure 2(b)). Blocking Na^+ influx with 1 μM TTX prevented the oxidative stress-induced reduction of motile mitochondria (11.460 ± 1.826%; Figure 2(b)). The effect of 100 nM TTX was not significant compared to the H_2O_2-treated group (Figure 2(b)).

3.3. Blocking Mitochondrial Ca^{2+} Uptake Prevents Oxidative Stress-Induced Alterations of Mitochondrial Length. Then, we examined the influence of mitochondrial Ca^{2+} on mitochondrial morphology. Oxidative stress was induced again with 100 μM H_2O_2. Blocking mitochondrial Ca^{2+} influx via mitochondrial Ca^{2+} uniporter channels was performed by simultaneous incubation of mitochondria with H_2O_2 and 5, 10, or 20 μM Ru360. We observed that H_2O_2 led to a decrease in mitochondrial length (untreated: 1.9260 ± 0.0343 μm; H_2O_2: 1.6920 ± 0.0302 μm) and area (untreated: 1.0890 ± 0.0292 μm^2; H_2O_2: 0.9756 ± 0.0268 μm^2) compared to the untreated group (Figures 3(c) and 3(d)). However, shape factor did not increase under H_2O_2-treatment (untreated: 0.4703 ± 0.0072; H_2O_2: 0.4841 ± 0.0071) when compared to the untreated group (Figure 3(b)). Blocking mitochondrial Ca^{2+} influx with 5 μM Ru360 prevented changes in shape factor (0.4474 ± 0.0090, Figure 3(b)). A similar trend was observed in roots treated with 10 μM Ru360 (0.4741 ± 0.0083; Figure 3(b)). However, at 20 μM, Ru360 induced an even more pronounced increase in shape factor values (0.5214 ± 0.0095) when compared to the H_2O_2-treated group (Figure 3(b)). Incubation with 5 μM Ru360 did not increase mitochondrial length compared to the H_2O_2-treated group (1.881 ± 0.0426 μm, Figure 3(c)). In the presence of 10 μM Ru360, mitochondrial length increased (1.7780 ± 0.0390 μm; Figure 3(c)), while at 20 μM Ru360 promoted decrease in mitochondrial length compared to treatment with oxidative stress alone (Figure 3(c)). Regarding area, we did not observe significant alterations in either of the treatment groups (Figure 3(d)).

3.4. Blocking Mitochondrial Ca^{2+} Uptake Prevents Reduction of Mitochondrial Motility in Stressed Axons. To investigate the effect of blocking MCU on oxidative stress-induced alterations in mitochondrial motility, we incubated explanted ventral spinal roots with DMSO alone, DMSO plus 100 μM H_2O_2, or with 100 μM H_2O_2 along with three different concentrations (5, 10 or 20 μM) of Ru360 (Figure 4(a)).

In the untreated group, we observed an average of 7% (7.103% ± 0.997) of moving mitochondria (Figure 4(b)). H_2O_2 at 100 μM caused a significant reduction in motile mitochondria (1.447% ± 0.507) as well as a decrease in track length (untreated: 8.2722 ± 0.8433 μm; H_2O_2-treated: 2.8750 ± 0.6442 μm) and track velocity (untreated: 0.2094 ± 0.0210 μm/s; H_2O_2-treated: 0.1265 ± 0.0320 μm/s) (Figures 4(a)–4(c)). H_2O_2-induced decrease in percentage of motile mitochondria, mitochondrial track length, and track velocity was prevented with 10 μM Ru360 (% of moving mitochondria: 7.393 ± 1.861%; track length: 8.9410 ± 0.7597 μm; track velocity: 0.2293 ± 0.0243 μm/s; Figures 4(a)–4(c)) and 20 μM Ru360 (% of moving mitochondria: 3.549 ± 1.124%; track length: 4.989 ± 0.6025 μm; track velocity: 0.1384 ± 0.0280 μm/s; Figures 4(a)–4(c)). However, in spinal roots treated with 5 μM Ru360, only H_2O_2-induced changes for track length (μm, Figure 4(c)) were prevented. No effects were observed on percentage of moving mitochondria or track velocity ((% of moving mitochondria: 5.205 ± 1.325%; track velocity: 0.1331 ± 0.0235 μm/s, Figures 4(a) and 4(d)).

3.5. Blocking Axonal Na^+ Influx Prevents Oxidative Stress-Induced Reduction of Mitochondrial Membrane Potential. Next, we investigated whether inhibition of axonal Na^+ influx may preserve mitochondrial functionality altered by H_2O_2. Four groups of spinal roots were treated for 30 min

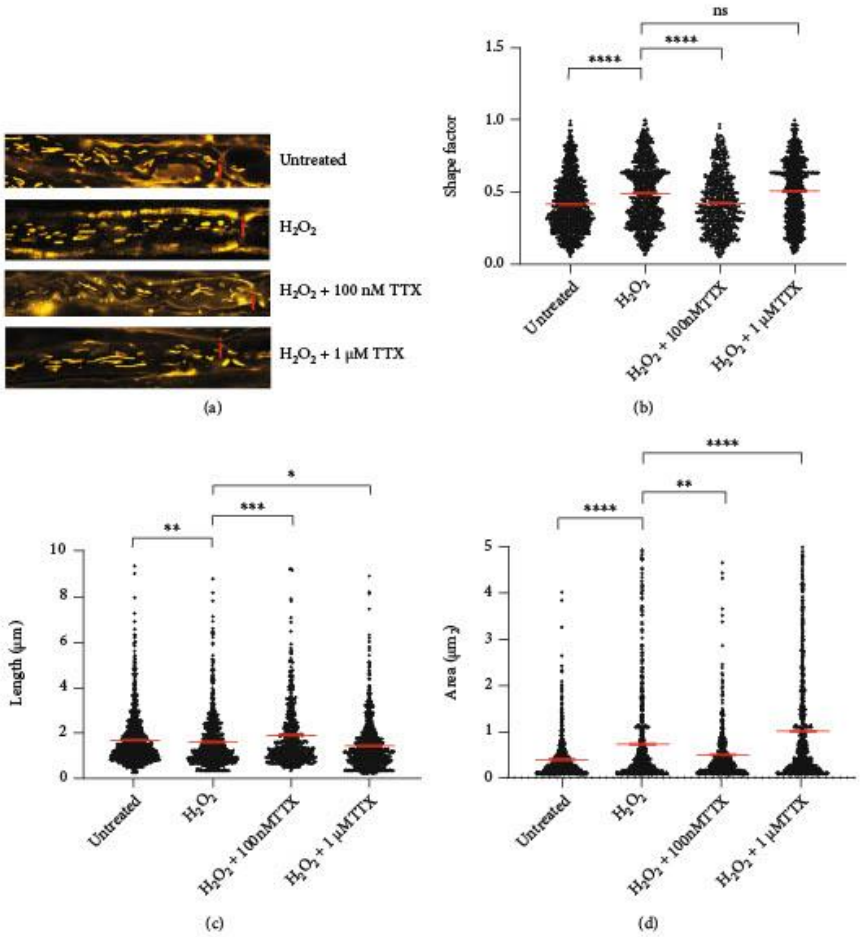

FIGURE 1: Blocking axonal Na^+ influx with tetrodotoxin (TTX) prevents oxidative stress-induced mitochondrial morphology alterations. (a) Representative original images of all different experimental conditions; axons incubated with aCSF alone contained elongated mitochondria; incubation with 100 μM H_2O_2 led to the generation of smaller and rounder mitochondria, and some diffuse MitoTracker® distribution; axon simultaneously incubated with 100 μM H_2O_2 and 100 nM TTX contained elongated mitochondria; axon simultaneously incubated with 100 μM H_2O_2 and 1 μM TTX contained short mitochondria but with increased area. (b–d) Shape factor (b), length (c), and area (d) of mitochondria located near the nodes of Ranvier in axons incubated with the above-mentioned treatments. Nodes of Ranvier are marked with a red "i". $^*p \leq 0.05$, $^{**}p \leq 0.01$, $^{***}p \leq 0.001$, and $^{****}p \leq 0.0001$. The error bars represent the standard error of mean; $n = 6$ animals and 22 roots; untreated 7 roots, H_2O_2 6 roots, H_2O_2+100 nM TTX 4 roots, and H_2O_2+1 μM TTX 5 roots.

with either aCSF alone (vehicle control group), 100 μM H_2O_2, 100 μM H_2O_2+1 μM TTX or 1 μM TTX alone, respectively. Since the incubation chamber permitted the simultaneous assessment of maximally 5 conditions, only the 1 μM TTX concentration, which showed best protecting effects in Figure 2(a), was tested in these experiments. Treated spinal roots were then incubated for 30 min with the ratiometric indicator JC-1. The red/green fluorescence ratio is an indication of the mitochondrial membrane potential and thereby mitochondrial ability to produce ATP (Figure 5(a)).

The application of 100 μM H_2O_2 resulted in a shift to green fluorescence (0.6374 ± 0.0291; Figures 5(a) and 5(b)), as a sign of a loss of mitochondrial membrane potential. 1 μM TTX applied simultaneously with 100 μM H_2O_2 prevented the loss of mitochondrial membrane potential (untreated: 1.0000 ± 0.0297; 1 μM TTX: 1.2410 ± 0.0432; Figures 5(a) and 5(b)). TTX alone led to higher

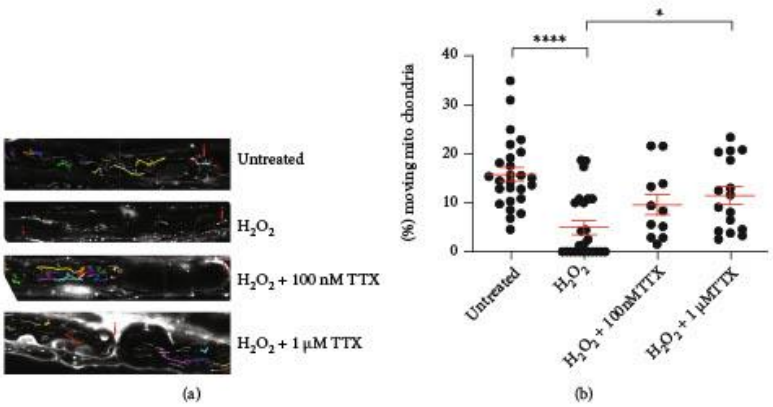

FIGURE 2: Blocking axonal Na^+ influx with TTX barely affects mitochondrial motility parameters altered due to oxidative stress. (a) Representative original images of all different experimental conditions: axon incubated with aCSF alone contained multiple moving mitochondria that c5over larger distances in the axon; 100 μM H_2O_2 induced a strong reduction of motile mitochondria; axons simultaneously incubated with 100 μM H_2O_2 and 100 nM TTX or 1 μM TTX contained more motile mitochondria, covering longer distances. (b) Percentage of moving mitochondria per axon. Nodes of Ranvier are marked with a red "i". $^*p \leq 0.05$, $^{****}p \leq 0.0001$. The error bars represent the standard error of mean; $n = 6$ animals and 22 roots; untreated 7 roots, H_2O_2 6 roots, H_2O_2+100 nM TTX 4 roots, and H_2O_2+1 μM TTX 5 roots.

mitochondrial membrane potential than in the untreated group (TTX: 1.1270 ± 0.0309; Figures 5(a) and 5(b)).

3.6. Blocking Mitochondrial Ca^{2+} Uptake Prevents Oxidative Stress-Induced Reduction of Mitochondrial Membrane Potential. To assess effects of Ca^{2+} uptake on mitochondrial functionality, four groups of spinal roots were treated for 30 min with either DMSO (vehicle control group), DMSO +100 μM H_2O_2, 100 μM H_2O_2+10 μM Ru360 or 10 μM Ru360 alone, respectively. We selected 10 μM Ru360 for these experiments because it was the concentration that showed the best protection against oxidative stress-induced loss of motility (Figure 4(a)). Treated spinal roots were then incubated for 30 min with the ratiometric indicator JC-1. The red/green fluorescence ratio is an indication of the mitochondrial membrane potential and thereby mitochondrial ability to produce ATP (Figure 6(a)).

The application of 100 μM H_2O_2 resulted in a shift to green fluorescence (0.5638 ± 0.0250; Figures 6(a) and 6(b)), as a sign of a severe loss of mitochondrial membrane potential. 10 μM Ru360 applied simultaneously with 100 μM H_2O_2 prevented the loss of mitochondrial membrane potential and restored it to values close to the untreated group (untreated: 1.0000 ± 0.0383; 10 μM Ru360: 0.8507 ± 0.0395; Figures 6(a) and 6(b)). With Ru360 alone, we did not observe any effects on mitochondrial membrane potential in comparison to DMSO treated condition (Figures 6(a) and 6(b)).

4. Discussion

Mitochondrial alterations linked to oxidative stress [9] are reported to occur in the early stages of MS [4, 12] and are believed to contribute to neurodegenerative processes observed in MS patients [2, 27–29]. Therefore, mitochondria have emerged as potential therapeutic targets to limit disease progression [30, 31]. In this study, we investigated using an ex vivo model of peripheral axons [17] whether the effects of oxidative stress on mitochondria can be prevented by targeting pathological ion alterations affecting, in particular, the levels of axonal Na^+ and mitochondrial Ca^{2+}.

In this model, oxidative stress was induced by a 30-minute incubation with 100 μM H_2O_2, a concentration that led to reversible structural and functional alterations in mitochondria [32]. We observed oxidative stress-induced decrease in mitochondrial length (Figures 1(c) and 3(c)) as well as a decrease in the number of motile mitochondria (Figures 2(b) and 4(b)). Additionally, consistent with our previous reports [16, 33] and those of others describing inhibition of axonal transport by oxidative stress [34–36], we observed a decrease in both track length and track velocity of mitochondria exposed to 100 μM H_2O_2 (Figures 4(c) and 4(d)). The observed reduction in mitochondrial length supports previous findings of our group [17] and may be the consequence of an increase in the fission process, which is induced in stressed and damaged mitochondria to get rid of the damaged portion [37].

We also expected that oxidative stress would damage mitochondria and reduce their functionality in our model causing ATP depletion as it has been reported for highly energy-dependent neuronal cells [9, 38]. We showed a decrease in mitochondrial membrane potential under oxidative stress conditions (Figures 5(a), 5(b), 6(a), and 6(b)). As an intact mitochondrial membrane potential is an important determinant for mitochondrial ATP production via oxidative phosphorylation [39], we assumed ATP depletion in oxidatively injured mitochondria. In a novel CNS model established in our lab, we were indeed able to show decreased ATP levels upon oxidative stress induced by

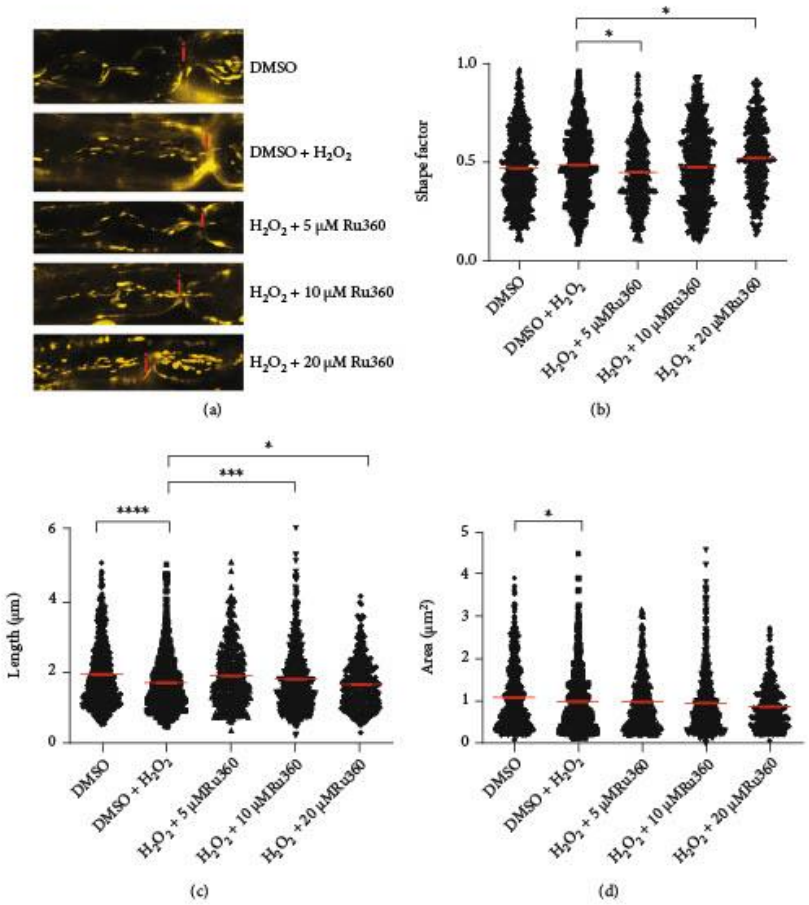

FIGURE 3: Blocking mitochondrial Ca^{2+} influx with Ru360 alters mitochondrial morphology. (a) Representative original images of all different experimental conditions; axon incubated with DMSO alone showed elongated mitochondria; 100 μM H_2O_2 induced shorter and smaller mitochondria; axonal mitochondria exposed to 100 μM H_2O_2 and 5 μM Ru360 showed slightly longer and less round morphology than mitochondria exposed to H_2O_2 alone; incubation with 100 μM H_2O_2 and 10 μM Ru360 led to the formation of longer mitochondria compared with H_2O2 control; axon incubated with 100 μM H_2O_2 and 20 μM Ru360 showed shorter mitochondria than oxidative stress control. (b–d) Mitochondrial shape factor (b), length (c), and area (d) of single mitochondria. Nodes of Ranvier are marked with a red "i". $^*p \leq 0.05$, $^{***}p \leq 0.001$, and $^{****}p \leq 0.0001$. The error bars represent the standard error of mean; $n = 7$ animals and 29 roots; DMSO 7 roots, H_2O_2 7 roots, H_2O_2+5 μM Rui360 4 roots, H_2O_2+10 μM Ru360 7 roots, and H_2O_2+20 μM Ru360 4 roots.

100 μM H_2O_2 [33]. Thus, our paradigm of stressed mitochondria in explanted roots may serve in the future to examine effects of antioxidative interventions on ATP levels.

We previously reported that alterations of mitochondria during oxidative stress initiate at the nodes of Ranvier [17]. NaVs are abundantly present at the nodes of Ranvier and are important for saltatory conduction [40, 41]. In MS lesions, the expression of these channels is reported to be altered [42–44]. In this line, during exposure to H_2O_2, blocking NaV with 100 nM TTX prevented the decrease in length and increase in shape factor and area (Figures 1(a)–1(c)). In contrast, 1 μM TTX along with H_2O_2 led to the generation of short mitochondria that display however large areas (Figures 1(b) and 1(c)). A large mitochondrial area could reflect either detrimental swelling [45, 46] or fusion [1, 35]. We speculate that in the group treated with H_2O_2 and 1 μM TTX, transient mitochondrial fusion followed by fission as reported by Liu et al. [45] may occur. Transient fusion seems to be central for maintaining metabolism and motility [45]. In this line, we observed that 1 μM TTX could

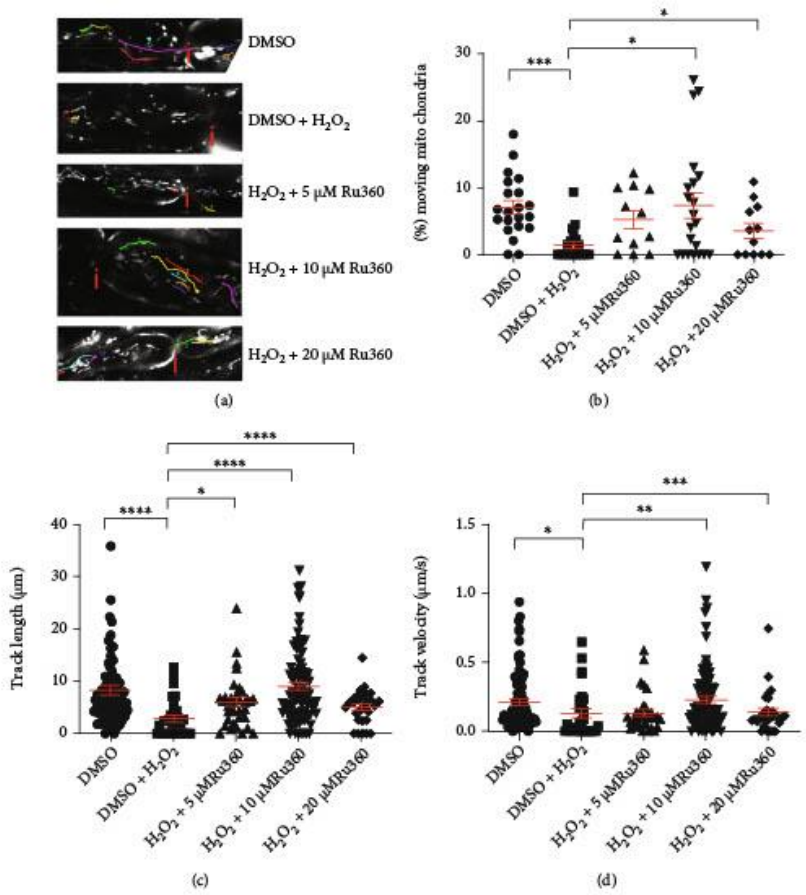

FIGURE 4: Blocking mitochondrial Ca^{2+} uptake with Ru360 prevents oxidative stress-induced loss of mitochondrial motility. (a) Representative original images of all different experimental conditions: axon incubated with DMSO alone contained multiple moving mitochondria that cover larger distances in the axon.; axon incubated with 100 μM H_2O_2, showed few motile mitochondria with short track length; simultaneous incubation with 100 μM H_2O_2 and 5 or 20 μM Ru360 led to more motile mitochondria that move longer distances; axon simultaneously incubated with 100 μM H_2O_2 and 10 μM Ru360 showed nearly normal mitochondrial motility. (b–d) Quantification of the percentage of motile mitochondria (a), track length (b), and track velocity (c). Nodes of Ranvier are marked with a red "i". $^*p \leq 0.05$, $^{**}p \leq 0.01$, $^{***}p \leq 0.001$, and $^{****}p \leq 0.0001$. The error bars represent the standard error of mean; $n = 7$ animals and 29 roots; DMSO 7 roots, H_2O_2 7 roots, H_2O_2+5 μM Rui360 4 roots, H_2O_2+10 μM Ru360 7 roots, and H_2O_2+20 μM Ru360 4 roots.

prevent the motility decrease and the loss of membrane potential observed in mitochondria exposed to H_2O_2 (Figures 2(a), 5(a), and 5(b)).

Interestingly, 1 μM TTX alone induced an elevation of the mitochondrial membrane potential when compared to the untreated group. This may reflect a state defined as mitochondrial hyperpolarization [46, 47]. We hypothesize that the presence of TTX and the consequent reduce Na^+ influx may lead to a diminished activity of the ATP-dependent Na^+/K^+-ATPase and induce an increase of ATP. Thus, in our setup, hyperpolarization may be generated by the ATP-consuming reverse action mode of complex V [46]. The exact mechanism underlying the elevation of the mitochondrial membrane potential with TTX alone will be part of future investigations.

Subsequently to Na^+ overload, intra-axonal Ca^{2+} accumulation occurs via reverse action mode of NCX, as described in other studies [13, 48]. During axonal Ca^{2+} overload, mitochondria may uptake Ca^{2+} and function as an intracellular Ca^{2+} buffering system [49]. However, excessive intramitochondrial Ca^{2+} may affect mitochondrial function and motility. It has been shown that dynamin-related protein 1 (Drp1), responsible for mitochondrial fission, as well as Miro, connecting mitochondria via other proteins to

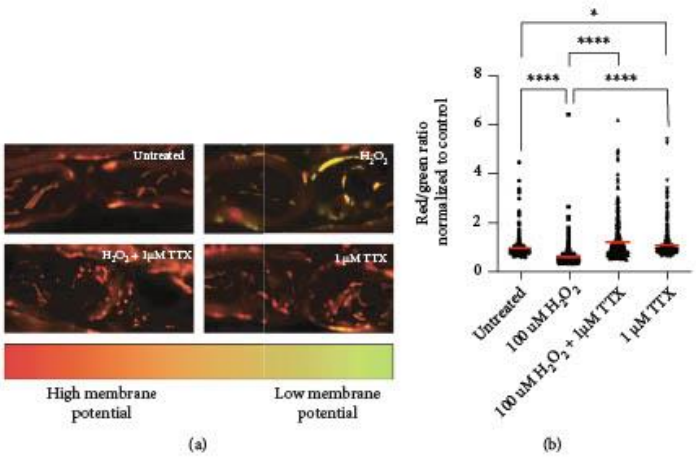

FIGURE 5: Blocking axonal Na^+ influx with TTX prevents loss of mitochondrial membrane potential. (a) Representative images of axons in the different treatment groups. The upper left image shows mitochondrial membrane potential in untreated condition. Oxidative stress led to loss of mitochondrial membrane potential (upper right image) and a shift to green fluorescence. TTX prevented the H_2O_2 effects (lower left image). The lower right image shows that the application of TTX alone led to preserved mitochondrial membrane potential. (b) Data represent normalized values of individual mitochondria to the mean of the control group (red/green ratio = 1 ± 0.0383). **** $p \leq 0.0001$. The error bars represent the standard error of mean; $n = 3$ animals and 12 roots; untreated 3 roots, H_2O_2 3 roots, H_2O_2+1 μM TTX 3 roots, and 1 μM TTX 3 roots.

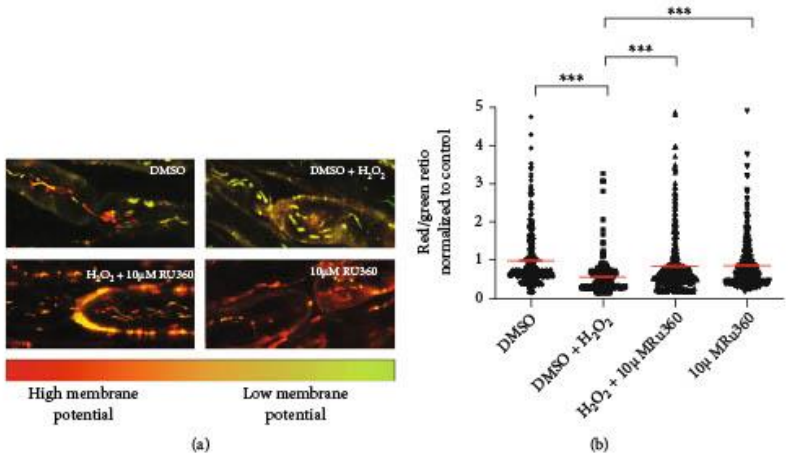

FIGURE 6: Blocking mitochondrial Ca^{2+} uptake with Ru360 prevents loss of mitochondrial membrane potential. (a) Representative images of axons in the different treatment groups. The upper left image shows mitochondrial membrane potential under negative control conditions containing mitochondria with high (red) and low (green) mitochondrial membrane potential. Oxidative stress led to loss of mitochondrial membrane potential (upper right image) and a shift to green fluorescence. Ru360 prevented the H_2O_2 effects (lower left image). The lower right image shows that the application of the Ru360 alone had no effects on mitochondrial functionality compared to control group. (b) Data represent normalized values of individual mitochondria to the mean of the control group (red/green ratio = 1 ± 0.0383). *** $p \leq 0.001$. The error bars represent the standard error of mean; $n = 5$ animals and 20 roots; DMSO 5 roots, H_2O_2 5 roots, H_2O_2+10 μM Ru360 5 roots, and 10 μM Ru360 5 roots.

motor proteins, are directly or indirectly controlled by Ca^{2+} [29, 50–52]. Moreover, mitochondrial swelling seems to be Ca^{2+}-related, too [53]. In this case, we demonstrated that inhibition of Ca^{2+} influx into mitochondria with 10 μM Ru360 completely prevents oxidative stress-induced reduction of mitochondrial length and all motility parameters (Figures 3(b) and 4(a)–4(c)). Further, with 10 μM Ru360, we observed preserved mitochondrial membrane potential (Figures 5(a) and 5(b)). Thus, a rise in intramitochondrial Ca^{2+} concentration appears to contribute to mitochondrial alterations during oxidative stress in our model. In the motility experiments, we observed a biphasic effect of Ru360 with similar absolute values for 5 and 20 μM and a clearly different response for 10 μM Ru360. This biphasic effect was observed in all investigated mitochondrial motility parameters, i.e., percentage of motile mitochondria, mitochondrial track length, and track velocity (Figures 3(a)–3(c)).

Our data confirm previous studies that indicated that ion concentrations show no linear correlation with mitochondrial morphology, motility, or membrane potential [54, 55]. While a slight increase in mitochondrial Ca^{2+} concentration may increase mitochondrial ATP production and be beneficial [55], elevated levels of mitochondrial Ca^{2+} may lead to the opening of the PTP with possible detrimental effects [56]. In addition, PTP opening does not only depend on ion concentrations but also on ATP/ADP levels, mitochondrial ROS, fatty acids, and magnesium levels [57–59]. ROS function as signaling molecules, reversibly oxidizing defined structures and thereby regulating transcription or enzyme activity [6, 31, 60–62]. ROS regulates among others the activity of MCU [63], as well as of voltage-gated sodium channels, including NaV1.7 [64]. These potential cellular mechanisms to cope with increased ROS should be kept in mind when dealing with oxidative stress and ion alterations.

Ru360 is a specific inhibitor of the MCU [65, 66]. However, blocking MCU may not result in a complete inhibition of mitochondrial Ca^{2+} influx. As described in metabolically inhibited cells [47], a reverse action mode of mitochondrial Na^+/Ca^{2+}-exchanger may enhance intramitochondrial Ca^{2+} in stressed axons. Additionally, mitochondria closely interact with the endoplasmic reticulum (ER), forming mitochondria-associated membranes (MAMs) [67]. MAMs play a role in the exchange of Ca^{2+} or metabolites [68, 69], mitochondrial fusion and fission processes, and induction of apoptosis [70].

Mitochondria possess different mechanisms of Ca^{2+} influx [71], but also of Ca^{2+} efflux. The two most important mechanisms are via mitochondrial Na^+/Ca^{2+}-exchanger and via $2H^+/Ca^{2+}$-exchanger [71, 72]. Mitochondrial Ca^{2+} uptake is therefore most likely directly influenced by intraaxonal Na^+ concentration because this affects mitochondrial Ca^{2+} efflux mechanisms via mitochondrial Na^+/Ca^{2+}-exchanger. Interestingly, a reverse action mode is also described for mitochondrial Na^+/Ca^{2+}-exchanger in metabolically inhibited cells [48]. Thus, blocking either axonal Na^+ influx or mitochondrial Ca^{2+} uptake may likely indirectly interfere with other pathways, for example via mitochondria-associated membranes (MAMs) or mitochondrial Na^+/Ca^{2+}-exchanger of a tightly regulated and interconnected Na^+- Ca^{2+}-homeostasis.

5. Limitations of the Study

One technical limitation of our setup was the restricted number of experimental conditions that could be conducted simultaneously within one experiment. The size of the incubation chamber and the narrow time-window, in which transplants could be imaged ex vivo, permitted only the comparison of maximally five different culture conditions. Therefore, using this setup, we were unable to compare effects on mitochondria of different concentrations of inhibitors both in the absence and the presence of the oxidative insult.

Therefore, using this setup, we were able to show only effects on mitochondria of different concentrations of inhibitors in the oxidative stress paradigm and not in the absence of H_2O_2.

Moreover, although our data indicate that modulation of Ca^{2+} influx with Ru360 protects mitochondria from oxidative stress-induced damage, we could not define which Ca^{2+} concentrations are protective and which concentrations are detrimental for mitochondria. Basically, we attested that the explanted root model was not suitable for intraaxonal Ca^{2+} quantification using, for instance, Ca^{2+}-sensitive dyes or roots from Ca^{2+} reporter mice.

6. Conclusion

In conclusion, explanted murine spinal roots appear to be a suitable model to investigate oxidative stress-induced ion alterations affecting axonal mitochondria, in particular, Na^+ and Ca^{2+} overload. Using the model, we demonstrated that inhibition of axonal Na^+ influx prevented oxidative stress-induced alterations of mitochondrial morphology. On the other hand, blocking mitochondrial Ca^{2+} uptake prevented the oxidative stress-induced reduction of both mitochondrial motility and mitochondrial membrane potential, which is crucial for ATP production.

The fact that H_2O_2-induced alterations in mitochondria morphology and motility were prevented by pharmacologic inhibitors of NaV and MCU indicates a direct participation of Na^+ and Ca^{2+} on oxidative stress-mediated mitochondrial changes. Further investigations in this direction are needed to explore the therapeutic potential of the modulation of Na^+ and Ca^{2+} ion channel for mitochondrial protection during oxidative stress.

Data Availability

The main data supporting the findings of this study are listed in Tables 1–6 of the Supplementary Materials.

Conflicts of Interest

The authors declare that there is no conflict of interest regarding the publication of this paper.

Authors' Contributions

Bimala Malla and Carmen Infante-Duarte contributed equally to this work.

Acknowledgments

We thank the Core Facility Advanced Medical Bioimaging (AMBIO) at Charité Universitätsmedizin Berlin for imaging infrastructure and technical support. The study was supported by the Charité Universitätsmedizin and by a fellowship from Berlin Institute of Health (BIH) to R. Ulshöfer. The work of C. Infante-Duarte was supported by the DFG (SFB1340-1, Project B05), and the work of R. Niesner and A. E. Hauser was supported by the DFG (SFB1444, Project 14).

Supplementary Materials

Supplementary 1. Table 1: summary of morphology parameters of untreated mitochondria, mitochondria under H_2O_2 treatment alone, and mitochondria treated with H_2O_2 in the presence of 100 nM and 1 μM TTX.

Supplementary 2. Table 2: summary of motility parameters of untreated mitochondria, mitochondria under H_2O_2 treatment alone, and mitochondria treated with H_2O_2 in the presence of 100 nM and 1 μM TTX.

Supplementary 3. Table 3: summary of morphology parameters of untreated mitochondria, mitochondria under H_2O_2 treatment alone, and mitochondria treated with H_2O_2 in the presence of 5 μM, 10 μM, and 20 μM Ru360.

Supplementary 4. Table 4: summary of motility parameters of untreated mitochondria, mitochondria under H_2O_2 treatment alone, and mitochondria treated with H_2O_2 in the presence of 5 μM, 10 μM, and 20 μM Ru360.

Supplementary 5. Table 5: summary of the red-green ratio normalized to untreated mitochondria, mitochondria treated with 100 μM H_2O_2 alone or in the presence of 1 μM TTX, and mitochondria treated with 1 μM TTX alone.

Supplementary 6. Table 6: summary of the red-green ratio normalized to untreated mitochondria, mitochondria treated with 100 μM H_2O_2 alone or in the presence of 10 μM Ru360, and mitochondria treated with 10 μM Ru360 alone.

References

[1] A. J. Thompson, S. E. Baranzini, J. Geurts, B. Hemmer, and O. Ciccarelli, "Multiple sclerosis," *The Lancet*, vol. 391, no. 10130, pp. 1622–1636, 2018.

[2] K. G. Su, G. Banker, D. Bourdette, and M. Forte, "Axonal degeneration in multiple sclerosis: the mitochondrial hypothesis," *Current Neurology and Neuroscience Reports*, vol. 9, no. 5, pp. 411–417, 2009.

[3] L. Haider, "Inflammation, iron, energy failure, and oxidative stress in the pathogenesis of multiple sclerosis," *Oxidative Medicine and Cellular Longevity*, vol. 2015, Article ID 725370, 10 pages, 2015.

[4] S. Patergnani, V. Fossati, M. Bonora et al., "Mitochondria in multiple sclerosis: molecular mechanisms of pathogenesis," *International Review of Cell and Molecular Biology*, vol. 328, pp. 49–103, 2017.

[5] S. G. Waxman, "Axonal conduction and injury in multiple sclerosis: the role of sodium channels," *Nature Reviews Neuroscience*, vol. 7, no. 12, pp. 932–941, 2006.

[6] K. Ohl, K. Tenbrock, and M. Kipp, "Oxidative stress in multiple sclerosis: central and peripheral mode of action," *Experimental Neurology*, vol. 277, pp. 58–67, 2016.

[7] A. A. Mossakowski, J. Pohlan, D. Bremer et al., "Tracking CNS and systemic sources of oxidative stress during the course of chronic neuroinflammation," *Acta Neuropathologica*, vol. 130, no. 6, pp. 799–814, 2015.

[8] H. Radbruch, D. Bremer, R. Guenther et al., "Ongoing oxidative stress causes subclinical neuronal dysfunction in the recovery phase of EAE," *Frontiers in Immunology*, vol. 7, no. 92, 2016.

[9] A. Federico, E. Cardaioli, P. Da Pozzo, P. Formichi, G. N. Gallus, and E. Radi, "Mitochondria, oxidative stress and neurodegeneration," *Journal of the Neurological Sciences*, vol. 322, no. 1-2, pp. 254–262, 2012.

[10] B. Kadenbach, "Introduction to mitochondrial oxidative phosphorylation," *Advances in Experimental Medicine and Biology*, vol. 748, pp. 1–11, 2012.

[11] D. F. Wilson, "Oxidative phosphorylation: regulation and role in cellular and tissue metabolism," *The Journal of Physiology*, vol. 595, no. 23, pp. 7023–7038, 2017.

[12] I. Nikić, D. Merkler, C. Sorbara et al., "A reversible form of axon damage in experimental autoimmune encephalomyelitis and multiple sclerosis," *Nature Medicine*, vol. 17, no. 4, pp. 495–499, 2011.

[13] A. K. Persson, I. Kim, P. Zhao, M. Estacion, J. A. Black, and S. G. Waxman, "Sodium channels contribute to degeneration of dorsal root ganglion neurites induced by mitochondrial dysfunction in an in vitro model of axonal injury," *The Journal of Neuroscience*, vol. 33, no. 49, pp. 19250–19261, 2013.

[14] V. Pegoretti, K. A. Swanson, J. R. Bethea, L. Probert, U. L. M. Eisel, and R. Fischer, "Inflammation and oxidative stress in multiple sclerosis: consequences for therapy development," *Oxidative Medicine and Cellular Longevity*, vol. 2020, Article ID 7191080, 19 pages, 2020.

[15] H. Bros, R. Niesner, and C. Infante-Duarte, "An ex vivo model for studying mitochondrial trafficking in neurons," *Methods in Molecular Biology*, vol. 1264, pp. 465–472, 2015.

[16] B. Malla, S. Cotten, R. Ulshoefer et al., "Teriflunomide preserves peripheral nerve mitochondria from oxidative stress-mediated alterations," *Therapeutic Advances in Chronic Disease*, vol. 11, 2020.

[17] H. Bros, J. M. Millward, F. Paul, R. Niesner, and C. Infante-Duarte, "Oxidative damage to mitochondria at the nodes of Ranvier precedes axon degeneration in ex vivo transected axons," *Experimental Neurology*, vol. 261, pp. 127–135, 2014.

[18] J. Wang, S.-W. Ou, and Y.-J. Wang, "Distribution and function of voltage-gated sodium channels in the nervous system," *Channels*, vol. 11, no. 6, pp. 534–554, 2017.

[19] X. Wang, W. Wang, L. Li, G. Perry, H.-g. Lee, and X. Zhu, "Oxidative stress and mitochondrial dysfunction in Alzheimer's disease," *Biochimica et Biophysica Acta (BBA) - Molecular Basis of Disease*, vol. 1842, no. 8, pp. 1240–1247, 2014.

[20] G. Criste, B. Trapp, and R. Dutta, "Axonal loss in multiple sclerosis: causes and mechanisms," *Handbook of Clinical Neurology*, vol. 122, pp. 101–113, 2014.

[21] Y. Lin, L.-L. Li, W. Nie et al., "Brain activity regulates loose coupling between mitochondrial and cytosolic Ca^{2+} transients," *Nature Communications*, vol. 10, no. 1, p. 5277, 2019.

[22] G. Csordás, P. Várnai, T. Golenár et al., "Imaging interorganelle contacts and local calcium dynamics at the ER-mitochondrial interface," *Molecular Cell*, vol. 39, no. 1, pp. 121–132, 2010.

[23] V. Granatiero, M. Pacifici, A. Raffaello, D. De Stefani, and R. Rizzuto, "Overexpression of mitochondrial calcium uniporter causes neuronal death," *Oxidative Medicine and Cellular Longevity*, vol. 2019, Article ID 1681254, 15 pages, 2019.

[24] B. Schattling, B. Eggert, and M. A. Friese, "Acquired channelopathies as contributors to development and progression of multiple sclerosis," *Experimental Neurology*, vol. 262, pp. 28–36, 2014.

[25] F. Sivandzade, A. Bhalerao, and L. Cucullo, "Analysis of the mitochondrial membrane potential using the cationic JC-1 dye as a sensitive fluorescent probe," *Bio-Protocol*, vol. 9, no. 1, article e3128, 2019.

[26] S. M. Kilbride, J. E. Telford, and G. P. Davey, "Complex I controls mitochondrial and plasma membrane potentials in nerve terminals," *Neurochemical Research*, vol. 46, no. 1, pp. 100–107, 2021.

[27] M. E. Witte, D. J. Mahad, H. Lassmann, and J. van Horssen, "Mitochondrial dysfunction contributes to neurodegeneration in multiple sclerosis," *Trends in Molecular Medicine*, vol. 20, no. 3, pp. 179–187, 2014.

[28] D. Mahad, H. Lassmann, and D. Turnbull, "Review: mitochondria and disease progression in multiple sclerosis," *Neuropathology and Applied Neurobiology*, vol. 34, no. 6, pp. 577–589, 2008.

[29] C. S. Palmer, L. D. Osellame, D. Stojanovski, and M. T. Ryan, "The regulation of mitochondrial morphology: intricate mechanisms and dynamic machinery," *Cellular Signalling*, vol. 23, no. 10, pp. 1534–1545, 2011.

[30] P. H. Reddy and T. P. Reddy, "Mitochondria as a therapeutic target for aging and neurodegenerative diseases," *Current Alzheimer Research*, vol. 8, no. 4, pp. 393–409, 2011.

[31] A. K. Camara, E. J. Lesnefsky, and D. F. Stowe, "Potential therapeutic benefits of strategies directed to mitochondria," *Antioxidants & Redox Signaling*, vol. 13, no. 3, pp. 279–347, 2010.

[32] M. Gülden, A. Jess, J. Kammann, E. Maser, and H. Seibert, "Cytotoxic potency of H2O2 in cell cultures: impact of cell concentration and exposure time," *Free Radical Biology and Medicine*, vol. 49, no. 8, pp. 1298–1305, 2010.

[33] B. Malla, A. Liotta, H. Bros et al., "Teriflunomide preserves neuronal activity and protects mitochondria in brain slices exposed to oxidative stress," *International Journal of Molecular Sciences*, vol. 23, no. 3, p. 1538, 2022.

[34] C. Fang, D. Bourdette, and G. Banker, "Oxidative stress inhibits axonal transport: implications for neurodegenerative diseases," *Molecular Neurodegeneration*, vol. 7, no. 1, p. 29, 2012.

[35] O. Errea, B. Moreno, A. Gonzalez-Franquesa, P. M. Garcia-Roves, and P. Villoslada, "The disruption of mitochondrial axonal transport is an early event in neuroinflammation," *Journal of Neuroinflammation*, vol. 12, no. 1, p. 152, 2015.

[36] R. Isonaka, H. Hiruma, and T. Kawakami, "Inhibition of axonal transport caused by tert-butyl hydroperoxide in cultured mouse dorsal root ganglion neurons," *Journal of Molecular Neuroscience*, vol. 45, no. 2, pp. 194–201, 2011.

[37] M. Carinci, B. Vezzani, S. Patergnani et al., "Different roles of mitochondria in cell death and inflammation: focusing on mitochondrial quality control in ischemic stroke and reperfusion," *Biomedicine*, vol. 9, no. 2, p. 169, 2021.

[38] M. T. Islam, "Oxidative stress and mitochondrial dysfunction-linked neurodegenerative disorders," *Neurological Research*, vol. 39, no. 1, pp. 73–82, 2017.

[39] M. D. Brand, "The efficiency and plasticity of mitochondrial energy transduction," *Biochemical Society Transactions*, vol. 33, no. 5, pp. 897–904, 2005.

[40] S. A. Freeman, A. Desmazières, D. Fricker, C. Lubetzki, and N. Sol-Foulon, "Mechanisms of sodium channel clustering and its influence on axonal impulse conduction," *Cellular and Molecular Life Sciences*, vol. 73, no. 4, pp. 723–735, 2016.

[41] A. H. Seidl, "Regulation of conduction time along axons," *Neuroscience*, vol. 276, pp. 126–134, 2014.

[42] J. A. Black, J. Newcombe, B. D. Trapp, and S. G. Waxman, "Sodium channel expression within chronic multiple sclerosis plaques," *Journal of Neuropathology and Experimental Neurology*, vol. 66, no. 9, pp. 828–837, 2007.

[43] M. J. Craner, J. Newcombe, J. A. Black, C. Hartle, M. L. Cuzner, and S. G. Waxman, "Molecular changes in neurons in multiple sclerosis: altered axonal expression of Nav1.2 and Nav1.6 sodium channels and Na^+/Ca^{2+} exchanger," *Proceedings of the National Academy of Sciences of the United States of America*, vol. 101, no. 21, pp. 8168–8173, 2004.

[44] A. Bouafia, J. L. Golmard, V. Thuries et al., "Axonal expression of sodium channels and neuropathology of the plaques in multiple sclerosis," *Neuropathology and Applied Neurobiology*, vol. 40, no. 5, pp. 579–590, 2014.

[45] X. Liu, D. Weaver, O. Shirihai, and G. Hajnóczky, "Mitochondrial 'kiss-and-run': interplay between mitochondrial motility and fusion-fission dynamics," *The EMBO Journal*, vol. 28, no. 20, pp. 3074–3089, 2009.

[46] M. Forkink, G. R. Manjeri, D. C. Liemburg-Apers et al., "Mitochondrial hyperpolarization during chronic complex I inhibition is sustained by low activity of complex II, III, IV and V," *Bioenergetics*, vol. 1837, no. 8, pp. 1247–1256, 2014.

[47] A. Y. Abramov, T. K. Smulders-Srinivasan, D. M. Kirby et al., "Mechanism of neurodegeneration of neurons with mitochondrial DNA mutations," *Brain: a Journal of Neurology*, vol. 133, no. 3, pp. 797–807, 2010.

[48] I. Smets, A. Caplanusi, S. Despa et al., "Ca^{2+} uptake in mitochondria occurs via the reverse action of the Na^+/Ca^{2+} exchanger in metabolically inhibited MDCK cells," *American Journal of Physiology Renal Physiology*, vol. 286, no. 4, pp. F784–F794, 2004.

[49] D. G. Nicholls, "Mitochondrial calcium function and dysfunction in the central nervous system," *Biochimica et Biophysica Acta (BBA)-Bioenergetics*, vol. 1787, no. 11, pp. 1416–1424, 2009.

[50] P. Mishra and D. C. Chan, "Metabolic regulation of mitochondrial dynamics," *The Journal of Cell Biology*, vol. 212, no. 4, pp. 379–387, 2016.

[51] G. M. Cereghetti, A. Stangherlin, O. M. de Brito et al., "Dephosphorylation by calcineurin regulates translocation of Drp1 to mitochondria," *Proceedings of the National Academy*

of Sciences of the United States of America, vol. 105, no. 41, pp. 15803–15808, 2008.

[52] Y. Chen and Z. H. Sheng, "Kinesin-1-syntaphilin coupling mediates activity-dependent regulation of axonal mitochondrial transport," *The Journal of Cell Biology*, vol. 202, no. 2, pp. 351–364, 2013.

[53] A. A. Courtes, N. R. de Carvalho, D. F. Gonçalves et al., "Guanosine protects against Ca^{2+}-induced mitochondrial dysfunction in rats," *Biomedicine & Pharmacotherapy*, vol. 111, pp. 1438–1446, 2019.

[54] R. Bagur and G. Hajnóczky, "Intracellular Ca^{2+} sensing: its role in calcium homeostasis and signaling," *Molecular Cell*, vol. 66, no. 6, pp. 780–788, 2017.

[55] E. J. Griffiths and G. A. Rutter, "Mitochondrial calcium as a key regulator of mitochondrial ATP production in mammalian cells," *Biochimica et Biophysica Acta (BBA)-Bioenergetics*, vol. 1787, no. 11, pp. 1324–1333, 2009.

[56] T. I. Peng and M. J. Jou, "Oxidative stress caused by mitochondrial calcium overload," *Annals of the New York Academy of Sciences*, vol. 1201, no. 1, pp. 183–188, 2010.

[57] N. Naumova and R. Šachl, "Regulation of cell death by mitochondrial transport systems of calcium and Bcl-2 proteins," *Membranes*, vol. 10, no. 10, p. 299, 2020.

[58] K. N. Belosludtsev, M. V. Dubinin, N. V. Belosludtseva, and G. D. Mironova, "Mitochondrial Ca^{2+} transport: mechanisms, molecular structures, and role in cells," *Biochemistry Biokhimiia*, vol. 84, no. 6, pp. 593–607, 2019.

[59] S. Golshani-Hebroni, "Mg^{++} requirement for MtHK binding, and Mg^{++} stabilization of mitochondrial membranes via activation of MtHK & MtCK and promotion of mitochondrial permeability transition pore closure: a hypothesis on mechanisms underlying Mg^{++}'s antioxidant and cytoprotective effects," *Gene*, vol. 581, no. 1, pp. 1–13, 2016.

[60] A. Kumar and R. R. Ratan, "Oxidative stress and Huntington's disease: the good, the bad, and the ugly," *Journal of Huntington's Disease*, vol. 5, no. 3, pp. 217–237, 2016.

[61] J. R. Stone and S. Yang, "Hydrogen peroxide: a signaling messenger," *Antioxidants & Redox Signaling*, vol. 8, no. 3-4, pp. 243–270, 2006.

[62] D. F. Stowe and A. K. Camara, "Mitochondrial reactive oxygen species production in excitable cells: modulators of mitochondrial and cell function," *Antioxidants & Redox Signaling*, vol. 11, no. 6, pp. 1373–1414, 2009.

[63] N. Nemani, S. Shanmughapriya, and M. Madesh, "Molecular regulation of MCU: implications in physiology and disease," *Cell Calcium*, vol. 74, pp. 86–93, 2018.

[64] R. Patel and F. Sesti, "Oxidation of ion channels in the aging nervous system," *Brain Research*, vol. 1639, pp. 174–185, 2016.

[65] K. C. Reed and F. L. Bygrave, "A low molecular weight ruthenium complex inhibitory to mitochondrial Ca^{2+} transport," *FEBS Letters*, vol. 46, no. 1-2, pp. 109–114, 1974.

[66] C. L. Moore, "Specific inhibition of mitochondrial Ca^{++} transport by ruthenium red," *Biochemical and Biophysical Research Communications*, vol. 42, no. 2, pp. 298–305, 1971.

[67] N. Bernard-Marissal, R. Chrast, and B. L. Schneider, "Endoplasmic reticulum and mitochondria in diseases of motor and sensory neurons: a broken relationship?," *Cell Death & Disease*, vol. 9, no. 3, p. 333, 2018.

[68] C. Giorgi, S. Missiroli, S. Patergnani, J. Duszynski, M. R. Wieckowski, and P. Pinton, "Mitochondria-associated membranes: composition, molecular mechanisms, and physiopathological implications," *Antioxidants & Redox Signaling*, vol. 22, no. 12, pp. 995–1019, 2015.

[69] R. Rizzuto, S. Marchi, M. Bonora et al., "Ca^{2+} transfer from the ER to mitochondria: when, how and why," *Biochimica et Biophysica Acta (BBA) - Bioenergetics*, vol. 1787, no. 11, pp. 1342–1351, 2009.

[70] M. Krols, G. van Isterdael, B. Asselbergh et al., "Mitochondria-associated membranes as hubs for neurodegeneration," *Acta Neuropathologica*, vol. 131, no. 4, pp. 505–523, 2016.

[71] R. F. Feissner, J. Skalska, W. E. Gaum, and S.-S. Sheu, "Crosstalk signaling between mitochondrial Ca^{2+} and ROS," *Frontiers in Bioscience*, vol. 14, no. 4, pp. 1197–1218, 2009.

[72] P. Pizzo, I. Drago, R. Filadi, and T. Pozzan, "Mitochondrial Ca^{2+} homeostasis: mechanism, role, and tissue specificities," *Pflügers Archiv - European Journal of Physiology*, vol. 464, no. 1, pp. 3–17, 2012.

Journal Data Filtered By: **Selected JCR Year: 2021** Selected Editions: SCIE,SSCI Selected Categories: **"BIOCHEMISTRY and MOLECULAR BIOLOGY"** Selected Category Scheme: WoS

Gesamtanzahl: 296 Journale

Rank	Full Journal Title	Total Cites	Journal Impact Factor	Eigenfaktor
1	NATURE MEDICINE	141,857	87.241	0.23255
2	CELL	362,236	66.850	0.53397
3	Molecular Cancer	32,250	41.444	0.03386
4	Signal Transduction and Targeted Therapy	11,026	38.104	0.01781
5	Annual Review of Biochemistry	25,139	27.258	0.01962
6	Molecular Plant	20,242	21.949	0.02339
7	MOLECULAR CELL	94,258	19.328	0.13937
8	NUCLEIC ACIDS RESEARCH	284,490	19.160	0.33755
9	NATURE STRUCTURAL & MOLECULAR BIOLOGY	33,999	18.361	0.04689
10	TRENDS IN MICROBIOLOGY	19,957	18.230	0.02015
11	CYTOKINE & GROWTH FACTOR REVIEWS	9,002	17.660	0.00625
12	MOLECULAR ASPECTS OF MEDICINE	8,986	16.337	0.00615
13	Nature Chemical Biology	31,125	16.174	0.04456
14	TRENDS IN MOLECULAR MEDICINE	14,585	15.272	0.01381
15	NATURAL PRODUCT REPORTS	14,564	15.111	0.01079
16	PROGRESS IN LIPID RESEARCH	7,982	14.673	0.00444
17	TRENDS IN BIOCHEMICAL SCIENCES	22,957	14.264	0.02170
18	EMBO JOURNAL	80,536	14.012	0.05438
19	MOLECULAR PSYCHIATRY	33,324	13.437	0.04914
20	Molecular Systems Biology	11,036	13.068	0.01483
21	EXPERIMENTAL AND MOLECULAR MEDICINE	12,199	12.153	0.01698

Rank	Full Journal Title	Total Cites	Journal Impact Factor	Eigenfaktor
22	PLANT CELL	67,319	12.085	0.02964
23	CELL DEATH AND DIFFERENTIATION	31,035	12.067	0.02639
24	BIOCHIMICA ET BIOPHYSICA ACTA-REVIEWS ON CANCER	8,255	11.414	0.00673
25	Cell Systems	8,047	11.091	0.03332
26	CURRENT BIOLOGY	85,124	10.900	0.10641
27	Redox Biology	20,557	10.787	0.02390
28	International Journal of Biological Sciences	14,100	10.750	0.01488
29	MATRIX BIOLOGY	9,415	10.447	0.00856
30	PLOS BIOLOGY	44,888	9.593	0.05920
31	Cell and Bioscience	4,564	9.584	0.00524
32	Science Signaling	17,426	9.517	0.02046
33	GENOME RESEARCH	51,169	9.438	0.05153
34	CELLULAR AND MOLECULAR LIFE SCIENCES	38,745	9.207	0.03204
35	Journal of Integrative Plant Biology	8,456	9.106	0.00730
36	EMBO REPORTS	21,705	9.071	0.02695
37	Cell Chemical Biology	6,651	9.039	0.01870
38	CURRENT OPINION IN CHEMICAL BIOLOGY	12,464	8.972	0.01277
39	MOLECULAR BIOLOGY AND EVOLUTION	67,311	8.800	0.07228
40	ONCOGENE	81,646	8.756	0.05014
41	CELLULAR & MOLECULAR BIOLOGY LETTERS	2,684	8.702	0.00250
42	CRITICAL REVIEWS IN BIOCHEMISTRY AND MOLECULAR BIOLOGY	5,108	8.697	0.00477
43	Molecular Ecology Resources	15,145	8.678	0.01553

Selected JCR Year: 2021; Selected Categories: "BIOCHEMISTRY and MOLECULAR BIOLOGY"

Rank	Full Journal Title	Total Cites	Journal Impact Factor	Eigenfaktor
44	Plant Communications	743	8.625	0.00148
45	FREE RADICAL BIOLOGY AND MEDICINE	55,523	8.101	0.02824
46	INTERNATIONAL JOURNAL OF BIOLOGICAL MACROMOLECULES	112,372	8.025	0.09445
47	Biomedical Journal	2,388	7.892	0.00301
48	CURRENT OPINION IN STRUCTURAL BIOLOGY	13,407	7.786	0.01689
49	AMERICAN JOURNAL OF RESPIRATORY CELL AND MOLECULAR BIOLOGY	16,259	7.748	0.01386
50	Antioxidants	21,453	7.675	0.01946
51	EXPERT REVIEWS IN MOLECULAR MEDICINE	2,282	7.615	0.00062
52	Reviews of Physiology Biochemistry and Pharmacology	920	7.500	0.00043
53	ANTIOXIDANTS & REDOX SIGNALING	29,117	7.468	0.01390
54	Essays in Biochemistry	4,569	7.258	0.00691
55	Genes & Diseases	2,732	7.243	0.00322
56	Open Biology	5,227	7.124	0.00994
57	PROTEIN SCIENCE	18,673	6.993	0.02822
58	BIOMACROMOLECULES	46,963	6.978	0.02347
59	JOURNAL OF PHOTOCHEMISTRY AND PHOTOBIOLOGY B-BIOLOGY	18,610	6.814	0.01229
60	JOURNAL OF LIPID RESEARCH	29,128	6.676	0.01485
61	BIOCHIMICA ET BIOPHYSICA ACTA-MOLECULAR BASIS OF DISEASE	22,719	6.633	0.01820
62	MOLECULAR ECOLOGY	45,664	6.622	0.03311
63	AMYLOID-JOURNAL OF PROTEIN FOLDING DISORDERS	2,335	6.571	0.00312

Selected JCR Year: 2021; Selected Categories: "BIOCHEMISTRY and MOLECULAR BIOLOGY"

Rank	Full Journal Title	Total Cites	Journal Impact Factor	Eigenfaktor
64	BIOFACTORS	5,614	6.438	0.00307
65	International Review of Cell and Molecular Biology	3,388	6.420	0.00314
66	MOLECULAR MEDICINE	7,039	6.376	0.00402
67	Food & Function	27,282	6.317	0.02290
68	Biochimica et Biophysica Acta-Gene Regulatory Mechanisms	8,926	6.304	0.00707
69	INTERNATIONAL JOURNAL OF MOLECULAR SCIENCES	211,517	6.208	0.24907
70	Computational and Structural Biotechnology Journal	6,436	6.155	0.00945
71	JOURNAL OF MOLECULAR BIOLOGY	66,672	6.151	0.03581
72	JOURNAL OF NUTRITIONAL BIOCHEMISTRY	15,277	6.117	0.00837
73	Frontiers in Molecular Biosciences	6,864	6.113	0.01068
74	BIOCONJUGATE CHEMISTRY	19,624	6.069	0.01508
75	Biomolecules	21,742	6.064	0.02602
76	GLYCOBIOLOGY	10,212	5.954	0.00650
77	STRUCTURE	17,734	5.871	0.01779
78	MACROMOLECULAR BIOSCIENCE	9,240	5.859	0.00565
79	FASEB JOURNAL	59,831	5.834	0.04452
80	ACS Chemical Neuroscience	12,168	5.780	0.01655
81	BIOELECTROCHEMISTRY	7,093	5.760	0.00463
82	JOURNAL OF ENZYME INHIBITION AND MEDICINAL CHEMISTRY	8,156	5.756	0.00580
83	Journal of Genetics and Genomics	3,129	5.723	0.00327
84	Acta Crystallographica Section D-Structural Biology	23,006	5.699	0.02041
85	REDOX REPORT	2,247	5.696	0.00082

Selected JCR Year: 2021; Selected Categories: "BIOCHEMISTRY and MOLECULAR BIOLOGY"

International Journal of *Molecular Sciences*

MDPI

Article

Teriflunomide Preserves Neuronal Activity and Protects Mitochondria in Brain Slices Exposed to Oxidative Stress

Bimala Malla [1], Agustin Liotta [2], Helena Bros [1], Rebecca Ulshöfer [1,3], Friedemann Paul [3,4], Anja E. Hauser [5,6], Raluca Niesner [5,7] and Carmen Infante-Duarte [1,3,*]

[1] Institute for Medical Immunology, Charité—Universitätsmedizin Berlin, Corporate Member of Freie Universität Berlin, Humboldt-Universität zu Berlin, Augustenburger Platz 1, 13353 Berlin, Germany; bimala.malla@charite.de (B.M.); hnbros@gmail.com (H.B.); rebecca.ulshofer@charite.de (R.U.)
[2] Klinik für Anästhesiologie mit Schwerpunkt Operative Intensivmedizin, Charité—Universitätsmedizin Berlin, Charitéplatz 1, 10117 Berlin, Germany; agustin.liotta@charite.de
[3] Experimental and Clinical Research Center (ECRC), MDC for Molecular Medicine and Charité—Universitätsmedizin Berlin, Lindenberger Weg 80, 13125 Berlin, Germany; friedemann.paul@charite.de
[4] NeuroCure Clinical Research Center, Charité—Universitätsmedizin Berlin, Charitéplatz 1, 10117 Berlin, Germany
[5] Deutsches Rheuma-Forschungszentrum, Charitéplatz 1, 10117 Berlin, Germany; hauser@drfz.de (A.E.H.); niesner@drfz.de (R.N.)
[6] Medizinische Klinik mit Schwerpunkt Rheumatologie und Klinische Immunologie, Charité—Universitätsmedizin Berlin, Corporate Member of Freie Universität Berlin, Humboldt-Universität zu Berlin, Charitéplatz 1, 10117 Berlin, Germany
[7] Dynamic and Functional In Vivo Imaging, Veterinary Medicine, Freie Universität Berlin, 14163 Berlin, Germany
* Correspondence: carmen.infante@charite.de

check for updates

Citation: Malla, B.; Liotta, A.; Bros, H.; Ulshöfer, R.; Paul, F.; Hauser, A.E.; Niesner, R.; Infante-Duarte, C. Teriflunomide Preserves Neuronal Activity and Protects Mitochondria in Brain Slices Exposed to Oxidative Stress. *Int. J. Mol. Sci.* **2022**, *23*, 1538. https://doi.org/10.3390/ijms23031538

Academic Editor: Salvatore Passarella

Received: 26 November 2021
Accepted: 26 January 2022
Published: 28 January 2022

Publisher's Note: MDPI stays neutral with regard to jurisdictional claims in published maps and institutional affiliations.

Abstract: Teriflunomide (TFN) limits relapses in relapsing–remitting multiple sclerosis (RRMS) by reducing lymphocytic proliferation through the inhibition of the mitochondrial enzyme dihydroorotate dehydrogenase (DHODH) and the subsequent modulation of de novo pyrimidine synthesis. Alterations of mitochondrial function as a consequence of oxidative stress have been reported during neuroinflammation. Previously, we showed that TFN prevents alterations of mitochondrial motility caused by oxidative stress in peripheral axons. Here, we aimed to validate TFN effects on mitochondria and neuronal activity in hippocampal brain slices, in which cellular distribution and synaptic circuits are largely preserved. TFN effects on metabolism and neuronal activity were investigated by assessing oxygen partial pressure and local field potential in acute slices. Additionally, we imaged mitochondria in brain slices from the transgenic Thy1-CFP/COX8A)S2Lich/J (mitoCFP) mice using two-photon microscopy. Although TFN could not prevent oxidative stress-related depletion of ATP, it preserved oxygen consumption and neuronal activity in CNS tissue during oxidative stress. Furthermore, TFN prevented mitochondrial shortening and fragmentation of puncta-shaped and network mitochondria during oxidative stress. Regarding motility, TFN accentuated the decrease in mitochondrial displacement and increase in speed observed during oxidative stress. Importantly, these effects were not associated with neuronal viability and did not lead to axonal damage. In conclusion, during conditions of oxidative stress, TFN preserves the functionality of neurons and prevents morphological and motility alterations of mitochondria.

Keywords: mitochondria; neurodegeneration; teriflunomide (TFN); oxidative stress; dihydroorotate dehydrogenase (DHODH); multiple sclerosis; mitochondrial morphology; mitochondrial motility; acute hippocampal slices; two-photon microscopy

1. Introduction

Multiple sclerosis (MS) is a chronic inflammatory and neurodegenerative disease that represents one of the most common non-traumatic incapacitating neurological diseases

in young adults [1]. Pathologically, MS is characterized by inflammation, demyelination, and neuroaxonal damage [1,2]. The MS course is generally characterized by an initial relapsing–remitting MS (RRMS) phase, in which acute attacks are followed by complete or partial recovery. Around 80–85% of the RRMS patients develops a secondary progressive MS (SPMS) within 20–30 years after diagnosis, which is characterized by the progressive accumulation of disability, generally independent of relapses [1,3]. About 10–15% of patients manifest a primary progressive MS [PPMS] characterized by chronic progression from the onset of the disease.

Although the exact disease pathogenesis remains unclear, it is assumed that an autoimmune attack mediated by autoreactive lymphocytes initiates the disease and leads to neurodegenerative processes [4,5]. In this context, oxidative stress caused by the sustained release of reactive oxygen and nitrogen species (ROS and NOS) by inflammatory cells appears to be implicated in the damaging cascade inside the CNS [6–9]. Numerous studies indicated that oxidative stress and mitochondria are the key players in neurodegeneration [9–11]. Moreover, mitochondrial alterations are considered one of the early contributors of the disease that leads to virtual hypoxia, causing energy deficiency, ionic imbalance, as well as tissue damage [12–14]. Hence, mitochondria could represent a target for therapies [4,9,15–18].

Teriflunomide (TFN) is a disease-modifying drug (DMT) that has been recently approved as an oral therapy for patients with RRMS [19,20]. TFN is the active metabolite of leflunomide, which has been widely used to treat rheumatic arthritis [21] and is known to exert its effect by non-competitively and reversibly inhibiting dihydroorotate dehydrogenase (DHODH). DHODH is a mitochondrial enzyme located on the inner mitochondrial membrane that is involved in de novo pyrimidine synthesis [19,20,22,23]. DHODH-inhibition, therefore, primarily leads to the regulation of rapidly dividing cells, reducing B and T cell proliferation and modulating inflammation in MS [22,24,25]. Due to its immunomodulatory potential, TFN has been implicated in RRMS.

Since TFN inhibits an enzyme that is closely associated with mitochondrial biology via the respiratory chain, we hypothesized that treatment of MS patients with TFN may also affect neuronal mitochondria. Although in MS, autoimmune attack is assumed to be one of the key players leading to neurodegenerative processes [26], numerous studies indicate that inflammation-induced oxidative stress in CNS leads to mitochondrial damage and consequently, to neurodegeneration [9–11,27].

Recently, we showed that TFN could prevent alterations in mitochondrial morphology, motility, as well as oxidation potential in peripheral spinal root explants during oxidative stress [28]. Considering the central role of inflammation-mediated oxidative stress and subsequent mitochondria damage in MS, we aimed here to determine whether TFN may also affect mitochondrial functionality and dynamics in hippocampal brain slices, which retain the complexity and physiology of central nervous system (CNS) structures and were exposed to oxidative stress conditions [29]. Thus, we have investigated the effect of TFN on synaptic transmission, metabolism, as well as on the dynamics of CNS mitochondria in a model of murine acute hippocampal slices exposed to exogenous hydrogen peroxide (H_2O_2) that induces oxidative stress in CNS cells.

2. Results

2.1. TFN Restores Tissue Respiration during Oxidative Stress

To understand the effects of TFN on the metabolic activity in the nervous tissue, we investigated changes in oxygen partial pressure (pO_2) levels in hippocampal slices at baseline and after treatments with H_2O_2 (200 µM) and H_2O_2 (200 µM) + TFN (50 µM). In vitro, changes in pO_2 correlates inversely with neuronal oxygen consumption and cellular metabolism due to the constant supply with oxygen and glucose. To determine pO_2, we performed a gradient descent of the oxygen electrode into the slice, which we refer to as 'steps' from the surface with the increment of 20 µm up to the core of the slice. A total of 10 slices were analyzed in three independent experiments. As depicted in Figure 1C, the

core was located between the depth of 240 and 280 µm, after which the pO_2 level no longer decreased (see methods). Thus, the depicted data covers only the descent to the core. Then, the oxygen electrode was raised to a 100 µm depth from the surface of the slice and 15 min of baseline activity was recorded. Immediately following the baseline recording, the H_2O_2 or H_2O_2 + TFN treatment in an artificial cerebrospinal fluid (aCSF) was applied for 30 min. Again, the steps were performed from the surface of the slice towards the core.

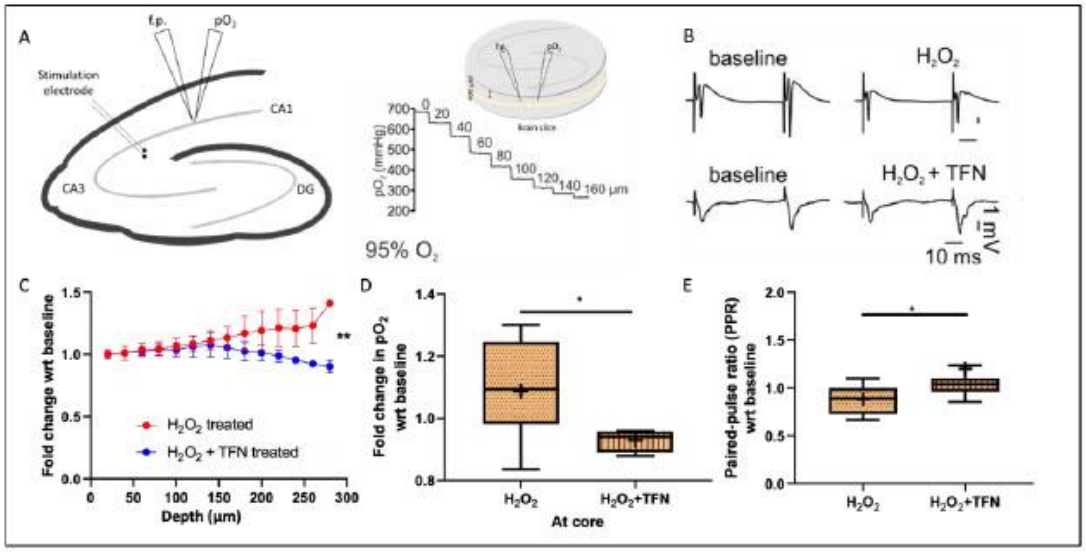

Figure 1. Electrophysiology recordings of pO_2 and local field potential in acute hippocampal slice: (**A**) Left, schematic representation of hippocampal slice and the placement of stimulation, recording, and pO_2 electrodes. The Schaffer collaterals were electrically stimulated in the stratum radiatum of the cornu ammonis (CA) and the O_2 recording and population spikes (PS) were simultaneously obtained between CA3 and CA1 in close vicinity. Middle upper, representation of 400 µM-thick brain slice in interface chamber which is supplied with carbogen from surface and bottom. The pO_2 decreases with each step inside the tissue up to the core (not shown in the figure), after which it starts increasing (due to the distance from the source of oxygen, i.e., from the surface and the bottom) providing a typical depth profile, as shown in middle lower figure—the pO_2 measurement steps at the interval of 20 µm from the surface to the core; (**B**) a typical population spike in a paired pulse at baseline, with H_2O_2 and H_2O_2 + TFN treatment; (**C**) fold change in the pO_2 at tissue depth in the interval of 20 µm with respect to the baseline; (**D**) fold change in pO_2 at the core with respect to the baseline recording; (**E**) the paired-pulse ratio (PPR) of PS2 and PS1 with respect to the respective baseline recordings between H_2O_2 treatment and H_2O_2 + TFN treatment. Graphs are shown in Tukey boxplots. Inside the box, '+' delineates the mean. * $p \leq 0.05$, ** $p \leq 0.01$.

Figure 1A shows the depth profile of the O_2 steps with the corresponding partial pressures of oxygen. At the slice surface, pO_2 of ~680 mmHg corresponded to carbogen. Figure 1C,D shows the fold change in the pO_2 with respect to the baseline measurement. We observed that the pO_2 increased near to the core, pointing to an increase in pO_2 due to a reduced oxygen consumption in H_2O_2-stressed tissue (1.09 ± 0.16-fold (mean ± SD) relative the baseline). In contrast, the pO_2 decreased towards the core when TFN treatment was added (H_2O_2 + TFN; 0.93 ± 0.04 fold (mean ± SD) relative to untreated), indicating an increase in the consumption of oxygen in the presence of TFN with respect to H_2O_2 treatment alone (Figure 1D,E).

2.2. TFN Prevents Oxidative Stress-Mediated Depression of Synaptic Transmission

Furthermore, we investigated the effect of oxidative stress and TFN application on synaptic transmission in acute hippocampal tissue. For that, stimulus-induced local field potential (LFP) signals were recorded in CA1 while stimulating the Schaffer collaterals using a paired-pulse facilitation protocol (see methods). The amplitudes of the population spike responses during baseline and treatment with H_2O_2 (200 µM) or H_2O_2 (200 µM) + TFN (50 µM) were measured.

Figure 1B shows a typical population spike (PS) in response to a paired-pulse stimulation. The amplitudes of the population spikes were measured by subtracting the maxima and minima of the spike. Then, we compared the short-term facilitation/paired-pulse ratio (PPR), which is the ratio of the amplitude of the second population spike (PS2) to the first population spike (PS1) and normalized to the baseline recordings. We observed a depression of PPR in H_2O_2-stressed brain slices treatment (0.88 ± 0.14-fold (mean ± SD) relative to the baseline), while the presence of TFN increased the PPR (H_2O_2 + TFN treatment (1.2 ± 0.62-fold (mean ± SD) relative to the baseline) (Figure 1E).

2.3. TFN Does Not Prevent Oxidative Stress-Mediated ATP Decrease in Acute Hippocampal Slices

To understand the effect on the energy metabolism of mitochondria, we investigated the effect of TFN on ATP levels in the acute hippocampal slices exposed to oxidative stress. We observed that the ATP amount in the slices treated with H_2O_2 significantly decreased (0.64 ± 0.16-fold (mean ± SD)) with respect to untreated controls. The treatment with TFN along with H_2O_2 did not affect or restore the ATP levels (0.65 ± 0.03-fold (mean ± SD)). (Figure 2).

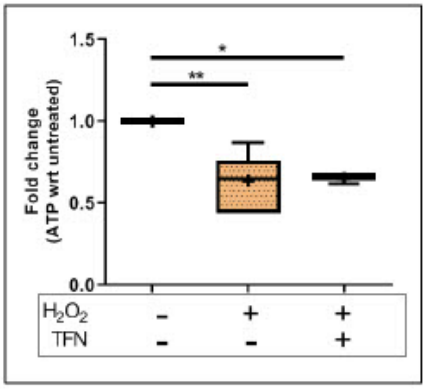

Figure 2. ATP levels in brain tissue exposed to oxidative stress with/out TFN treatment. Graphs are expressed as fold change with respect to the baseline and shown in Tukey boxplots. Inside the box, '+' delineates the mean. * $p \leq 0.05$ and ** $p \leq 0.01$.

2.4. TFN Prevented Oxidative Stress-Induced Decrease in Mitochondrial Area in Acute Hippocampal Slices

We have shown previously that in peripheral nerves, mitochondria exposed to oxidative stress are affected even prior to the axonal damages [28,30] and that TFN prevents these mitochondrial alterations [28]. To monitor how TFN affects changes of mitochondria morphology during oxidative stress within the CNS, hippocampal slices from transgenic Tg(Thy1-CFP/COX8A)S2Lich/J mice (mitoCFP mice) that express cyan fluorescence protein (CFP) in neuronal mitochondria were imaged before (baseline image) and after the treatment with H_2O_2 or H_2O_2 + TFN. Then, the values of treated slices were normalized with their respective baseline images.

We observed that H_2O_2 reduced mitochondrial length (0.96 ± 0.37-fold (mean ± SD)) and that this effect was not abolished in the presence of TFN (0.97 ± 0.34-fold (mean ± SD)) (Figure 3C). However, the H_2O_2-induced reduction of mitochondrial area was partly prevented in presence of TFN treatment (data shown as mean ± SD: untreated: 0.97 ± 0.56-fold; H_2O_2: 0.82 ± 0.48-fold; and H_2O_2 ± TFN: 0.89 ± 0.47-fold) (Figure 3D) (Tables 1 and 2).

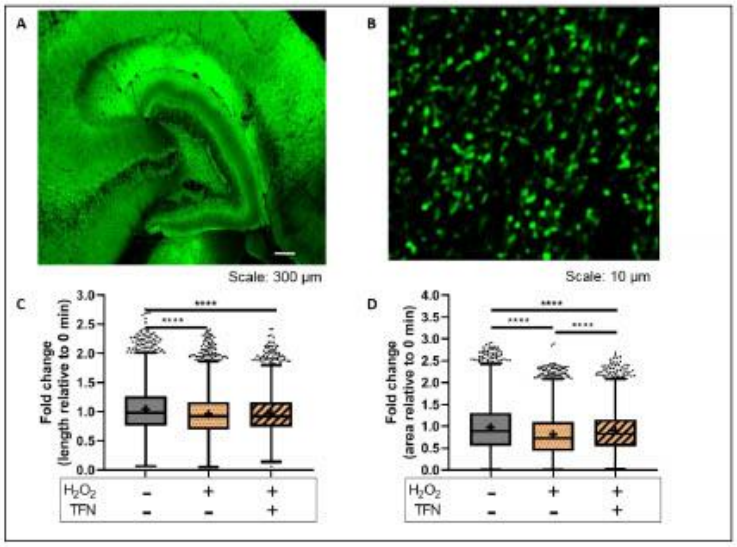

Figure 3. Mitochondrial morphology in brain tissue exposed to oxidative stress with/out TFN: (**A**) Representative confocal image of murine hippocampal section from mitoCFP mice. The fluorescence of cyan fluorescence protein in mitochondria is shown in green; (**B**) representative two-photon microscope image of murine hippocampal section from mitoCFP mice. Mitochondria are shown in green; fold change in (**C**) mitochondrial length and (**D**) mitochondrial area with respect to 0 min slice. Graphs are expressed as fold change with respect to the baseline and shown in Tukey boxplots. Inside the box, '+' delineates the mean. **** $p \leq 0.0001$.

Table 1. Mitochondrial length in acute hippocampal slices.

Length	All mitochondria Mean ± SD	Rod Mean + SD	Puncta Mean + SD	Network Mean + SD	Large Mean + SD
Untreated	1.04±0.40	1.12±0.52	1.02±0.43	0.96±0.45	0.98±0.45
H_2O_2	0.96±0.36	0.90±0.40	1.01±0.43	0.77±0.50	1.08±0.43
H_2O_2+TFN	0.97±0.34	0.88±0.41	1.00±0.36	0.98±0.45	0.94±0.33

*** $p \leq 0.001$, **** $p \leq 0.0001$.

Table 2. Mitochondrial area in acute hippocampal slices.

Area	All mitochondria Mean ± SD	Rod Mean + SD	Puncta Mean + SD	Network Mean + SD	Large Mean + SD
Untreated	0.97±0.56	1.04±0.66	1.01±0.65	0.85±0.60	0.61±0.48
H_2O_2	0.81±0.48	0.61±0.39	0.91±0.56	0.50±0.44	1.05±0.76
H_2O_2+TFN	0.89±0.47	0.63±0.40	0.96±0.51	0.92±0.62	0.91±0.60

** $p \leq 0.01$, **** $p \leq 0.0001$.

2.5. TFN Did Not Prevent Oxidative Stress-Mediated Alterations in Mitochondrial Motility in Acute Hippocampal Slices

To monitor effects of TFN on oxidative stress-induced motility alterations, we obtained time-lapse images of the slices before (baseline image) and after the treatment with H_2O_2 or H_2O_2 + TFN, as mentioned above. Mitochondrial motility-related parameters of treated slices were normalized to their respective baseline images as explained in the methods.

In our setup, the H_2O_2-induced decrease in mitochondrial displacement was further decreased in the presence of TFN (data shown as mean ± SD: H_2O_2 treated: 1.06 ± 0.66-fold and H_2O_2 + TFN treated: 0.88 ± 0.59-fold) (Figure 4A). Similarly, the H_2O_2- induced increase in mitochondrial speed was further increased by TFN treatment (H_2O_2: 0.78 ± 0.40-fold and H_2O_2 + TFN: 0.94 ± 0.56-fold) (Figure 4B) (Tables 3 and 4).

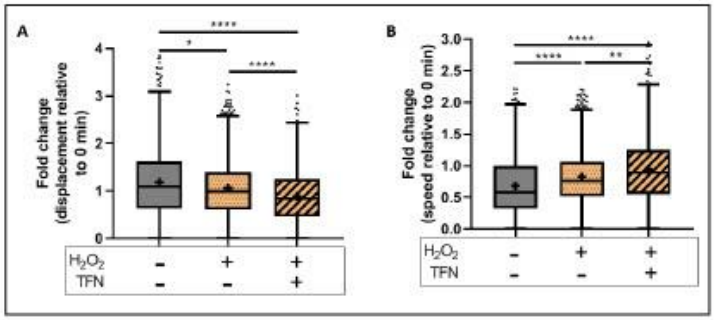

Figure 4. Mitochondrial motility in brain slices exposed to oxidative stress with the presence/absence of TFN: Fold change in (**A**) mitochondrial displacement and (**B**) motility speed with respect to 0 min slice. Graphs are expressed as fold change with respect to the baseline and shown in Tukey boxplots. Inside the box, '+' delineates the mean. '–' horizontally aligned with H_2O_2 and TFN denotes no H_2O_2 or TFN treatment. * $p \leq 0.05$, ** $p \leq 0.01$, and **** $p \leq 0.0001$.

Table 3. Mitochondrial displacement in acute hippocampal slices.

Displacement	All mitochondria Mean ± SD	Rod Mean + SD	Puncta Mean + SD	Network Mean + SD	Large Mean + SD
Untreated	1.18±0.78	1.28±0.80	1.18±0.55	1.18±0.93	1.65±1.77
H_2O_2	1.06±0.66	1.24±0.78	1.07±0.60	1.78±2.16	1.02±1.24
H_2O_2+TFN	0.88±0.59	0.41±0.54	1.01±0.56	0.90±0.60	0.74±1.10

* $p \leq 0.05$, ** $p \leq 0.01$, *** $p \leq 0.001$, and **** $p \leq 0.0001$.

Table 4. Mitochondrial speed in acute hippocampal slices.

Speed	All mitochondria Mean ± SD	Rod Mean + SD	Puncta Mean + SD	Network Mean + SD	Large Mean + SD
Untreated	0.66±0.45	0.96±0.34	1.03±0.36	0.98±0.80	1.18±1.29
H_2O_2	0.78±0.40	1.36±0.73	1.00±0.35	1.04±0.73	1.04±1.02
H_2O_2+TFN	0.94±0.55	1.35±2.30	1.06±0.39	1.21±1.03	0.75±0.91

* $p \leq 0.05$, ** $p \leq 0.01$, **** $p \leq 0.0001$.

2.6. TFN Prevented the Oxidative Stress-Promoted Decrease in Length of Network Mitochondria and Size of Puncta-Shaped and Network Mitochondria in Acute Hippocampal Slices

We know that mitochondria are dynamic organelles that can change their shape, ranging from punctuate structures to tubular networks depending on the cellular needs. Hence,

we processed the images and segmented the fluorescent mitochondria into four different morphological categories: rod-shaped, puncta-shaped, network, and large mitochondria. Morphological parameters of mitochondria in treated slices were renormalized to their respective baseline images (Figure 5).

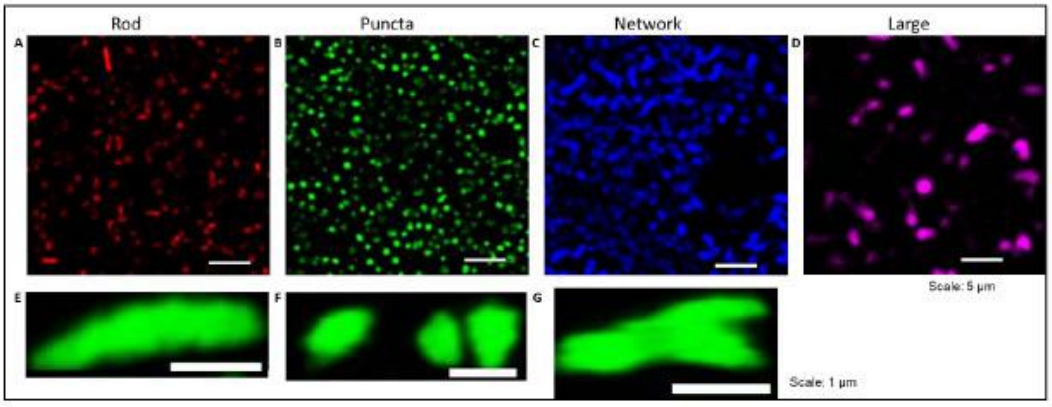

Figure 5. Morphotypes of mitochondria in murine acute hippocampal slices during oxidative stress with/out TFN. Representative segmented image of rod-shaped, puncta-shaped, network, and large mitochondria respectively (**A**–**D**). Representative image of an individual rod (**E**), puncta (**F**), and network (**G**) mitochondria.

To evaluate the morphological parameters of mitochondria in treated slices, data were normalized to their respective baseline images. We showed that oxidative stress reduced the length of rod-shaped, network, and large mitochondria, while the addition of TNF prevented these alterations in network and large types but not in rod-shaped mitochondria (Figure 6A–D) (in rod-shaped mitochondria shown as mean ± SD; untreated: 1.12 ± 0.52 length and 1.04 ± 0.66 area; H_2O_2: 0.90 ± 0.41 length and 0.62 ± 0.39 area; and H_2O_2 + TFN: 0.88 ± 0.41 length and 0.64 ± 0.40 area) (Tables 1 and 2).

TFN also prevented H_2O_2- induced area reduction in puncta, network, and large (here only a trend) forms (Figure 6E–H). Again, in rod-shaped mitochondria, TFN has no effects on H_2O_2-promoted size reduction. In the case of puncta-shaped mitochondria, there was no difference in the length (data shown as mean ± SD: untreated: 1.03 ± 0.43; H_2O_2: 1.01 ± 0.43; H_2O_2 + TFN: 1.00 ± 0.36); however, mitochondria became smaller (data shown as mean ± SD: untreated: 1.02 ± 0.65; H_2O_2: 0.91 ± 0.57) after exposure to H_2O_2. TFN-treatment prevented the reduction of mitochondrial size (0.96 ± 0.52). Similarly, TFN- treatment could prevent reduction in length and size of network-shaped mitochondria induced by H_2O_2 (data shown as mean ± SD: untreated: 0.96 ± 0.46 length, 0.85 ± 0.60 area; H_2O_2: 0.77 ± 0.51 length, 0.51 ± 0.45 area; H_2O_2 + TFN: 0.99 ± 0.45 length, 0.93 ± 0.62 area). In contrast, H_2O_2 induced the increase in length and size of large mitochondria (data shown as mean ± SD: untreated: 0.98 ± 0.46 and 0.61 ± 0.48 area; H_2O_2: 1.08 ± 0.44 length and 1.05 ± 0.76 area). TFN prevented the oxidative stress-related increase in length but not the area of large mitochondria (data shown as mean ± SD: 0.95 ± 0.33 length and 0.91 ± 0.61 area) (Tables 1 and 2).

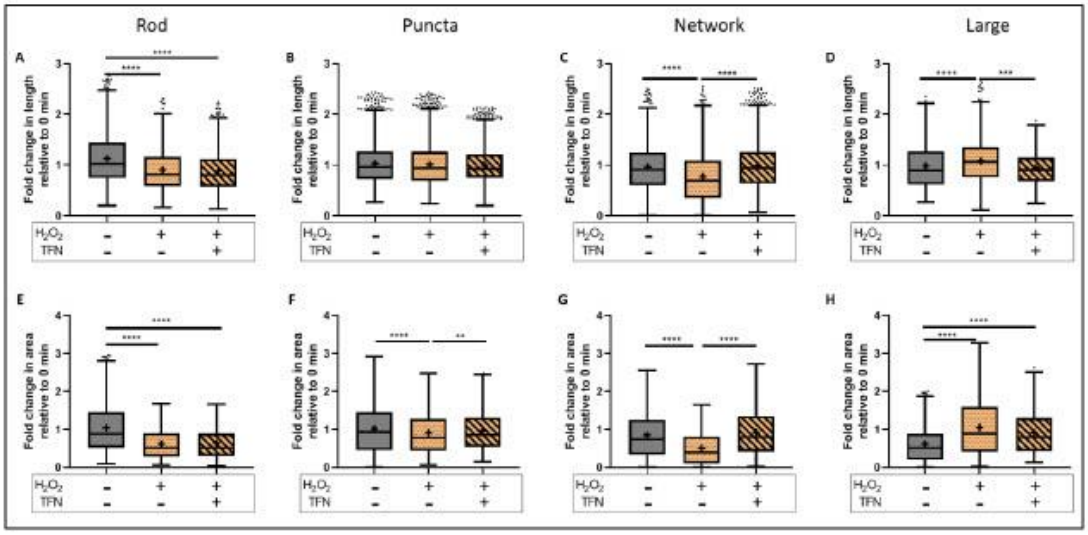

Figure 6. Morphological alterations in different mitochondrial morphotypes during induced oxidative stress with/out TFN. Fold change in length of rod-shaped (**A**), puncta-shaped (**B**), network (**C**), and large mitochondria (**D**) during oxidative stress with/out TFN relative to 0 min slices. Fold change in area of rod-shaped (**E**), puncta-shaped (**F**), network (**G**), and large mitochondria (**H**) during oxidative stress with/out TFN relative to 0 min slices. Graphs are expressed as fold change with respect to the baseline and shown in Tukey boxplots. Inside the box, '+' delineates the mean. '−' horizontally aligned with H_2O_2 and TFN denotes no H_2O_2 or TFN treatment. ** $p \leq 0.01$, *** $p \leq 0.001$, and **** $p \leq 0.0001$.

2.7. TFN Enhanced Mitochondrial Speed in Puncta-Shaped Mitochondria in Acute Hippocampal Slices Exposed to Oxidative Stress

Similarly, we investigated the motility parameters using the time-lapse images (Figure 7). We observed that TFN reduced the displacement of all mitochondrial forms as shown in Figure 7A–D (data shown as mean ± SD: untreated: 1.08 ± 0.8 (rod), 1.18 ± 0.55 (puncta), 1.19 ± 0.93 (network), 1.65 ± 1.77 (large); H_2O_2 + TFN: 0.42 ± 0.55 (rod), 1.01 ± 0.57 (puncta), 0.91 ± 0.60 (network), and 0.75 ± 1.11 (large)). Additionally, in case of rod-shaped and network mitochondria, it accentuated the effect of H_2O_2 (data shown as mean ± SD: 1.08 ± 0.68 (rod), 1.08 ± 0.60 (puncta), 1.78 ± 2.16 (network), and 1.02 ± 1.25 (large)) (Table 3). Furthermore, TFN enhanced the effect of H_2O_2, increasing the speed in puncta-shaped and network mitochondria and decreasing speed of the large morphotype (Figure 7E–H) (data shown as mean ± SD: untreated: 0.73 ± 0.38 (rod), 0.78 ± 0.43 (puncta), 0.44 ± 0.31 (network), 1.18 ± 1.29 (large); H_2O_2: 0.85 ± 0.60 (rod), 0.91 ± 0.37 (puncta), 0.94 ± 0.65 (network), 1.05 ± 1.03 (large); H_2O_2 + TFN: 0.56 ± 0.51 (rod), 1.07 ± 0.39 (puncta), 1.01 ± 0.76 (network), and 0.75 ± 0.91 (large)) (Table 4).

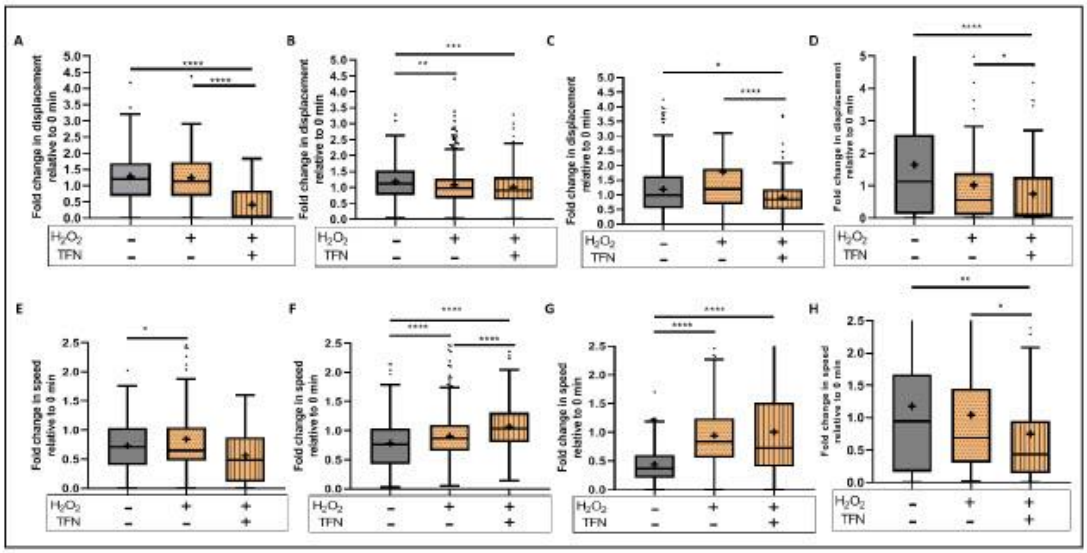

Figure 7. Motility alterations in different mitochondrial morphotypes during induced oxidative stress with/out TFN: Fold change in displacement of rod-shaped (**A**), puncta-shaped (**B**), network (**C**), and large mitochondria (**D**) during oxidative stress with/out TFN relative to 0 min slices. Fold change in transportation speed of rod-shaped (**E**), puncta-shaped (**F**), network (**G**), and large mitochondria (**H**) during oxidative stress with/out TFN relative to 0 min slices. Graphs are expressed as fold change with respect to the baseline and shown in Tukey boxplots. Inside the box, '+' delineates the mean. '−' horizontally aligned with H_2O_2 and TFN denotes no H_2O_2 or TFN treatment. * $p \leq 0.05$, ** $p \leq 0.01$, *** $p \leq 0.001$, and **** $p \leq 0.0001$.

3. Discussion

Mitochondrial alteration during inflammation is one of the major factors that contribute to neurodegeneration in inflammatory diseases such as MS. Thus, besides the importance of controlling inflammation, MS treatments should also aim at protecting mitochondria from damage [17]. In this context, we have investigated the therapeutic potential of the DHODH inhibitor TFN, an approved drug for the treatment of RRMS [19,20], on both neuronal and mitochondrial protection. Using a model in peripheral root explants, we have previously shown that mitochondria become shorter and rounder, and were less motile, during oxidative stress [28,30]. Importantly, using this model of peripheral nerves, we recently demonstrated that TFN could prevent the morphologic alterations of axonal mitochondria caused by oxidative stress [28]. To understand the effect of TFN on neuronal activity and neuronal mitochondria within the CNS, we used here acute hippocampal sections from transgenic mice that express CFP in neuronal mitochondria. To induce oxidative stress on neurons, slices were treated with H_2O_2, and the effects of TFN on H_2O_2-mediated neuronal and mitochondria changes were investigated. In the CNS slice model, TFN was used at a concentration of 50 µM. Using peripheral spinal root explants, we have already previously shown that TFN prevented oxidative stress-induced mitochondrial alterations at 1 µM concentrations [28]. However, since in the CNS sections the TFN dissolved in DMSO had to penetrate to depths of 50–100 µm, 50 µM of TFN was used to ensure sufficient diffusion into the tissue slices.

Our findings with electrophysiological recordings of pO_2 and LFP revealed that TFN treatment could prevent the reduction of oxygen consumption and synaptic transmission upon the induced oxidative insult. An increment in pO_2 with respect to the baseline recording during oxidative stress (Figure 1C,D) suggested a decrease in the consumption

of oxygen, and hence, slower oxidative metabolism in the tissue. TFN could prevent this effect (Figure 1D), as pO_2 decrease corresponds to increased oxygen consumption, and hence, suggests a restoration of the metabolic activity.

In addition, in the tissue exposed to oxidative stress we observed a decrement in LFP, clearly signaling the depression of neuronal firing. This is in line with the report of Ohashi et al., 2016, which showed H_2O_2-induced reduction in neuronal excitability in ventral horn neurons [31]. The depression in neuronal firing was prevented by TFN (Figure 1E). Importantly, inhibition of DHODH by TFN does not seem to cause depletion in neuronal activity. DHODH is associated with the mitochondrial respiratory chain, and according to Scialo et al., 2017, DHODH reduces ubiquinone in the process of the conversion of dihydroorotate during pyrimidine biosynthesis. Evidence shows that when ubiquinone becomes over-reduced, it can cause reverse electron transfers that are associated with excessive ROS production and causes Complex V to stop producing ATP [32]. Thus, DHODH-inhibition with TFN might affect mitochondrial respiratory chains/electron transport chains (ETC) and preserve neuronal functions. Moreover, we could not discount that these observations may be mediated by DHODH-independent effects of TFN, since it has been well established that TFN can inhibit different kinases at concentrations higher than 50 µM [20]. In our model, TFN does not cause any neuronal or tissue damage, however, based on the recent reports of existence of the de novo pathway for pyrimidine synthesis in the adult brain, we cannot exclude that in other contexts, TFN may affect neuronal cells by altering pyrimidine biosynthesis, [33].

Additionally, we observed that the amount of ATP decreases during oxidative stress, as already reported in the context of neuroinflammation [26,34]. ATP depletion could not be prevented by TFN in our set-up (Figure 2). However, diminished amounts of ATP do not appear to affect neuronal activity. This could mean that with TFN treatment, ATP synthesis has decreased either in response to acute stress or as a result of increasing mitochondrial movement. Another possible explanation could be that ATP consumption increased without negatively affecting the mitochondrial electron transport chain (ETC).

Furthermore, looking at the mitochondrial dynamics, we observed a reduction in mitochondrial length and area in acute hippocampal slices exposed to oxidative stress (Figure 3C,D), which is in line with our previous observations in peripheral root explants [28,30]. TFN reduced the length of mitochondria but not their area, implying changes in mitochondrial morphology, but not necessarily fragmentation. In consistent with this, a segregated morphological analysis of puncta, rod, network, and large mitochondria indicated an increase in networks rather than fragmentation (Figure 3C,D and Figure 6A–D). Thus, in consistent with our reports on peripheral root explants [28], TFN could prevent both oxidative stress-induced reductions in the mitochondrial area and fragmentation of mitochondria in acute brain slices. However, within the CNS, TFN promoted a reduction in mitochondrial displacement [28]. Interestingly, an increment of speed was observed during both oxidative stress alone and with TFN treatment along with oxidative stress (Figure 4A,B), suggesting the differences in mitochondrial dynamics in different tissue types.

To better understand which alterations of mitochondrial dynamics occur during the treatments, we categorized mitochondria in four different morphological categories. It is well established that, depending upon the cellular demand, mitochondria undergo fusion, fission, or biogenesis, and adopt a variety of forms or stages as part of mitochondrial homeostasis [35]. Mitochondrial shape could reflect different functional stages associated for instance with ATP generation, mitochondrial DNA segregation, calcium buffering, and the removal of damaged portions from mitochondria or mitophagy [36–41]. In this context, we observed a decrease in the length and area of rod-shaped and network mitochondria during oxidative stress (Figure 6A,C,E,G), suggesting that mitochondria are undergoing fragmentation, probably to eliminate depolarized mitochondria as a compensatory mechanism to increase the number of healthy functional mitochondria during stress situations [41]. On the other hand, the network mitochondria that are formed due

to mitochondrial fusion [37,39,40] (Figure 5C,G) are important for buffering the damages, to get rid of the damaged portions, and distribution of functional portions [40,41]. The formation of large networks in response to stress was demonstrated in 2009 by Tondera et al. Importantly, the authors showed that this process of stress-induced mitochondrial hyperfusion (SIMH) is associated with an elevated production of mitochondrial ATP and represents an adaptive pro-survival response against stress [42]. Van der Bliek, 2009, further suggests that the fate of mitochondria is determined by the level of stress. While low stress might lead the mitochondria into SIMH, high and prolonged stress might promote the apoptotic fragmentation path [35]. Thus, TFN seems to reduce stress induced by H_2O_2 on neurons via DHODH-inhibition. The changes affecting network mitochondria may also lead to deficient ATP, also observed under oxidative stress, since, depending upon energy demand, mitochondria may form a network and get involved in ATP synthesis [36,38].

Additionally, during oxidative stress, the length and area increased for large mitochondria (Figure 6D,H), suggesting mitochondrial swelling. In general, large, and intensely fluorescent mitochondria indicate mitochondrial swelling and mitochondria undergoing mitophagy [37,39] (Figure 5D). Thus, the observed oxidative stress-mediated mitochondrial fragmentation and swelling within the CNS tissue suggests that mitochondria are unable to recover and do undergo degradation [37,39]. The addition of TFN during oxidative stress prevented oxidative stress-induced reduction in size of puncta-shaped mitochondria, and the reduction of both the length and size of network mitochondria (Figure 6B,F,G). It could be that TFN either prevented mitochondrial fission or promoted mitochondrial fusion to buffer the damages during oxidative stress. Moreover, the polarization of mitochondria seems to be maintained, as depicted by their ability to fuse [41] and form networks with TFN treatment. This is consistent with the findings by Miret-Casals et al. on mitochondrial fusion and elongation during DHODH-inhibition and limitation in the respiratory chain in proliferating cells [43].

Regarding mitochondrial motility, we observed during oxidative stress a significant reduction in the displacement of puncta-shaped mitochondria (Figure 7B), and an increment in the speed of rod-shaped, puncta-shaped and network mitochondria (Figure 7E–G), implying short distance mitochondrial transportation, in consistent with our observation in peripheral root explants [28]. However, oxidative stress induced comparatively faster mitochondrial movement with respect to the untreated slices (Figure 7E–H). This observation differs from the slow transport observed in peripheral root explants upon oxidative stress [28]. As we observed an increase in mitochondrial networks, the mitochondria that might fuse together to form networks might not need to travel longer and faster. TFN did not prevent these alterations but, apparently, induced an additional decrease in displacement and increase in the speed of puncta-shaped mitochondria, probably because they were forming the networks. Moreover, it has been reported that other factors, such as the depolymerization of cytoskeletal systems, may lead to impaired mitochondrial transportation. In this context, Zhang et al., 2018, demonstrated a H_2O_2- induced depolymerization of ß-actin filaments in neuronal cell lines incubated for 24 h with 200 µM H_2O_2 [44]. Such an effect is, however, very improbable in our experimental brain slices, which were incubated for only 30 min with H_2O_2.

Our study presents several limitations. Although the concentrations of H_2O_2 and TFN added to the brain sections were known, and in the case of H_2O_2 could be considered as unphysiological, the exact concentration of both substances at the depths at which we imaged the slices remained undetermined and are probably much lower. Moreover, the measurement of activity of DHODH in our experiment would have given more confirmative value to our existing results. Furthermore, we performed a two-dimensional analysis of the mitochondria, which may lead to errors in the estimations of shape and motility. However, since images under H_2O_2 stress and/or TFN conditions were corrected for time and compared to their corresponding baseline images, we consider that the errors introduced by the 2D analyses were minimized. An additional limitation is that, due to extremely high amounts of measured mitochondria, the semi-automated analysis could

not be accurately confirmed by manual analysis. Additionally, we were unable to precisely determine mitochondrial boundary for the measurement using manual analysis, unlike in pixel-based measurements performed by the semi-automated analysis.

In summary, preventing the depletion of the oxidative metabolism and the alterations in mitochondrial motility might contribute to the preservation of neuronal firing in neuronal tissue treated with TFN during oxidative stress. We believe that the depletion of ATP does not necessarily mean energy failure but may reflect an enhanced consumption of ATP or slight shortcoming of ATP synthesis, while still maintaining the ETC as well as neuronal activity. In this context, as mentioned before, TFN may not negatively affect ETC when applied alone or together with hydrogen peroxide [45], but it seems to efficiently buffer mitochondrial damage, which could protect mitochondria against degradation. Thus, TFN seem to protect CNS tissue from oxidative damage. The protective effect seems to be mediated by its ability to prevent decrease in oxygen metabolism and neuronal activity, and its effect on mitochondrial dynamics.

4. Materials and Methods

4.1. Experimental Design and Settings

All the experiments were performed on the acute hippocampal slices of murine brain. The investigation of oxygen metabolism and synaptic transmission was performed simultaneously in an interface recording chamber with a continuous flow of carbogenated aCSF. After the initial baseline recording, the slices were treated with TFN and/or H_2O_2 and the second recordings were performed. For the analysis, after-treatment recordings were normalized to the baseline recordings. For the ATP assay, we treated acute hippocampal slices in continuously carbogenated HEPES aCSF. For the investigation of mitochondrial dynamics, we prepared acute hippocampal slices from mitoCFP mice brains and continuously supplied carbogenated HEPES aCSF to the slices. Mitochondrial images were taken using a two-photon microscope. Initial control images of mitochondria in the region of interest were captured. Then, the second images of the same region of interest were captured after the treatment. After-treatment analyses were normalized to the initial control images.

4.2. Experimental Animals and Ethics Statement

WT C57BL/6 mice were obtained from the Research Institute for Experimental Medicine—Forschungseinrichtungen für Experimentelle Medizin (FEM) at the Charité- Universitätsmedizin (Berlin, Germany). Breeding of transgenic Tg(Thy1-CFP/COX8A)S2Lich/J mice (*mitoCFP* mice) that express cyan fluorescence protein (CFP) in neuronal mitochondria was conducted at the FEM under specific pathogen-free conditions. All experimental procedures were conducted in strict accordance with Directive 2010/63/EU of the European Parliament and of the Council of 22 September 2010 and were approved by the Regional Animal Study Committee of Berlin, (LAGeSo-Landesamt für Gesundheit und Soziales Berlin), approvals ID: G0101-14 and T0002-10.

4.3. Preparation of Acute Hippocampal Sections

A quantity of 400 µm-thick acute brain slices were prepared based on the modified protocol from Nitsch et al., 2004 [29]. Hippocampal sections were obtained by slicing the 2/3rd of the caudal cerebral region. The intermediate hippocampal sections were used for the imaging experiments, as sections with comparable sizes could be generated from this region. Once the slices were obtained, the hippocampal region was dissected, preserving the hippocampal formation using the scalpel and the light microscope.

Brain slices were continuously supplied with carbogen (95% O_2 and 5% CO_2) in HEPES artificial cerebrospinal fluid (HEPES aCSF) (in mM: 92 NaCl, 2.5 KCl, 1.25 NaH_2PO_4, 30 $NaHCO_3$, 20 HEPES, 25 Glucose, 5 Sodium ascorbate, 2 Thiourea, 3 Sodium pyruvate, 2 $MgCl_2$, 2 $CaCl_2$). The solutions were freshly prepared, and the pH adjusted between 7.3 and 7.4. The whole procedure was performed in temperatures between 34 and 37 °C.

To induce oxidative stress, acute slices were incubated for 30 min with hydrogen peroxide (H_2O_2) dissolved in aCSF. In our previous studies, 200 µM H_2O_2 induced mitochondrial damage [30], while 50 µM H_2O_2 induced only mitochondrial alterations [28]. Gülden et al., 2010, reported minimal cytotoxicity in cells cultured with 100 or 200 µM H_2O_2 for 1 h [46]. Hence, in our CNS model, we used 100 µM H_2O_2 for incubation in submerged chamber during mitochondrial imaging experiments to ensure diffusion of H_2O_2 inside the 400 µm-thick brain slices. Since, H_2O_2 concentrations are known to quickly decrease after short period of time [46,47], 200 µM H_2O_2 was used in the interface chamber during the electrophysiology experiments to ensure adequate H_2O_2 availability to the slices in air-water interface, unlike in submerged chamber where the slices are inside the solution. The other treatment groups were DMSO (0.0005%), H_2O_2 (100 µM) +DMSO (0.0005%), and H_2O_2 (100 µM), along with TFN (50 µM) and TFN (50 µM) alone. DMSO was used as a vehicle control for TFN.

4.4. Simultaneous Electrophysiology and Oxygen Partial Pressure (pO_2) Recordings in Hippocampal Slices

Hippocampal slices (400 µm thickness) were prepared using a Leica VT1200 S vibratome (Leica, Wetzlar, Germany), as mentioned above. The slices were stored in an interface chamber and continuously supplied with freshly prepared and carbogenated aCSF (in mM: 129 NaCl, 21 $NaHCO_3$, 10 Glucose, 3 KCl, 1.25 NaH_2PO_4, 1.6 $CaCl_2$, and 1.8 $MgCl_2$) for at least 90 min before the investigation (temperature ~34 °C). To induce oxidative stress, 200 µM H_2O_2 was added to the bath solution for 30 min.

Stimulus-induced population spikes (PS) and pO_2 were recorded using a glass microelectrode filled with 154 mM NaCl and a Clark-style oxygen electrode (tip diameter: 10 µm; Unisense, Aarhus, Denmark), respectively. Both electrodes were placed in the stratum pyramidale of the CA1 area while stimulation (2 pulses of 100 µs duration with a 50 ms interval every minute) was performed with a stimulation electrode placed in the stratum radiatum between CA3 and CA1 using a Master 8 system (A.M.P.I., Jerusalem, Israel). To measure changes in neuronal respiration, the pO_2 electrode was advanced in 20 µm steps through the slices using a calibrated micromanipulator (Narishige, Tokyo, Japan). In the in vitro condition, pO_2 distribution depends on cellular O_2-consumption since O_2 diffusion and solubility are constant [48]. Typically, a vertical O_2-gradient can be measured, from the surface till the core of the slice, the depth in which pO_2 ceases to decrease. For electrophysiology measurements, baseline measurements were performed at 100 µm below the tissue surface for 15 min before and after 30 min treatment with H_2O_2 and H_2O_2 + TFN. Analog signals were digitalized using a Power1401 and recorded using Spike 2 software (Cambridge Electronic Design Limited, Cambridge, UK) for the recording. Offline analysis of the data was performed using Spike2.

4.5. Adenosine Triphosphate (ATP) Assay

After the treatment of the slices, ATP assay was performed using the Abcam ATP assay kit (Abcam, ab83355) according to the manufacture's protocol. Briefly, the tissue was homogenized in ATP assay buffer and centrifuged at 13,000× *g* for 5 min. Then, the supernatant was collected and deproteinization with perchloric acid (PCA) was performed. ATP standards, in the range of 0 to 1 nmol, as well as samples, were then incubated with reaction-mix for 30 min. The fluorometric detection was performed at 535/587 nm in a plate reader (GloMax®-Multi Detection System, Promega Corporation, Madison, WI, USA). The calculation of the amount of the ATP in each slice was performed after the subtraction of the sample background and with the multiplication of the dilution factor, as described in the protocol by the manufacture.

4.6. Mitochondrial Imaging Using Two-Photon Laser Scanning Microscope in Acute Hippocampus Sections

To image mitochondria in slices prepared from the mitoCFP transgenic mouse (Tg(Thy1-CFP/COX8A)S2Lich/J), an 830nm excitation wavelength and photomultiplier at 525 nm with 50 nm bandwidth was selected.

At first, a region of interest (ROI) was selected and a time-lapse image stack of 30 steps with intervals of 3.6 s was obtained. Then, aCSF along with treatment was added without moving the objective or the holding chamber. After 30 min, the same region was imaged again with same setting. This procedure was repeated with each single treatment group.

4.7. Image Analysis of Mitochondrial Morphology and Dynamics in Acute Hippocampal Slices

Huygens deconvolution Scientific Volume Imaging software (SVI, The Netherlands) was applied for the restoration of mitochondrial images obtained with two-photon microscopy. Images were opened in Huygens professional X11 and enabled automatic computation of point spread function (PSF). Then, the images were inspected with the logarithmic vertical mapping function. Once, the PSF was computed, the Classic Maximum Likelihood Estimation (CMLE) algorithm was applied to obtain effectively deconvolved images.

Images were corrected for the background noise and image movement using Fiji Is Just ImageJ (Fiji) software [49,50]. The correction of the movement of the images was conducted using StackReg plugin [51]. After the preprocessing of the images, segmentation of mitochondria was preformed using Trainable Weka segmentation plugin in Image J software. All the automation for the analysis was controlled and supervised by the experimenter.

For morphology analysis, the corrected images were first segmented with Trainable Weka segmentation plugin in Image J software [52]. A few mitochondria and backgrounds were selected in each image for the plugin to train itself. However, the segmentation output was not satisfactory; subsequently, the plugin was given more examples of mitochondria and backgrounds. Then, the probability map of the segmented mitochondria was used for the analysis with Volocity 6.3 software (Perkin Elmer, Rodgau, Germany). In Volocity software, the mitochondria were identified based on the fluorescence intensity threshold against the background and noises, and the measurements for the length and area of the selected objects were extracted.

For motility analysis, from the corrected images, five random ROIs within the image were selected. Then, each ROI was separately processed into Track mate plugin [53] for tracking mitochondrial transport (Supplementary Videos S1 and S2. The measurements of mitochondrial speed and displacement were extracted for further analysis).

4.8. Statistical Analysis

The data were analyzed with the Prism software (GraphPad, San Diego, CA, USA). First, the Gaussian distribution of the variables was confirmed using all the three normality tests— KS, D'Agostino and Pearson omnibus, and Shapiro–Wilk. Non-normally distributed data were treated as non-parametric. Comparisons between the two groups were performed by *t*-test for the normal parametric data. Comparisons between two groups of non-parametric data were performed by Mann–Whitney U test. Comparison between more than two groups were analyzed with one-way analysis of variance and with Kruskal–Wallis test for non-parametric data followed by Dunn's post hoc test. All the data are shown as mean ± SD. The data are shown as Tukey boxplot where the central line denotes the median; the lower and upper boundaries denote the 1st and 3rd quartile, and the whiskers denote the data except the outliers presented as individual dots. The outliers were not included in the analysis. p values ≤ 0.05 were considered significant. The significance of the data was further depicted as * $p \leq 0.05$, ** $p \leq 0.01$, *** $p \leq 0.001$, and **** $p \leq 0.0001$.

5. Conclusions

Here, we conclude that TFN contributes to mitochondrial protection during oxidative stress. The drug might influence mitochondrial bioenergetics by reversibly limiting the

reduction of flavin mononucleotide (FMN) via DHODH and thus, electron transport in the ETC [54]. This in turn reduces ROS production, as ETC is one of the major ROS producers, while the intracellular antioxidants work against the extracellular ROS. Additionally, due to the presence of multiple electron donor complexes, the ETC is not completely shut off. Thus, TFN does not significantly depress the ATP synthesis and helps maintain mitochondrial dynamics and neuronal activity.

Supplementary Materials: The following supporting information can be downloaded at: https://www.mdpi.com/article/10.3390/ijms23031538/s1.

Author Contributions: Conceptualization: B.M., H.B., F.P., A.E.H., R.N. and C.I.-D.; data curation, B.M.; formal analysis, B.M. and A.L.; funding acquisition, C.I.-D.; investigation, B.M. and A.L.; methodology, B.M., A.L., H.B. and R.U.; project administration, C.I.-D.; resources, A.E.H., R.N. and C.I.-D.; supervision, F.P. and C.I.-D.; visualization, B.M.; writing—original draft, B.M.; writing—review and editing, B.M., R.U., F.P., A.E.H., R.N. and C.I.-D. All authors have read and agreed to the published version of the manuscript.

Funding: This study was funded by a research grant from Sanofi Genzyme (grant number GZ-2015-11386). The study was also supported by the Charité Universitätsmedizin and by a fellowship from Berlin Institute of Health (BIH) to R. Ulshöfer. The work of C. Infante-Duarte and A. Hauser was supported by the DFG (SFB1340-1 to C.I.D) and SPP2332 (HA5354/11-1) and SFB 1444/P14 to A.E.H.

Institutional Review Board Statement: All experimental procedures were reviewed and approved by the local authority on animal studies in Berlin Landesamt für Gesundheit und Soziales Berlin (LaGeSo). Animal studies were performed in strict accordance with the European Communities Council Directive of 22 September 2010 (2010/63/EU).

Informed Consent Statement: Not applicable.

Data Availability Statement: The datasets during and/or analyzed during the current study available from the corresponding author on reasonable request.

Acknowledgments: We thank Natascha Asselborn, Robert Günther, Daniel Bremer, Ruth Leben, and Asylkhan Rakhymzhan for their support, valuable suggestions and constructive criticism.

Conflicts of Interest: B.M., A.L., H.B., R.U., A.E.H. and R.N. declare no conflict of interest. F.P. reports funding for travel or speaker honoraria from Bayer, Novartis, Biogen Idec, Teva, Sanofi-Aventis/Genzyme, Merck Serono, Alexion, Chugai, MedImmune, Shire, Roche, Actelion, and Celgene and research support from Bayer, Novartis, Biogen Idec, Teva, Sanofi-Aventis/Genzyme, Alexion, Merck Serono, and the German Research Council (DFG Exc 257). C.I.-D. reports research grants from Novartis, Sanofi Genzyme, and DFG (German Research Council), as well as conference honoraria from Sanofi Genzyme and Novartis.

References

1. Dobson, R.; Giovannoni, G. Multiple sclerosis—A review. *Eur. J. Neurol.* **2019**, *26*, 27–40. [CrossRef] [PubMed]
2. Lassmann, H. Multiple Sclerosis Pathology. *Cold Spring Harb. Perspect. Med.* **2018**, *8*, a028936. [CrossRef] [PubMed]
3. Thompson, A.J.; Baranzini, S.E.; Geurts, J.; Hemmer, B.; Ciccarelli, O. Multiple sclerosis. *Lancet* **2018**, *391*, 1622–1636. [CrossRef]
4. Dendrou, C.A.; Fugger, L.; Friese, M.A. Immunopathology of multiple sclerosis. *Nat. Rev. Immunol.* **2015**, *15*, 545–558. [CrossRef] [PubMed]
5. Sospedra, M.; Martin, R. Immunology of Multiple Sclerosis. *Semin. Neurol.* **2016**, *36*, 115–127. [CrossRef]
6. Mossakowski, A.A.; Pohlan, J.; Bremer, D.; Lindquist, R.; Millward, J.M.; Bock, M.; Pollok, K.; Mothes, R.; Viohl, L.; Radbruch, M.; et al. Tracking CNS and systemic sources of oxidative stress during the course of chronic neuroinflammation. *Acta Neuropathol.* **2015**, *130*, 799–814. [CrossRef]
7. Barsukova, A.G.; Forte, M.; Bourdette, D. Focal Increases of Axoplasmic Ca^{2+}, Aggregation of Sodium-Calcium Exchanger, N-type Ca^{2+} Channel, and Actin Define the Sites of Spheroids in Axons Undergoing Oxidative Stress. *J. Neurosci.* **2012**, *32*, 12028–12037. [CrossRef]
8. Lassmann, H. Targets of therapy in progressive MS. *Mult. Scler. J.* **2017**, *23*, 1593–1599. [CrossRef]
9. De Barcelos, I.P.; Troxell, R.M.; Graves, J.S. Mitochondrial Dysfunction and Multiple Sclerosis. *Biology* **2019**, *8*, 37. [CrossRef]
10. Federico, A.; Cardaioli, E.; Da Pozzo, P.; Formichi, P.; Gallus, G.N.; Radi, E. Mitochondria, oxidative stress and neurodegeneration. *J. Neurol. Sci.* **2012**, *322*, 254–262. [CrossRef]

11. Mahad, D.H.; Trapp, B.D.; Lassmann, H. Pathological mechanisms in progressive multiple sclerosis. *Lancet Neurol.* **2015**, *14*, 183–193. [CrossRef]
12. Nikic, I.; Merkler, D.; Sorbara, C.; Brinkoetter, M.; Kreutzfeldt, M.; Bareyre, F.M.; Brück, W.; Bishop, D.; Misgeld, T.; Kerschensteiner, M. A reversible form of axon damage in experimental autoimmune encephalomyelitis and multiple sclerosis. *Nat. Med.* **2011**, *17*, 495–499. [CrossRef] [PubMed]
13. Mahad, D.; Ziabreva, I.; Lassmann, H.; Turnbull, D. Mitochondrial defects in acute multiple sclerosis lesions. *Brain* **2008**, *131*, 1722–1735. [CrossRef] [PubMed]
14. Stys, P.K.; Zamponi, G.W.; Van Minnen, J.; Geurts, J.J.G. Will the real multiple sclerosis please stand up? *Nat. Rev. Neurosci.* **2012**, *13*, 507–514. [CrossRef] [PubMed]
15. Faissner, S.; Plemel, J.R.; Gold, R.; Yong, V.W. Progressive multiple sclerosis: From pathophysiology to therapeutic strategies. *Nat. Rev. Drug Discov.* **2019**, *18*, 905–922. [CrossRef]
16. Campbell, G.; Licht-Mayer, S.; Mahad, D. Targeting mitochondria to protect axons in progressive MS. *Neurosci. Lett.* **2019**, *710*, 134258. [CrossRef]
17. Bargiela, D.; Chinnery, P.F. Mitochondria in neuroinflammation—Multiple sclerosis (MS), leber hereditary optic neuropathy (LHON) and LHON-MS. *Neurosci. Lett.* **2019**, *710*, 132932. [CrossRef]
18. Baecher-Allan, C.; Kaskow, B.J.; Weiner, H.L. Multiple Sclerosis: Mechanisms and Immunotherapy. *Neuron* **2018**, *97*, 742–768. [CrossRef]
19. Miller, A.E. Oral teriflunomide in the treatment of relapsing forms of multiple sclerosis: Clinical evidence and long-term experience. *Ther. Adv. Neurol. Disord.* **2017**, *10*, 381–396. [CrossRef]
20. O'Connor, P.; Comi, G.; Freedman, M.S.; Miller, A.E.; Kappos, L.; Bouchard, J.-P.; Lebrun-Frenay, C.; Mares, J.; Benamor, M.; Thangavelu, K.; et al. Long-term safety and efficacy of teriflunomide: Nine-year follow-up of the randomized TEMSO study. *Neurology* **2016**, *86*, 920–930. [CrossRef]
21. Keen, H.I.; Conaghan, P.; Tett, S.E. Safety evaluation of leflunomide in rheumatoid arthritis. *Expert Opin. Drug Saf.* **2013**, *12*, 581–588. [CrossRef] [PubMed]
22. Bar-Or, A. Teriflunomide (Aubagio®) for the treatment of multiple sclerosis. *Exp. Neurol.* **2014**, *262 Pt A*, 57–65. [CrossRef]
23. Boukalova, S.; Hubackova, S.; Milosevic, M.; Ezrova, Z.; Neuzil, J.; Rohlena, J. Dihydroorotate dehydrogenase in oxidative phosphorylation and cancer. *Biochim. Biophys. Acta (BBA)-Mol. Basis Dis.* **2020**, *1866*, 165759. [CrossRef] [PubMed]
24. Kretzschmar, B.; Pellkofer, H.; Weber, M.S. The Use of Oral Disease-Modifying Therapies in Multiple Sclerosis. *Curr. Neurol. Neurosci. Rep.* **2016**, *16*, 38. [CrossRef] [PubMed]
25. Kieseier, B.C.; Warnke, C.; zu Horste, G.M.; Hartung, H.-P.; Stüve, O. Review of teriflunomide and its potential in the treatment of multiple sclerosis. *Neuropsychiatr. Dis. Treat.* **2009**, *5*, 333–340. [CrossRef]
26. Friese, M.A.; Schattling, B.; Fugger, L. Mechanisms of neurodegeneration and axonal dysfunction in multiple sclerosis. *Nat. Rev. Neurol.* **2014**, *10*, 225–238. [CrossRef] [PubMed]
27. Tanaka, M.; Vécsei, L. Monitoring the Redox Status in Multiple Sclerosis. *Biomedicines* **2020**, *8*, 406. [CrossRef] [PubMed]
28. Malla, B.; Cotten, S.; Ulshoefer, R.; Paul, F.; Hauser, A.E.; Niesner, R.; Bros, H.; Infante-Duarte, C. Teriflunomide preserves peripheral nerve mitochondria from oxidative stress-mediated alterations. *Ther. Adv. Chronic Dis.* **2020**, *11*, 2040622320944773. [CrossRef]
29. Nitsch, R.; Pohl, E.E.; Smorodchenko, A.; Infante-Duarte, C.; Aktas, O.; Zipp, F. Direct Impact of T Cells on Neurons Revealed by Two-Photon Microscopy in Living Brain Tissue. *J. Neurosci.* **2004**, *24*, 2458–2464. [CrossRef]
30. Bros, H.; Millward, J.M.; Paul, F.; Niesner, R.; Infante-Duarte, C. Oxidative damage to mitochondria at the nodes of Ranvier precedes axon degeneration in ex vivo transected axons. *Exp. Neurol.* **2014**, *261*, 127–135. [CrossRef]
31. Ohashi, M.; Hirano, T.; Watanabe, K.; Shoji, H.; Ohashi, N.; Baba, H.; Endo, N.; Kohno, T. Hydrogen peroxide modulates neuronal excitability and membrane properties in ventral horn neurons of the rat spinal cord. *Neuroscience* **2016**, *331*, 206–220. [CrossRef]
32. Scialò, F.; Fernández-Ayala, D.J.; Sanz, A. Role of Mitochondrial Reverse Electron Transport in ROS Signaling: Potential Roles in Health and Disease. *Front. Physiol.* **2017**, *8*, 428. [CrossRef] [PubMed]
33. Löffler, M.; Carrey, E.A.; Zameitat, E. New perspectives on the roles of pyrimidines in the central nervous system. *Nucleosides Nucleotides Nucleic Acids* **2018**, *37*, 290–306. [CrossRef] [PubMed]
34. Armstrong, J.A.; Cash, N.J.; Ouyang, Y.; Morton, J.; Chvanov, M.; Latawiec, D.; Awais, M.; Tepikin, A.; Sutton, R.; Criddle, D.N. Oxidative stress alters mitochondrial bioenergetics and modifies pancreatic cell death independently of cyclophilin D, resulting in an apoptosis-to-necrosis shift. *J. Biol. Chem.* **2018**, *293*, 8032–8047. [CrossRef] [PubMed]
35. Van Der Bliek, A.M. Fussy mitochondria fuse in response to stress. *EMBO J.* **2009**, *28*, 1533–1534. [CrossRef] [PubMed]
36. Aryaman, J.; Johnston, I.G.; Jones, N.S. Mitochondrial Heterogeneity. *Front. Genet.* **2019**, *9*, 718. [CrossRef]
37. Campello, S.; Scorrano, L. Mitochondrial shape changes: Orchestrating cell pathophysiology. *EMBO Rep.* **2010**, *11*, 678–684. [CrossRef]
38. Hoitzing, H.; Johnston, I.G.; Jones, N.S. What is the function of mitochondrial networks? A theoretical assessment of hypotheses and proposal for future research. *BioEssays* **2015**, *37*, 687–700. [CrossRef]
39. Palmer, C.S.; Osellame, L.D.; Stojanovski, D.; Ryan, M.T. The regulation of mitochondrial morphology: Intricate mechanisms and dynamic machinery. *Cell. Signal.* **2011**, *23*, 1534–1545. [CrossRef]
40. Rafelski, S.M. Mitochondrial network morphology: Building an integrative, geometrical view. *BMC Biol.* **2013**, *11*, 71. [CrossRef]

41. Zorov, D.B.; Vorobjev, I.A.; Popkov, V.A.; Babenko, V.A.; Zorova, L.D.; Pevzner, I.B.; Silachev, D.N.; Zorov, S.D.; Andrianova, N.V.; Plotnikov, E.Y. Lessons from the Discovery of Mitochondrial Fragmentation (Fission): A Review and Update. *Cells* **2019**, *8*, 175. [CrossRef] [PubMed]
42. Tondera, D.; Grandemange, S.; Jourdain, A.; Karbowski, M.; Mattenberger, Y.; Herzig, S.; Da Cruz, S.; Clerc, P.; Raschke, I.; Merkwirth, C.; et al. SLP-2 is required for stress-induced mitochondrial hyperfusion. *EMBO J.* **2009**, *28*, 1589–1600. [CrossRef] [PubMed]
43. Casals, L.M.; Sebastián, D.; Brea, J.; Rico-Leo, E.M.; Palacín, M.; Fernández-Salguero, P.M.; Loza, M.I.; Albericio, F.; Zorzano, A. Identification of New Activators of Mitochondrial Fusion Reveals a Link between Mitochondrial Morphology and Pyrimidine Metabolism. *Cell Chem. Biol.* **2018**, *25*, 268–278.e4. [CrossRef] [PubMed]
44. Zhang, X.; Li, Z.; Zhang, Q.; Chen, L.; Huang, X.; Zhang, Y.; Liu, X.; Liu, W.; Li, W. Mechanisms Underlying H_2O_2-Evoked Carbonyl Modification of Cytoskeletal Protein and Axon Injury in PC-12 Cells. *Cell. Physiol. Biochem.* **2018**, *48*, 1088–1098. [CrossRef] [PubMed]
45. Löffler, M.; Carrey, E.A.; Knecht, W. The pathway to pyrimidines: The essential focus on dihydroorotate dehydrogenase, the mitochondrial enzyme coupled to the respiratory chain. *Nucleosides Nucleotides Nucleic Acids* **2020**, *39*, 1281–1305. [CrossRef] [PubMed]
46. Gülden, M.; Jess, A.; Kammann, J.; Maser, E.; Seibert, H. Cytotoxic potency of H_2O_2 in cell cultures: Impact of cell concentration and exposure time. *Free Radic. Biol. Med.* **2010**, *49*, 1298–1305. [CrossRef]
47. Iwakami, S.; Misu, H.; Takeda, T.; Sugimori, M.; Matsugo, S.; Kaneko, S.; Takamura, T. Concentration-dependent Dual Effects of Hydrogen Peroxide on Insulin Signal Transduction in H4IIEC Hepatocytes. *PLoS ONE* **2011**, *6*, e27401. [CrossRef]
48. Berndt, N.; Rösner, J.; Haq, R.U.; Kann, O.; Kovács, R.; Holzhütter, H.-G.; Spies, C.; Liotta, A. Possible neurotoxicity of the anesthetic propofol: Evidence for the inhibition of complex II of the respiratory chain in area CA3 of rat hippocampal slices. *Arch. Toxicol.* **2018**, *92*, 3191–3205. [CrossRef]
49. Schindelin, J.; Rueden, C.T.; Hiner, M.C.; Eliceiri, K.W. The ImageJ ecosystem: An open platform for biomedical image analysis. *Mol. Reprod. Dev.* **2015**, *82*, 518–529. [CrossRef]
50. Schneider, C.A.; Rasband, W.S.; Eliceiri, K.W. NIH Image to ImageJ: 25 Years of image analysis. *Nat. Methods* **2012**, *9*, 671–675. [CrossRef]
51. Thevenaz, P.; Ruttimann, U.; Unser, M. A pyramid approach to subpixel registration based on intensity. *IEEE Trans. Image Process.* **1998**, *7*, 27–41. [CrossRef] [PubMed]
52. Arganda-Carreras, I.; Kaynig, V.; Rueden, C.; Eliceiri, K.W.; Schindelin, J.; Cardona, A.; Seung, H.S. Trainable Weka Segmentation: A machine learning tool for microscopy pixel classification. *Bioinformatics* **2017**, *33*, 2424–2426. [CrossRef] [PubMed]
53. Jaqaman, K.; Loerke, D.; Mettlen, M.; Kuwata, H.; Grinstein, S.; Schmid, S.L.; Danuser, G. Robust single-particle tracking in live-cell time-lapse sequences. *Nat. Methods* **2008**, *5*, 695–702. [CrossRef] [PubMed]
54. Rawls, J.; Knecht, W.; Diekert, K.; Lill, R.; Löffler, M. Requirements for the mitochondrial import and localization of dihydroorotate dehydrogenase. *Eur. J. Biochem.* **2000**, *267*, 2079–2087. [CrossRef]

Journal Data Filtered By: **Selected JCR Year: 2021** Selected Editions: SCIE,SSCI Selected Categories: **"PHARMACOLOGY and PHARMACY"** Selected Category Scheme: WoS

Gesamtanzahl: 279 Journale

Rank	Full Journal Title	Total Cites	Journal Impact Factor	Eigenfaktor
1	NATURE REVIEWS DRUG DISCOVERY	47,615	112.288	0.04911
2	DRUG RESISTANCE UPDATES	4,905	22.841	0.00358
3	PHARMACOLOGICAL REVIEWS	15,259	18.923	0.00720
4	ADVANCED DRUG DELIVERY REVIEWS	47,828	17.873	0.02501
5	TRENDS IN PHARMACOLOGICAL SCIENCES	16,714	17.638	0.01363
6	Annual Review of Pharmacology and Toxicology	9,807	16.459	0.00557
7	INTERNATIONAL JOURNAL OF ANTIMICROBIAL AGENTS	21,098	15.441	0.02309
8	Acta Pharmaceutica Sinica B	9,420	14.903	0.00922
9	Journal of Pharmaceutical Analysis	3,869	14.026	0.00404
10	PHARMACOLOGY & THERAPEUTICS	23,869	13.400	0.01921
11	MEDICINAL RESEARCH REVIEWS	7,973	12.388	0.00665
12	JOURNAL OF CONTROLLED RELEASE	67,680	11.467	0.03824
13	DRUGS	18,328	11.431	0.01713
14	European Heart Journal-Cardiovascular Pharmacotherapy	1,529	11.177	0.00282
15	PHARMACOLOGICAL RESEARCH	26,468	10.334	0.02692
16	ANTIVIRAL RESEARCH	17,486	10.103	0.01806
17	ALIMENTARY PHARMACOLOGY & THERAPEUTICS	27,559	9.524	0.03078
18	BRITISH JOURNAL OF PHARMACOLOGY	46,366	9.473	0.02492
19	Asian Journal of Pharmaceutical Sciences	3,744	9.273	0.00288
20	DRUG DISCOVERY TODAY	21,224	8.369	0.01633
21	NEUROPSYCHOPHARMACOLOGY	34,562	8.294	0.03279

Rank	Full Journal Title	Total Cites	Journal Impact Factor	Eigenfaktor
22	Expert Opinion on Drug Delivery	10,532	8.129	0.00604
23	BIODRUGS	3,113	7.744	0.00409
24	Current Neuropharmacology	7,580	7.708	0.00713
25	Reviews of Physiology Biochemistry and Pharmacology	920	7.500	0.00043
26	BIOMEDICINE & PHARMACOTHERAPY	52,615	7.419	0.05905
27	Journal of Neuroimmune Pharmacology	4,036	7.285	0.00302
28	ACTA PHARMACOLOGICA SINICA	14,909	7.169	0.01116
29	Expert Opinion on Drug Discovery	5,789	7.050	0.00575
30	CNS Neuroscience & Therapeutics	6,186	7.035	0.00600
31	International Journal of Nanomedicine	39,405	7.033	0.02657
32	DRUG METABOLISM REVIEWS	3,548	6.984	0.00162
33	CLINICAL PHARMACOLOGY & THERAPEUTICS	21,749	6.903	0.01987
34	DRUG DELIVERY	10,117	6.819	0.00867
35	EXPERT OPINION ON THERAPEUTIC TARGETS	6,787	6.797	0.00562
36	LIFE SCIENCES	42,960	6.780	0.03206
37	EXPERT OPINION ON THERAPEUTIC PATENTS	4,626	6.714	0.00389
38	PHYTOMEDICINE	18,290	6.656	0.00959
39	Pharmaceutics	19,762	6.525	0.01881
40	INTERNATIONAL JOURNAL OF PHARMACEUTICS	67,742	6.510	0.03053
41	EXPERT OPINION ON INVESTIGATIONAL DRUGS	6,588	6.498	0.00566
42	CNS DRUGS	6,627	6.497	0.00642
43	PHYTOTHERAPY RESEARCH	22,172	6.388	0.00999
44	PHARMACOTHERAPY	8,339	6.251	0.00772

Selected JCR Year: 2021; Selected Categories: "PHARMACOLOGY and PHARMACY"

Rank	Full Journal Title	Total Cites	Journal Impact Factor	Eigenfaktor
45	JOURNAL OF FOOD AND DRUG ANALYSIS	5,700	6.157	0.00412
46	BIOCHEMICAL PHARMACOLOGY	35,841	6.100	0.01726
47	Neurotherapeutics	7,998	6.088	0.00899
48	Marine Drugs	25,935	6.085	0.01716
49	ARCHIVES OF PHARMACAL RESEARCH	9,416	6.010	0.00366
50	Frontiers in Pharmacology	51,909	5.988	0.06585
51	ANTIMICROBIAL AGENTS AND CHEMOTHERAPY	81,074	5.938	0.05338
52	Expert Review of Anti-Infective Therapy	6,348	5.854	0.00589
53	ENVIRONMENTAL TOXICOLOGY AND PHARMACOLOGY	10,920	5.785	0.00651
54	JOURNAL OF ANTIMICROBIAL CHEMOTHERAPY	40,176	5.758	0.03462
55	VASCULAR PHARMACOLOGY	4,143	5.738	0.00360
56	INTERNATIONAL IMMUNOPHARMACOLOGY	27,838	5.714	0.02325
57	International Journal of Pharmaceutics-X	346	5.679	0.00041
58	INTERNATIONAL JOURNAL OF NEUROPSYCHOPHARMACOLOGY	8,630	5.678	0.00655
59	Drug Delivery and Translational Research	4,147	5.671	0.00371
60	EUROPEAN JOURNAL OF PHARMACEUTICS AND BIOPHARMACEUTICS	21,938	5.589	0.01003
61	JOURNAL OF LIPOSOME RESEARCH	1,990	5.586	0.00101
61	CLINICAL PHARMACOKINETICS	11,657	5.577	0.00781
63	EUROPEAN NEUROPSYCHOPHARMACOLOGY	9,792	5.415	0.00876
64	Journal of Clinical Lipidology	4,145	5.365	0.00693
65	MOLECULAR PHARMACEUTICS	24,761	5.364	0.01723
66	NEUROPHARMACOLOGY	28,216	5.273	0.02363

Selected JCR Year: 2021; Selected Categories: "PHARMACOLOGY and PHARMACY"

Rank	Full Journal Title	Total Cites	Journal Impact Factor	Eigenfaktor
67	DRUG SAFETY	7,184	5.228	0.00592
68	Antibiotics-Basel	9,403	5.222	0.01055
69	Pharmaceuticals	9,157	5.215	0.00810
70	PROGRESS IN NEURO-PSYCHOPHARMACOLOGY & BIOLOGICAL PSYCHIATRY	15,970	5.201	0.01295
71	JOURNAL OF ETHNOPHARMACOLOGY	53,915	5.195	0.01839
72	EUROPEAN JOURNAL OF PHARMACOLOGY	43,213	5.195	0.02078
73	CHEMICO-BIOLOGICAL INTERACTIONS	17,307	5.168	0.00980
74	EUROPEAN JOURNAL OF PHARMACEUTICAL SCIENCES	19,713	5.112	0.01254
75	JOURNAL OF DRUG DELIVERY SCIENCE AND TECHNOLOGY	10,771	5.062	0.00905
76	JOURNAL OF DRUG TARGETING	5,583	5.016	0.00339
77	DRUG DEVELOPMENT RESEARCH	2,964	5.004	0.00219
78	Advanced Therapeutics	1,966	5.003	0.00287
79	Therapeutic Advances in Psychopharmacology	1,293	4.988	0.00184
80	Therapeutic Advances in Chronic Disease	1,668	4.970	0.00234
81	Expert Opinion on Drug Metabolism & Toxicology	5,511	4.936	0.00438
81	JOURNAL OF PHARMACY AND PHARMACOLOGY	12,820	4.810	0.00439
83	JOURNAL OF NATURAL PRODUCTS	34,341	4.803	0.01481
84	Cannabis and Cannabinoid Research	1,526	4.786	0.00252
85	CURRENT OPINION IN PHARMACOLOGY	8,367	4.768	0.00564
86	Biomedicines	7,005	4.757	0.00710
87	CURRENT MEDICINAL CHEMISTRY	22,717	4.740	0.01145
88	ARCHIV DER PHARMAZIE	4,298	4.613	0.00210

Selected JCR Year: 2021; Selected Categories: "PHARMACOLOGY and PHARMACY"

Therapeutic Advances in Chronic Disease

Original Research

Teriflunomide preserves peripheral nerve mitochondria from oxidative stress-mediated alterations

Ther Adv Chronic Dis

2020, Vol. 11: 1–14

DOI: 10.1177/2040622320944773

Bimala Malla, Samuel Cotten, Rebecca Ulshoefer, Friedemann Paul, Anja E. Hauser, Raluca Niesner, Helena Bros* and Carmen Infante-Duarte*

Abstract: Mitochondrial dysfunction is a common pathological hallmark in various inflammatory and degenerative diseases of the central nervous system, including multiple sclerosis (MS). We previously showed that oxidative stress alters axonal mitochondria, limiting their transport and inducing conformational changes that lead to axonal damage. Teriflunomide (TFN), an oral immunomodulatory drug approved for the treatment of relapsing forms of MS, reversibly inhibits dihydroorotate dehydrogenase (DHODH). DHODH is crucial for *de novo* pyrimidine biosynthesis and is the only mitochondrial enzyme in this pathway, thus conferring a link between inflammation, mitochondrial activity and axonal integrity.

Here, we investigated how DHODH inhibition may affect mitochondrial behavior in the context of oxidative stress. We employed a model of transected murine spinal roots, previously developed in our laboratory. Using confocal live imaging of axonal mitochondria, we showed that in unmanipulated axons, TFN increased significantly the mitochondria length without altering their transport features. In mitochondria challenged with 50 µM hydrogen peroxide (H_2O_2) to induce oxidative stress, the presence of TFN at 1 µM concentration was able to restore mitochondrial shape, motility, as well as mitochondrial oxidation potential to control levels. No effects were observed at 5 µM TFN, while some shape and motility parameters were restored to control levels at 50 µM TFN.

Thus, our data demonstrate an undescribed link between DHODH and mitochondrial dynamics and point to a potential neuroprotective effect of DHODH inhibition in the context of oxidative stress-induced damage of axonal mitochondria.

Keywords: dihydroorotate dehydrogenase (DHODH), mitochondria, mitochondrial dynamics, neurodegeneration, oxidative stress, teriflunomide (TFN)

Received: 17 January 2020; revised manuscript accepted: 2 July 2020.

Introduction

Multiple sclerosis (MS) is a chronic inflammatory disease of central nervous system (CNS) that affects more than 2.5 million people worldwide.[1] In MS, inflammation, demyelination and neurodegeneration are considered to contribute to disease development.[2,3] It is assumed that in MS, a misguided immune response against the CNS is initiated and orchestrated by autoreactive T cells, leading to progressive demyelination, oligodendrocyte injury and axonal loss,[4,5] that affect not only the white but also the grey matter.[6]

The mechanisms by which neuroinflammation and myelin damage lead to neurodegeneration have not been fully elucidated; however, the sustained release of reactive oxygen species (ROS) and nitrogen species (NOS) by macrophages and activated microglia during inflammation appears to contribute to the damaging cascade.[7–9] Also in cortical lesions, demyelination appears to be associated with excessive oxidative damage.[10] Mitochondrial pathology and subsequent focal axonal injury appears also to be triggered by inflammation-associated ROS and NOS and to

Correspondence to:
Carmen Infante-Duarte
Institute for Medical Immunology, Charité – Universitätsmedizin Berlin and Experimental & Clinical Research Center (ECRC), MDC for Molecular Medicine and Charité – Universitätsmedizin, Campus Virchow Klinikum, Augustenburger Platz 1, Berlin 13353, Germany
carmen.infante@charite.de

Bimala Malla
Samuel Cotten
Rebecca Ulshoefer

Helena Bros
Charité – Universitätsmedizin Berlin, corporate member of Freie Universität Berlin, Humboldt-Universität zu Berlin and Berlin Institute of Health, Institute for Medical Immunology, Berlin, Germany

Friedemann Paul
NeuroCure Clinical Research Center, Charité – Universitätsmedizin Berlin and Experimental & Clinical Research Center (ECRC), Max Delbrueck Center (MDC) for Molecular Medicine, Berlin, Germany and Charité – Universitätsmedizin Berlin, Berlin, Germany

Anja E. Hauser
Medizinische Klinik mit Schwerpunkt Rheumatologie und Klinische Immunologie, Charité – Universitätsmedizin Berlin, corporate member of Freie Universität Berlin, Humboldt – Universität zu Berlin, and Berlin Institute of Health, Berlin, Germany
Deutsches Rheuma-Forschungszentrum, Berlin, Germany

Raluca Niesner
Dynamic and Functional in vivo Imaging, Deutsches Rheuma-Forschungszentrum, Berlin, Germany and Veterinary Medicine, Freie Universität Berlin, Germany

*These senior authors contributed equally to the work

be independent of demyelinating processes.[11] Axonal mitochondrial damage is an early sign of neurodegeneration that precedes and contributes to focal and reversible alterations in axon morphology. The alterations of the mitochondrial function within axons have been proposed to occur in the early stages of the disease, even before demyelination,[11,12] and to precede neuronal death.[13–16] In autopsied tissue from chronic progressive MS, respiratory deficient neurons were detected both in white and grey matter. Respiration deficits were shown to be caused by multiple deletions of mitochondrial DNA, probably subsequent to inflammation and oxidative stress, that contributed to an enhanced susceptibility of axons and neurons to additional damaging insults.[17] In this line, we and others have shown that oxidative stress disrupts the transport of mitochondria in the axon.[14,18] Hence, mitochondrial dysfunction is considered as one of the major contributors of neuroaxonal damage in MS.

With regard to MS management and treatment, teriflunomide (TFN) (Aubagio; Genzyme, Cambridge, MA, USA) is a once-daily oral immunomodulatory drug for the treatment of patients with relapsing forms of MS.[19] TFN has been shown to reduce relapse events and increase the periods of remission.[20,21]

TFN seems to exert its therapeutic effect by non-competitively and reversibly inhibiting the mitochondrial respiratory chain-associated enzyme dihydroorotate dehydrogenase (DHODH).[22–25] DHODH is involved in *de novo* pyrimidine biosynthesis, thus limiting lymphocytic proliferation and inflammation. However, whether the inhibition of DHODH alone may affect neuronal mitochondria remains uncertain. Importantly, a very recent retrospective, single-center, observational study indicated that the effect of TFN in reducing cortical grey matter atrophy is superior to the effect of the anti-oxidative and anti-inflammatory dimethyl fumarate.[26] Moreover, it has been reported that TFN penetrates into the CNS and exerts its effect directly within the brain.[27] Thus, TFN may indeed have the potential to affect axonal mitochondria directly.

To explore the possible effects of TFN on the nervous system, we have used in this study a previously established model of explanted spinal roots, in which we had shown that mitochondria undergo a series of alterations in response to oxidative stress.[18,28]

In patients treated daily with 14 mg TFN, average steady-state maximum TFN concentration (C_{max}) in plasma is 168 µM.[29] The half maximum concentration (IC_{50}) for interaction of TFN with human DHODH is 1 µM[30,31] and 50–100 µM is considered sufficient to inhibit protein tyrosine kinase *in vitro*.[29,31] Moreover, a study assessing the effect of TFN on eryptosis indicated that concentrations ranging from 3.7 to 37 µM TFN might compensate oxidative stress-mediated erythrocyte changes *in vitro*.[32] In rats, it has been shown that after one single injection of 10 µg/g TFN, approximately 2–4% of the blood concentration was found in the brain (~2.5–4.1 µM).[30] Although an extrapolation to the human reality is not exact, we could suppose in treated patients a TFN concentration within the nervous system of about 3–7 µM. Therefore, in our study, we investigated the effect of TFN on oxidative stress-induced mitochondrial alterations in murine root explants using three different TFN concentrations, 1 µM, 5 µM and 50 µM.

We show that TFN is able to prevent mitochondrial alterations induced by hydrogen peroxide (H_2O_2), suggesting that TFN has additional therapeutically relevant properties related to mitochondrial protection in axons.[31]

Materials and methods

Ethics

All experimental procedures were approved by the local authority on animal studies in Berlin (Landesamt für Gesundheit und Soziales Berlin; ID: T0002/10). Animal studies were performed in strict accordance with the European Communities Council Directive of 22 September 2010 (2010/63/EU).

Solutions and drugs

Explanted roots were bathed in artificial cerebrospinal fluid (aCSF) containing the following: solution I: 124 mM sodium chloride (NaCl), 1.25 mM sodium dihydrogen phosphate (NaH_2PO_4), 10.0 mM glucose, 1.80 mM magnesium sulphate ($MgSO_4$), 1.60 mM calcium chloride ($CaCl_2$), 3.00 mM potassium chloride (KCl);

solution II: 26.0 mM sodium bicarbonate ($NaHCO_3$). Solutions I and II were mixed immediately before use. Hydrogen peroxide (H_2O_2; 30% w/w in H_2O, with a stabilizer) and dimethyl sulfoxide (DMSO) were purchased from Sigma-Aldrich. To induce oxidative stress, explanted roots were incubated with 50 µM of H_2O_2 dissolved in aCSF for 30 min. TFN was applied at different concentrations along with H_2O_2 for 30 min. TFN was provided in powder form by the manufacturer (Sanofi Genzyme), which was dissolved in DMSO and stored at −20°C.

Preparation of ventral spinal roots

Ventral spinal roots were prepared as described in our previous work.[18,28,33] Briefly, C57BL/6 mice at least 3 weeks of age were anesthetized with isoflurane prior to cervical dislocation. After separating the connective tissue and exposing the dorsal side of the spinal cord, an initial sectioning was made at the thoracic level, which proceeded in a rostral to caudal direction until the last vertebrae. The spinal cord was lifted gently to expose the ventral roots, which were cut distal to the spinal cord but before the formation of the peripheral nerves. The explanted spinal cord with attached roots was transferred to aCSF saturated with carbogen (95% oxygen [O_2]; 5% carbon dioxide [CO_2]). Under a dissecting microscope, lumbar ventral roots of at least 0.8 cm were selected and separated from the spinal cord.

Labeling of mitochondria

All experimental incubations were conducted in a submerged incubation chamber (Brain Slice Keeper- BSK6-6; Scientific Systems Design Inc., Ontario, Canada), which allows for multiple treatment conditions and continuous carbogen perfusion of each submersion well. Transected ventral spinal roots were transferred to fresh aCSF containing 300 nM, MitoTracker CMTMRos orange (Life Technologies, Darmstadt, Germany) for 30 min and washed with aCSF.

Confocal microscopy

Explanted ventral roots were placed onto a glass coverslip and transferred to an imaging chamber filled with carbogenated aCSF. To prevent movement of the roots during imaging, a custom-built net was placed on the top of the roots.[28] For all imaging experiments, we used an inverted laser-scanning confocal microscope adapted for live cell imaging (LSM 710; Carl Zeiss, Jena, Germany). MitoTracker Orange was excited with a diode-pumped solid state (DPSS) laser at 561 nm. After finding the middle of the root, 3 × 60-sec videos (2 sec/frame) with a resolution of 512 × 512 pixels were acquired in three separate regions of interest (ROI) according to the following criteria: (a) there was a clearly defined node of Ranvier; (b) there were visibly labeled mitochondria; and (c) the areas were no closer than 0.2 cm from the ends of the roots. Typically, the first ROI was located at the middle of the root, whereas the following two were to the right and left of the middle region.

Analysis of mitochondrial dynamics

Mitochondrial morphology was assessed using an automated analysis function of the Volocity 6.3 software (Perkin Elmer, Rodgau, Germany). The first frame of every video was used for analysis. Shape factor, a measure of circularity ranging from 0 and 1 (closer to '0' was a longer mitochondrion, whereas '1' was a perfect circle), length (µm) and area of individual mitochondria were quantified for assessing change in mitochondrial morphology.

Mitochondrial transport was quantified in terms of the number of moving mitochondria, velocity, displacement, and track length of moving mitochondria. Displacement is the measure of shortest distance in µm, covered by a mitochondrion; it was measured as a straight line from the start to the end position during the 30 frames. Track length is the measure of real distance path longitude followed by the mitochondrion. Mitochondria were tracked manually using Volocity 6.3 software (Perkin Elmer, Rodgau, Germany). Any mitochondrion with a displacement of at least 1 µm was considered 'mobile'. Measurements from three ROI were averaged for each root.

In total, 15 different mice in 15 independent experiments were investigated. Depending on the quality of the explants, at least five independent roots and 15 ROI per culturing condition were included into the analysis (usually up to three different ROI per root). Specifically, 39 and 44 ROI were analyzed for the untreated group and H_2O_2 treated groups, respectively; 15–21 ROI were used to investigate treatments with H_2O_2 + TFN.

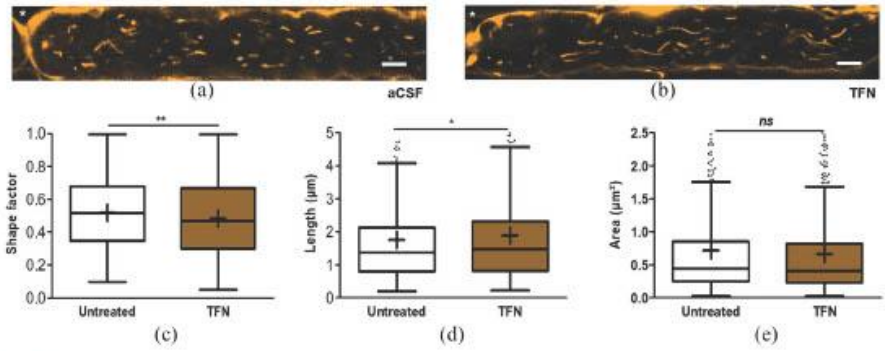

Figure 1. Teriflunomide (TFN) affected mitochondrial shape and length in untreated root explants.
(a) Representative confocal picture of the mitochondria within single axons in an untreated peripheral root explant and (b) treated with TFN. The node of Ranvier is located on the left side shown with an asterix (*). Scale bar: 5µm. (c) Shape factor (circularity), (d) length and (e) area of mitochondria. The mitochondrial shape and length is significantly less round and longer after treating the axons with TFN (50µM).
Graphs are shown in Tukey box plots, where the central line denotes the median; the lower and upper boundaries denote the first and third quartile, and the whiskers denote the spread of the data.
Inside the box, '+' delineates the mean.
ns, not significant statistically.
$^{*}p < 0.05$, $^{**}p < 0.01$.

For the morphological investigations, the number of mitochondria in the selected ROI were 2586, 2860, 1306, 875 and 1550 for untreated, H_2O_2-treated, H_2O_2 + TFN (1µM), H_2O_2 + TFN (5µM) and H_2O_2 + TFN (50µM), respectively. Analyses of motility included 201, 70, 83, 52 and 64 motile mitochondria for each of the above-mentioned groups.

For the comparison of untreated *versus* TFN-treated nerves, four independent experiments were performed. Analyses include 12 ROI per condition. In total, 568 and 672 individual mitochondria were analyzed, respectively.

Quantification of relative change in intracellular ROS

The fluorescence intensity of the MitoTracker Orange was quantified as a measure of intracellular ROS as described by Kweon *et al.*,[34] The images obtained from confocal microscopy were used for the quantification of mitochondrial fluorescence intensity using Image J software.

Statistical analysis and data representation

The data were analyzed with Prism 5.01 software (GraphPad, CA, USA). All datasets were subjected first to D'Agostino and Pearson omnibus K2 normality test for Gaussian distribution. All data fitting the criteria for a normal distribution were subsequently analyzed using a one-way analysis of variance (ANOVA) with Bonferroni's *post hoc* test. All data following a non-parametric distribution were analyzed using a Kruskal–Wallis test followed by a *post hoc* Dunn's multiple comparisons test. All data are given in mean ± SD.

Data are shown in Tukey box and whisker plots. The box and whisker plot shows simultaneously the minimum, first quartile, mean (+), median (dissecting line inside the box), third quartile, and maximum of the data set. Whiskers indicate variability outside the upper and lower quartiles. Outliers are plotted as individual dots that are in line with whiskers. The mean + SD values are given in the corresponding tables.

Results

TFN altered mitochondrial dynamics in peripheral root explants

We labelled peripheral root mitochondria with MitoTracker Orange and the explants were imaged for morphological investigation (Figure 1a, b). Then, the effects of TFN on mitochondrial morphology and transport in unmanipulated explanted roots were investigated. Explanted roots were

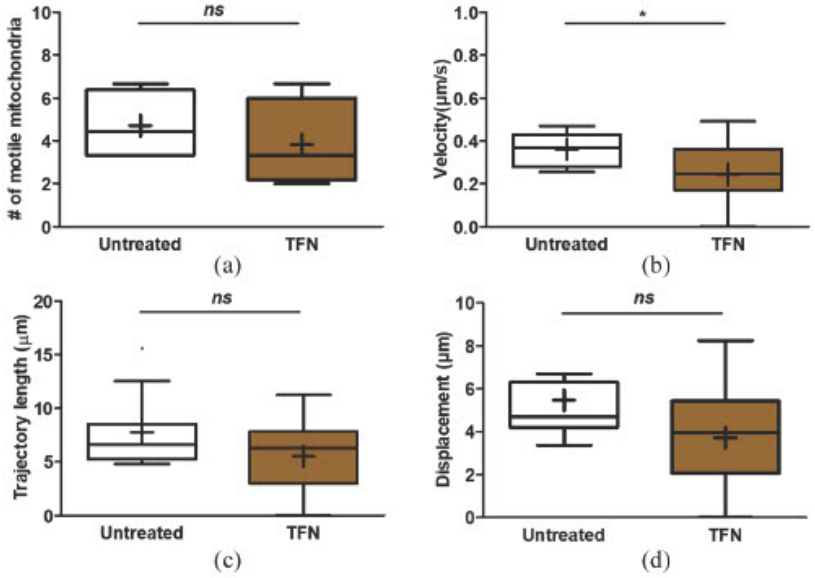

Figure 2. Teriflunomide (TFN) reduced mitochondrial velocity without influencing motile number, trajectory length and displacement of mitochondria in untreated root explants.
(a) Number of moving mitochondria per root during 1 min in untreated *versus* TFN-treated roots, (b) velocity of mitochondrial transport, (c) length of the mitochondrial trajectories and (d) displacement (final position minus initial position) of mitochondria.
Graphs are shown in Tukey boxplots, where the central line denotes the median; the lower and upper boundaries denote the first and third quartile, and the whiskers denote the spread of the data. Inside the box, '+' delineates the mean.
ns, not significant statistically.
*$p < 0.05$.

incubated in the presence or absence of 50µM TFN. TFN treatment resulted in a statistically significant decrease in mitochondrial circularity (Figure 1c) and an increase in mitochondrial length (Figure 1d). There were no significant changes in mitochondrial area (Figure 1e) after TFN treatment compared with the untreated controls.

For mitochondrial motility, TFN did not significantly change the number of motile mitochondria (Figure 2a) as well as the distance covered by the mitochondria (Figure 2c, d). However, it induced a significant reduction of the mean velocity of mitochondrial transport (Figure 2b). Corresponding statistical information is summarized in Table 1.

TFN prevented oxidative stress-induced morphological changes in mitochondria

We previously reported that oxidative stress leads to substantial changes to both morphology and transport of axonal mitochondria.[18] Here, we investigated whether TFN, applied together with H_2O_2, would be able to prevent these effects. We treated the roots with 50 µM H_2O_2 (both groups containing the vehicle DMSO), and 3 different concentrations of TFN: 1, 5 and 50 µM in aCSF (Figure 3a–e). We analyzed a total of 39 untreated ROI, 44 ROI treated with H_2O_2, and 18, 15 and 21 ROI treated with 1 µM, 5 µM and 50 µM TFN in the presence of 50 µM H_2O_2, respectively, from 15 independent experiments. Consistent with our previous findings, we observed that treatment with 50 µM H_2O_2 induced an overall increase of mitochondrial circularity and a corresponding decrease in mitochondrial length and area. In particular, mitochondria were significantly more circular (Figure 3f), shorter (Figure 3g) and smaller (Figure 3h) than their untreated counterparts.

In the presence of 1 µM TFN, the shape factor of the mitochondria was reduced, that is,

Table 1. Summary of morphology and motility parameters of mitochondria in untreated and teriflunomide-treated peripheral root explants.

	n=	Shape factor	Length (μm)	Area (μm²)	No. of motile mitochondria	Velocity (μm/s)	Trajectory length (μm)	Displacement (μm)
Untreated	39	0.52 ± 0.21	1.75 ± 1.52	0.77 ± 0.86	4.72 ± 1.67	0.36 ± 0.07	7.77 ± 3.26	5.46 ± 2.39
TFN (50 μM)	12	0.48 ± 0.23	1.89 ± 1.67	0.66 ± 0.82	3.83 ± 2.06	0.24 ± 0.15	5.51 ± 3.49	3.71 ± 2.43
Mann–Whitney test		**	*	>0.1	>0.1	*	>0.1	>0.1

Values are shown as mean ± SD.
*$p < 0.05$; **$p < 0.01$

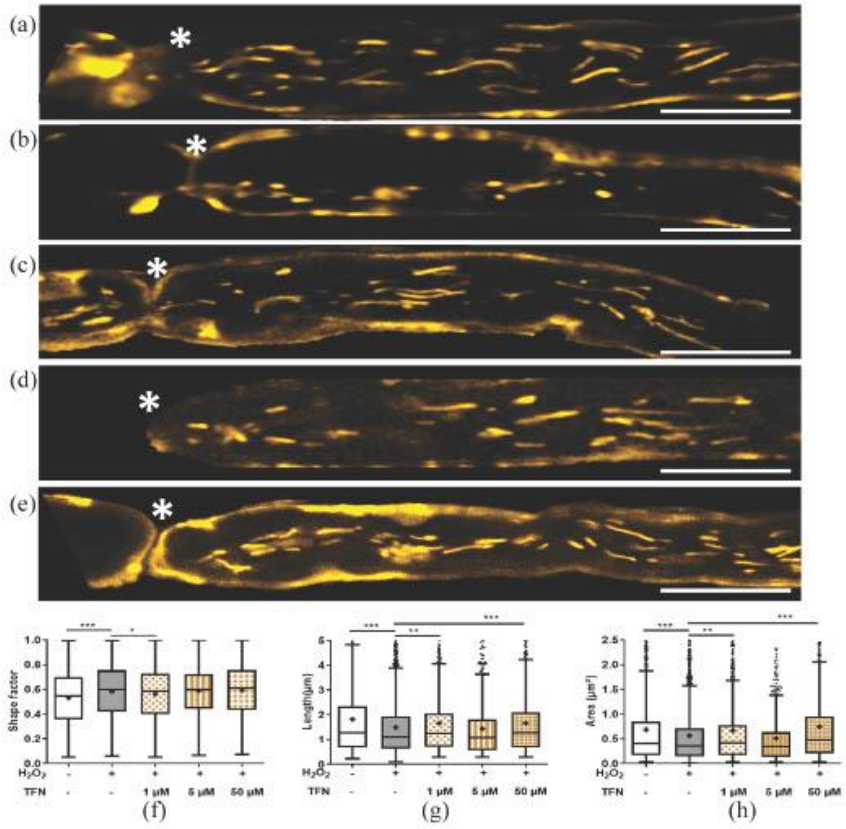

Figure 3. Mitochondrial morphology altered during oxidative stress with/out teriflunomide (TFN) treatment.
Representative image of mitochondria in (a) untreated, (b) hydrogen peroxide (H_2O_2)-treated, and (c, d, and e) H_2O_2-TFN-treated, where TFN was 1, 5 and 50 μM, respectively, in murine peripheral root explants. Scale bar: 10 μm. (f) Change in mitochondrial shape factor, (g) length, and (h) area of mitochondria in the presence of H_2O_2 with or without TFN.
Graphs are shown in Tukey boxplots, where the central line denotes the median; the lower and upper boundaries denote the 1st and 3rd quartile, and the whiskers denote the spread of the data. Inside the box, '+' delineates the mean.
*$p < 0.05$, **$p < 0.01$, ***$p < 0.001$.

Table 2. Summary of shape factor, length and area of mitochondria under H_2O_2 treatment alone, and with 50 µM H_2O_2 in the presence of 1 µM, 5 µM and 50 µM teriflunomide.

	n=	Shape factor	KW test	Length (µm)	KW test	Area (µm²)	KW test
Untreated	39	0.53 ± 0.22	***	1.82 ± 1.79	***	0.69 ± 0.92	***
H_2O_2-treated	44	0.58 ± 0.21		1.49 ± 1.29		0.57 ± 0.65	
H_2O_2 + TFN (1 µM)	18	0.57 ± 0.21	*	1.66 ± 1.50	**	0.67 + 0.85	**
H_2O_2 + TFN (5 µM)	15	0.59 ± 0.19	>0.1	1.43 ± 1.29	>0.1	0.51 + 0.69	>0.1
H_2O_2 + TFN (50 µM)	21	0.59 ± 0.21	>0.1	1.66 ± 1.42	***	0.75 + 0.93	***

KW, Kruskal–Wallis; H_2O_2, hydrogen peroxide.
Values are shown as mean ± SD.
*$p < 0.05$; **$p < 0.01$; ***$p < 0.001$.

mitochondria became elongated or rod-shaped (Figure 3f). In contrast, no effects were observed at higher concentration of TFN. Moreover, the lowest and highest TFN concentrations (1 µM and 50 µM) induced a significant increase in mitochondrial length (Figure 3g) and area (Figure 3h), in comparison with the mitochondria exposed to H_2O_2 alone. Paradoxically, treatment with 5 µM TFN with 50 µM H_2O_2, showed no statistically significant effect on H_2O_2-induced morphological alterations (Figure 3f–h) (0.59 ± 0.19 shape factor, 1.43 ± 1.29 µm length, and 0.51 ± 0.69 µm² area; Kruskal-Wallis test followed by Dunn's *post hoc* test $p > 0.1$ in all cases).

Corresponding statistical information is summarized in Table 2.

TFN prevented oxidative stress-induced changes in mitochondrial motility

To investigate TFN effects on mitochondrial motility, roots were treated either with aCSF, 50 µM H_2O_2 (both groups containing DMSO) or 50 µM H_2O_2 in the presence of three different concentrations of TFN: 1, 5 and 50 µM (Figure 4a–e). We observed that H_2O_2 treatment led to an overall decrease in the number of motile mitochondria (Figure 4f). In addition, the moving mitochondria had lower mean velocity (Figure 4g), trajectory length (Figure 4h), and displacement (Figure 4i) than the untreated mitochondria.

Again, the lowest and highest TFN concentration (1 µM and 50 µM) restored the motility-related parameters to control levels, except for the mitochondrial velocity with 50 µM TFN, when compared with the mitochondria exposed to H_2O_2 alone; for the number of moving mitochondria (Figure 4f), velocity (Figure 4g), trajectory (Figure 4h), and displacement (Figure 4i). In contrast, 5 µM TFN had no effect. Corresponding statistical information is summarized in Table 3.

TFN prevented change in mitochondrial oxidation potential in peripheral nerve explants during oxidative stress

MitoTracker Orange CMTMRos is a reduced, non-fluorescent dye that fluoresces on oxidation. Thus, in conditions of high oxidative stress, mitochondria acquire higher fluorescence intensity.[34] We observed that fluorescence intensity was higher in H_2O_2-treated roots compared with untreated controls (Figure 5). In the presence of 1 µM TFN, the fluorescence intensity in the mitochondria was reduced, approaching the values of the untreated axons (Table 4), suggesting that the H_2O_2-mediated increase in the oxidation potential could be prevented by TFN. In contrast, no effect was observed at 5 or 50 µM TFN. Corresponding statistical information is summarized in Table 4.

Discussion

While current treatments for MS focus on reducing inflammation *via* modulation of the

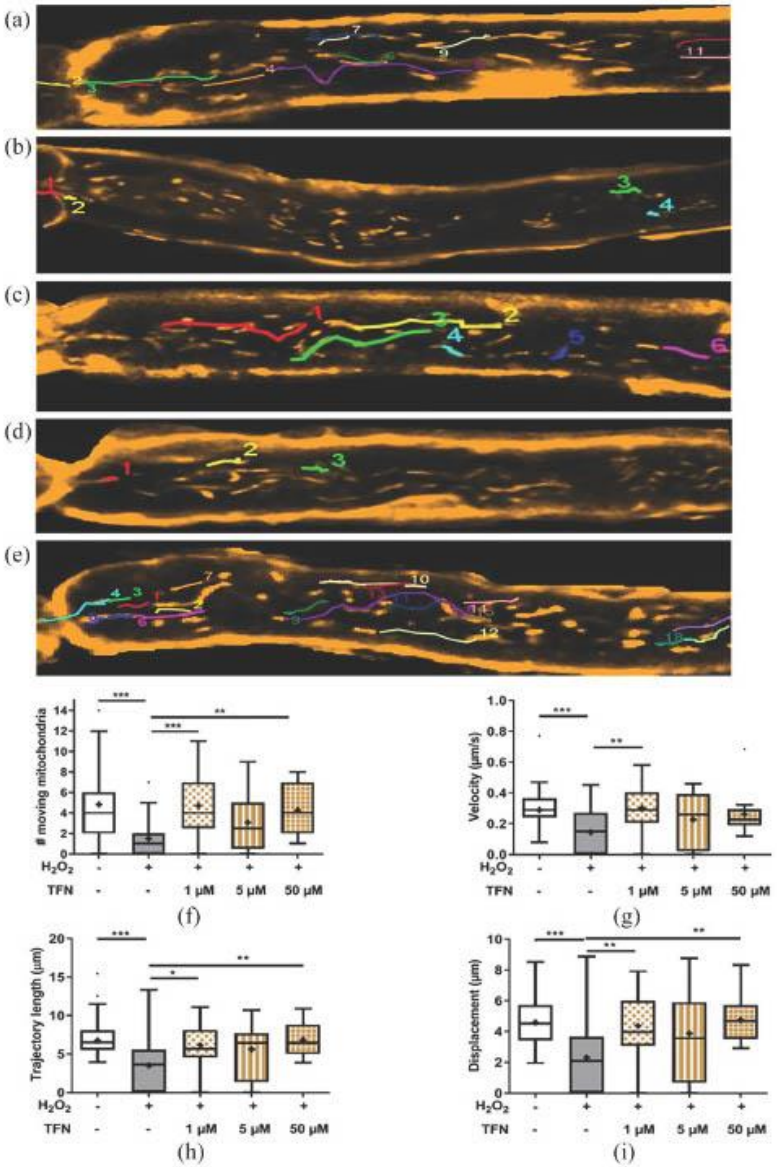

Figure 4. Mitochondrial motility altered during oxidative stress with or without teriflunomide (TFN) treatment. A representative image of mitochondrial tracking in (a) untreated, (b) hydrogen peroxide (H_2O_2)-treated, and (c, d, and e) H_2O_2-TFN treated where TFN was 1, 5 and 50 µM, respectively, in murine peripheral root explants. (f) Number, (g) velocity, (h) trajectory, and (i) displacement of mitochondria.
Graphs are shown in Tukey boxplots, where the central line denotes the median; the lower and upper boundaries denote the first and third quartile and the whiskers denote the spread of the data. Inside the box, '+' delineates the mean.
*$p < 0.05$; **$p < 0.01$; ***$p < 0.001$.

Table 3. Summary of mitochondrial motility, velocity, displacement and trajectory length under H_2O_2 treatment alone, and along with different concentrations of teriflunomide.

	n=	# motile mitochondria (axon)	KW test	Velocity (μm/s)	KW test	Trajectory length (μm)	KW test	Displacement (μm)	KW test
Untreated	39	4.85 ± 3.72 (39)	***	0.29 ± 0.14	***	6.77 ± 3.13	***	4.59 ± 2.16	***
H_2O_2-treated	44	1.52 ± 1.71 (39)		0.15 ± 0.14		3.53 ± 3.67		2.30 ± 2.60	
H_2O_2 + TFN (1 μM)	18	4.71 ± 3.08 (21)	***	0.30 ± 0.13	**	6.13 ± 2.59	*	4.37 ± 1.97	**
H_2O_2 + TFN (5 μM)	15	3.08 ± 2.75 (12)	>0.1	0.23 ± 0.17	>0.1	5.61 ± 3.69	>0.1	3.87 ± 2.96	>0.1
H_2O_2 + TFN (50 μM)	21	4.27 ± 2.34 (15)	**	0.26 ± 0.13	>0.1	6.84 ± 2.15	**	4.75 ± 1.45	**

KW, Kruskal–Wallis; H_2O_2, hydrogen peroxide.
Values are shown as mean ± SD.
*$p < 0.05$; **$p < 0.01$; ***$p < 0.001$.

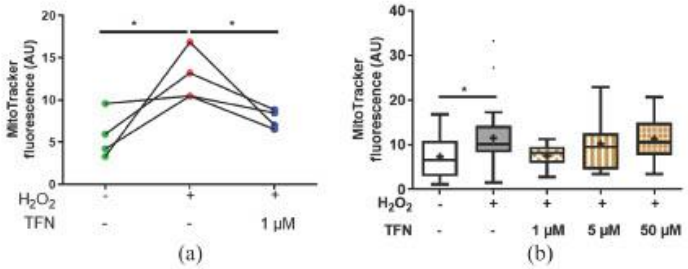

Figure 5. Teriflunomide (TFN) at 1 μM altered the oxidation potential of mitochondria, reducing oxidative MitoTracker Orange fluorescence intensity Fluorescence intensity of MitoTracker Orange staining depicting significant reduction of oxidation potential of 1 μM TFN. (b) MitoTracker Orange fluorescence intensity at 1, 5 and 50 μM TFN treatment during oxidative stress in comparison with untreated and H_2O_2-treated roots.
*Statistical significance with *p* value < 0.05.

Table 4. Summary of mean fluorescence intensities of mitochondria.

	n=	MitoTracker fluorescence (AU)	Mann–Whitney test
Untreated	39	7.35 ± 4.76	*
H_2O_2-treated	44	11.49 ± 6.44	
H_2O_2 + TFN (1 μM)	18	7.48 ± 2.75	*
H_2O_2 + TFN (5 μM)	15	10.22 ± 6.45	>0.1
H_2O_2 + TFN (50 μM)	21	11.27 ± 4.79	>0.1

AU, arbitrary units.
Values are shown as mean ± SD.
*$p < 0.05$.

immune system,[25,35] there is a general lack of treatment targeting inflammation-promoted neurodegeneration,[36,37] which is an integral component of disability progression.[37,38] As early mitochondrial alterations are reported in inflammatory neurodegenerative diseases,[8,11–16] the maintenance of mitochondrial integrity could be a key goal to achieve neuronal protection during neuroinflammation.[39] Here, we hypothesized that TFN, due to its ability to inhibit DHODH,[40] an enzyme functionally linked with complex III activity of the mitochondrial respiratory chain,[41] may influence mitochondrial stability in the context of oxidative stress. To test our hypothesis, we used our previously established model of murine explanted ventral roots, in which the morphology and the transport of mitochondria can be analyzed within peripheral axons.[18,28]

After excluding any relevant effect of DMSO (the dilution vehicle), in both untreated and H_2O_2-treated mitochondria (Supplemental Figures 1–2), we investigated the effect of TFN treatment in unmanipulated or oxidative stress-exposed spinal root explants.

Interestingly, in non-stressed roots, TFN seems to promote mitochondrial fusion, induce mitochondrial elongation (Figure 1d, e), and reduce mitochondrial velocity (Figure 2b). Mitochondrial fusion is important for the formation of mitochondrial networking that assists in reshuffling and redistributing the mitochondrial content.[42,43] Thus, the inhibition of DHODH and subsequent effects on complex III of the electron transport chain (ETC) and respiration[41] may promote mitochondrial fusion as an attempt to redistribute the electron transport complexes that are still capable of maintaining the proton gradient and synthesizing adenosine triphosphate (ATP).

In contrast, during oxidative stress, we observed a reduction in mitochondrial length and size, which is indicative of fragmentation/fission of mitochondria that might undergo mitophagy. Mitochondrial fission has also been proposed to increase the number of mitochondria and their cellular distribution in order to meet the increasing energy demands of the cell.[44,45] Although mitochondrial fission is extensively discussed in terms of mitophagy as well as apoptosis,[43–46] intensive mitochondrial fission may translate into mitochondrial failure and the strategy to optimize mitochondrial functionality before undergoing apoptosis. It also serves to get rid of damaged, irreparable mitochondrial parts.[45,47] Importantly, in the presence of 1 μM and 50 μM TFN, reduction in mitochondrial length and area due to oxidative insult could be prevented (Figure 3g, h). Intensive fragmentation during oxidative stress could not be prevented with 5 μM TFN.

Further, consistent with previous findings, we observed a reduced mitochondrial motility during oxidative stress,[14,18] that is, reduced trajectories and transport velocity. The impairment of mitochondrial transport was preserved with TFN treatment. In axons, around 10–30% of mitochondria are motile, while more than 70% remain stationary.[48] This motile and stationary pool of mitochondria is dependent on the current energy demands of the cell.[40,50] In addition, disrupted motility could lead to impairment of mitochondrial fusion.[46,40,51] Thus, TFN may promote fusion by influencing the motility. On the other hand, it has been proposed that inhibition of DHODH by TFN may reduce the total amount of ROS in the cell.[52] Thus, TFN-mediated ROS reduction may also lead indirectly to an increased motility of stressed mitochondria.

Along this line, to assess the effects of TFN on ROS in our system, we monitored the fluorescence intensity of MitoTracker Orange CMTMRos (see Methods).[34] As expected, fluorescence intensity of CMTMRos significantly increased with H_2O_2 treatment, while inhibition of DHODH with 1 μM TFN reduced the ROS level (Figure 5). As complex III of the ETC is considered one of the major contributors to ROS formation, its compromised activity in the presence of TFN might reduce ROS production in mitochondria in peripheral spinal root explants. 5 μM and 50 μM TFN could not effectively reduce ROS, which might be attributed to the inhibition at higher concentrations of additional signaling pathways including tyrosine kinases.[53]

On the other hand, the intermediate dose of 5 μM TFN showed no effects on H_2O_2-induced shape or motility changes. Why, in our experimental setup a dose effect is missing, remains uncertain. The high variability of our data, which is intrinsic to the nature of mitochondrial dynamics and reflects the heterogeneity of the mitochondrial population in both physiological and diseased conditions, could have contributed to mask a true dose effect. To minimize this problem, several experiments

with large amounts of mitochondria were analyzed (see Methods section). Moreover, depending on its concentration, TFN may function by a different mode of action. While low TFN concentrations are effective in inhibiting DHODH (1–1.5 µM), concentrations needed to achieve DHODH-independent effects such as inhibition of protein tyrosine kinase or cyclooxygenase-2 are much higher (50–200 µM).[29] However, little is known about the mode of action of intermediate concentrations. One could speculate that in our model, TFN at 5 µM may achieve partially known or yet undefined DHODH-independent effects that rather counterbalance the beneficial effects observed at 1 µM, while at 50 µM DHODH-dependent and independent mechanisms may synergize against dysfunctions observed under oxidative stress. Future experiments using long-living explants are needed to evaluate to what extent TFN effects at different concentration are DHODH-dependent and thus reversible.

Our previous data on root explants demonstrated that mitochondrial alterations caused by oxidative stress precede axonal damage.[18] Now, we show that these alterations could be pharmacologically reversed *in vitro* by TFN. Targeting dysfunction of axonal mitochondria should become one of the key goals in drug development not only for MS but also for other classic neurodegenerative disorders such as Parkinson's or Alzheimer diseases.[54] In this line, we showed in the animal model of MS a protective effect of epigallocatechin-3-gallate (EGCG),[55,56] a polyphenol, that among others, inhibits the formation of ROS and protects neurons.[57,58] Also dimethyl fumarate, used to treat MS, prevents oxidative stress-related mitochondrial dysfunction, apoptosis and autophagy in murine oligodendrocytes *in vitro*.[59] Importantly, endogenous substances currently being investigated in MS may be exploited as therapeutics due their mitoprotective capacities, such as high dose biotin,[60] vitamin D[61] or octadecaneuropeptide, a neurotrophic peptide produced principally by astrocytes, which is able to counteract oxidative stress-induced alterations.[62]

In summary, our present findings suggest a protective effect of TFN on axonal mitochondria exposed to oxidative stress. Investigations expanding on these findings are needed to determine whether mitochondrial protection at the axonal level can be translated into protection of axons and neurons.

Conflict of interest

The authors declare that there is no conflict of interest.

Funding

The authors disclosed receipt of the following financial support for the research, authorship, and/or publication of this article: This work was funded by a research grant from Sanofi Genzyme to C.I-D. A.E.H, was supported by DFG TRR130, TP17. The authors also acknowledge support from the German Research Foundation (DFG) and the Open Access Publication Funds of Charité- Universitätsmedizin.

ORCID iD

Carmen Infante-Duarte https://orcid.org/0000-0003-3005-351X

Supplemental material

Supplemental material for this article is available online.

References

1. Chen AY, Chonghasawat AO and Leadholm KL. Multiple sclerosis: frequency, cost, and economic burden in the United States. *J Clin Neurosci* 2017; 45: 180–186.
2. Compston A and Coles A. Multiple sclerosis. *Lancet* 2008; 372: 1502–1517.
3. Dutta R and Trapp BD. Pathogenesis of axonal and neuronal damage in multiple sclerosis. *Neurology* 2007; 68 (Suppl. 3): S22–S31; discussion S43–S54.
4. Lublin FD, Reingold SC, Cohen JA, *et al.* Defining the clinical course of multiple sclerosis: the 2013 revisions. *Neurology* 2014; 83: 278–286.
5. Mäurer M and Rieckmann P. Relapsing–remitting multiple sclerosis: what is the potential for combination therapy? *BioDrugs* 2000; 13: 149–158.
6. Geurts JJG and Barkhof F. Grey matter pathology in multiple sclerosis. *Lancet Neurol* 2008; 7: 841–851.
7. Barsukova AG, Forte M and Bourdette D. Focal increases of axoplasmic Ca^{2+}, aggregation of sodium-calcium exchanger, N-type Ca^{2+} channel, and actin define the sites of spheroids in axons undergoing oxidative stress. *J Neurosci* 2012; 32: 12028–12037.

8. Coleman M. Axon degeneration mechanisms: commonality amid diversity. *Nat Rev Neurosci* 2005; 6: 889–898.

9. Mossakowski AA, Pohlan J, Bremer D, *et al.* Tracking CNS and systemic sources of oxidative stress during the course of chronic neuroinflammation. *Acta Neuropathol* 2015; 130: 799–814.

10. Fischer MT, Wimmer I, Höftberger R, *et al.* Disease-specific molecular events in cortical multiple sclerosis lesions. *Brain* 2013; 136: 1799–1815.

11. Nikić I, Merkler D, Sorbara C, *et al.* A reversible form of axon damage in experimental autoimmune encephalomyelitis and multiple sclerosis. *Nat Med* 2011; 17: 495–499.

12. Mahad D, Ziabreva I, Lassmann H, *et al.* Mitochondrial defects in acute multiple sclerosis lesions. *Brain* 2008; 131: 1722–1735.

13. Court FA and Coleman MP. Mitochondria as a central sensor for axonal degenerative stimuli. *Trends Neurosci* 2012; 35: 364–372.

14. Fang C, Bourdette D and Banker G. Oxidative stress inhibits axonal transport: implications for neurodegenerative diseases. *Mol Neurodegener* 2012; 7: 29.

15. Medana IM and Esiri MM. Axonal damage: a key predictor of outcome in human CNS diseases. *Brain* 2003; 126: 515–530.

16. Saxton WM and Hollenbeck PJ. The axonal transport of mitochondria. *J Cell Sci* 2012; 125: 2095–2104.

17. Campbell GR, Ziabreva I, Reeve AK, *et al.* Mitochondrial DNA deletions and neurodegeneration in multiple sclerosis. *Ann Neurol* 2011; 69: 481–492.

18. Bros H, Millward JM, Paul F, *et al.* Oxidative damage to mitochondria at the nodes of Ranvier precedes axon degeneration in ex vivo transected axons. *Exp Neurol* 2014; 261: 127–135.

19. Armstrong JA, Cash NJ, Ouyang Y, *et al.* Oxidative stress alters mitochondrial bioenergetics and modifies pancreatic cell death independently of cyclophilin D, resulting in an apoptosis-to-necrosis shift. *J Biol Chem* 2018; 293: 8032–8047.

20. Miller AE, Wolinsky JS, Kappos L, *et al.* Oral teriflunomide for patients with a first clinical episode suggestive of multiple sclerosis (TOPIC): a randomised, double-blind, placebo-controlled, phase 3 trial. *Lancet Neurol* 2014; 13: 977–986.

21. O'Connor P, Wolinsky JS, Confavreux C, *et al.* Randomized trial of oral teriflunomide for relapsing multiple sclerosis. *N Engl J Med* 2011; 365: 1293–1303.

22. Bar-Or A. Teriflunomide (Aubagio®) for the treatment of multiple sclerosis. *Exp Neurol* 2014; 262: 57–65.

23. Li L, Liu J, Delohery T, *et al.* The effects of teriflunomide on lymphocyte subpopulations in human peripheral blood mononuclear cells in vitro. *J Neuroimmunol* 2013; 265: 82–90.

24. Warnke C, zu Hörste GM, Hartung HP, *et al.* Review of teriflunomide and its potential in the treatment of multiple sclerosis. *Neuropsychiatr Dis Treat* 2009; 5: 333–340.

25. Warnke C, Stüve O and Kieseier BC. Teriflunomide for the treatment of multiple sclerosis. *Clin Neurol Neurosurg* 2013; 115 (Suppl. 1): S90–S94.

26. Zivadinov R, Bergsland N, Carl E, *et al.* Effect of teriflunomide and dimethyl fumarate on cortical atrophy and leptomeningeal inflammation in multiple sclerosis: a retrospective, observational, case–control pilot study. *J Clin Med* 2019; 8: 344.

27. Rzagalinski I, Hainz N, Meier C, *et al.* Spatial and molecular changes of mouse brain metabolism in response to immunomodulatory treatment with teriflunomide as visualized by MALDI-MSI. *Anal Bioanal Chem* 2019; 411: 353–365.

28. Bros H, Niesner R and Infante-Duarte C. An ex vivo model for studying mitochondrial trafficking in neurons. *Methods Mol Biol* 2015; 1264: 465–472.

29. Oh J and O'Connor PW. An update of teriflunomide for treatment of multiple sclerosis. *Ther Clin Risk Manag* 2013; 9: 177–190.

30. Kaplan J, Cavalier S and Turpault S. Biodistribution of teriflunomide in naive rats vs rats with experimental autoimmune encephalomyelitis. *ECTRIMS Online Library*, 2015.

31. Palmer AM. Efficacy and safety of teriflunomide in treatment of multiple sclerosis. *J Symptoms Signs* 2013; 2: 444–457.

32. Zierle J, Bissinger R and Lang F. Inhibition by teriflunomide of erythrocyte cell membrane scrambling following energy depletion, oxidative stress and ionomycin. *Cell Physiol Biochem* 2016; 39: 1877–1890.

33. Bros H, Hauser A, Paul F, *et al.* Assessing mitochondrial movement within neurons: manual versus automated tracking methods. *Traffic* 2015; 16: 906–917.

34. Kweon SM, Kim HJ, Lee ZW, *et al.* Real-time measurement of intracellular reactive oxygen species using mito tracker orange (CMH2TMRos). *Biosci Rep* 2001; 21: 341–352.

35. Breedveld FC and Dayer JM. Leflunomide: mode of action in the treatment of rheumatoid arthritis. *Ann Rheum Dis* 2000; 59: 841–849.

36. Claussen MC and Korn T. Immune mechanisms of new therapeutic strategies in MS: teriflunomide. *Clin Immunol* 2012; 142: 49–56.

37. Rudick RA and Trapp BD. Gray-matter injury in multiple sclerosis. *N Engl J Med* 2009; 361: 1505–1506.

38. Aktas O, Smorodchenko A, Brocke S, *et al.* Neuronal damage in autoimmune neuroinflammation mediated by the death ligand TRAIL. *Neuron* 2005; 46: 421–432.

39. Moreira PI, Zhu X, Wang X, *et al.* Mitochondria: a therapeutic target in neurodegeneration. *Biochim Biophys Acta* 2010; 1802: 212–220.

40. Fang J, Uchiumi T, Yagi M, *et al.* Dihydro-orotate dehydrogenase is physically associated with the respiratory complex and its loss leads to mitochondrial dysfunction. *Biosci Rep* 2013; 33: e00021.

41. Khutornenko AA, Dalina AA, Chernyak BV, *et al.* The role of dihydroorotate dehydrogenase in apoptosis induction in response to inhibition of the mitochondrial respiratory chain complex III. *Acta Naturae* 2014; 6: 69–75.

42. Rafelski SM. Mitochondrial network morphology: building an integrative, geometrical view. *BMC Biol* 2013; 11: 71.

43. Chan DC. Fusion and fission: interlinked processes critical for mitochondrial health. *Annu Rev Genet* 2012; 46: 265–287.

44. Kaasik A, Safiulina D, Choubey V, *et al.* Mitochondrial swelling impairs the transport of organelles in cerebellar granule neurons. *J Biol Chem* 2007; 282: 32821–32826.

45. Safiulina D and Kaasik A. Energetic and dynamic: how mitochondria meet neuronal energy demands. *PLoS Biol* 2013; 11: e1001755.

46. Detmer SA and Chan DC. Functions and dysfunctions of mitochondrial dynamics. *Nat Rev Mol Cell Biol* 2007; 8: 870–879.

47. Chan DC. Mitochondria: dynamic organelles in disease, aging, and development. *Cell* 2006; 125: 1241–1252.

48. Misgeld T, Kerschensteiner M, Bareyre FM, *et al.* Imaging axonal transport of mitochondria in vivo. *Nat Methods* 2007; 4: 559–561.

49. Schwarz TL. Mitochondrial trafficking in neurons. *Cold Spring Harb Perspect Biol* 2013; 5: a011304.

50. Ohno N, Kidd GJ, Mahad D, *et al.* Myelination and axonal electrical activity modulate the distribution and motility of mitochondria at CNS nodes of Ranvier. *J Neurosci* 2011; 31: 7249–7258.

51. Cagalinec M, Safiulina D, Liiv M, *et al.* Principles of the mitochondrial fusion and fission cycle in neurons. *J Cell Sci* 2013; 126: 2187–2197.

52. Fairus AKM, Choudhary B, Hosahalli S, *et al.* Dihydroorotate dehydrogenase (DHODH) inhibitors affect ATP depletion, endogenous ROS and mediate S-phase arrest in breast cancer cells. *Biochimie* 2017; 135: 154–163.

53. Herrmann ML, Schleyerbach R and Kirschbaum BJ. Leflunomide: an immunomodulatory drug for the treatment of rheumatoid arthritis and other autoimmune diseases. *Immunopharmacology* 2000; 47: 273–289.

54. Area-Gomez E, Guardia-Laguarta C, Schon EA, *et al.* Mitochondria, OxPhos, and neurodegeneration: cells are not just running out of gas. *J Clin Invest* 2019; 129: 34–45.

55. Janssen A, Fiebiger S, Bros H, *et al.* Treatment of chronic experimental autoimmune encephalomyelitis with epigallocatechin-3-gallate and glatiramer acetate alters expression of heme-oxygenase-1. *PLoS One* 2015; 10: e0130251.

56. Herges K, Millward JM, Hentschel N, *et al.* Neuroprotective effect of combination therapy of glatiramer acetate and epigallocatechin-3-gallate in neuroinflammation. *PLoS One* 2011; 6: e25456.

57. Aktas O, Prozorovski T, Smorodchenko A, *et al.* Green tea epigallocatechin-3-gallate mediates T cellular NF-κB inhibition and exerts neuroprotection in autoimmune encephalomyelitis. *J Immunol* 2004; 173: 5794–5800.

58. Schroeder EK, Kelsey NA, Doyle J, *et al.* Green tea epigallocatechin 3-gallate accumulates in mitochondria and displays a selective antiapoptotic effect against inducers of mitochondrial oxidative stress in neurons. *Antioxid Redox Signal* 2009; 11: 469–480.

59. Sghaier R, Nury T, Leoni V, *et al.* Dimethyl fumarate and monomethyl fumarate

attenuate oxidative stress and mitochondrial alterations leading to oxiapoptophagy in 158N murine oligodendrocytes treated with 7β-hydroxycholesterol. *J Steroid Biochem Mol Biol* 2019; 194: 105432.

60. Sedel F, Bernard D, Mock DM, *et al.* Targeting demyelination and virtual hypoxia with high-dose biotin as a treatment for progressive multiple sclerosis. *Neuropharmacology* 2016; 110: 644–653.

61. Rodney C, Rodney S and Millis RM. Vitamin D and demyelinating diseases: neuromyelitis optica (NMO) and multiple sclerosis (MS). *Autoimmune Dis* 2020; 2020: 8718736.

62. Namsi A, Nury T, Khan AS, *et al.* Octadecaneuropeptide (ODN) induces N2a cells differentiation through a PKA/PLC/PKC/MEK/ERK-dependent pathway: incidence on peroxisome, mitochondria, and lipid profiles. *Molecules* 2019; 24: 3310.

41. Zorov, D.B.; Vorobjev, I.A.; Popkov, V.A.; Babenko, V.A.; Zorova, L.D.; Pevzner, I.B.; Silachev, D.N.; Zorov, S.D.; Andrianova, N.V.; Plotnikov, E.Y. Lessons from the Discovery of Mitochondrial Fragmentation (Fission): A Review and Update. *Cells* **2019**, *8*, 175. [CrossRef] [PubMed]
42. Tondera, D.; Grandemange, S.; Jourdain, A.; Karbowski, M.; Mattenberger, Y.; Herzig, S.; Da Cruz, S.; Clerc, P.; Raschke, I.; Merkwirth, C.; et al. SLP-2 is required for stress-induced mitochondrial hyperfusion. *EMBO J.* **2009**, *28*, 1589–1600. [CrossRef] [PubMed]
43. Casals, L.M.; Sebastián, D.; Brea, J.; Rico-Leo, E.M.; Palacín, M.; Fernández-Salguero, P.M.; Loza, M.I.; Albericio, F.; Zorzano, A. Identification of New Activators of Mitochondrial Fusion Reveals a Link between Mitochondrial Morphology and Pyrimidine Metabolism. *Cell Chem. Biol.* **2018**, *25*, 268–278.e4. [CrossRef] [PubMed]
44. Zhang, X.; Li, Z.; Zhang, Q.; Chen, L.; Huang, X.; Zhang, Y.; Liu, X.; Liu, W.; Li, W. Mechanisms Underlying H_2O_2-Evoked Carbonyl Modification of Cytoskeletal Protein and Axon Injury in PC-12 Cells. *Cell. Physiol. Biochem.* **2018**, *48*, 1088–1098. [CrossRef] [PubMed]
45. Löffler, M.; Carrey, E.A.; Knecht, W. The pathway to pyrimidines: The essential focus on dihydroorotate dehydrogenase, the mitochondrial enzyme coupled to the respiratory chain. *Nucleosides Nucleotides Nucleic Acids* **2020**, *39*, 1281–1305. [CrossRef] [PubMed]
46. Gülden, M.; Jess, A.; Kammann, J.; Maser, E.; Seibert, H. Cytotoxic potency of H_2O_2 in cell cultures: Impact of cell concentration and exposure time. *Free Radic. Biol. Med.* **2010**, *49*, 1298–1305. [CrossRef]
47. Iwakami, S.; Misu, H.; Takeda, T.; Sugimori, M.; Matsugo, S.; Kaneko, S.; Takamura, T. Concentration-dependent Dual Effects of Hydrogen Peroxide on Insulin Signal Transduction in H4IIEC Hepatocytes. *PLoS ONE* **2011**, *6*, e27401. [CrossRef]
48. Berndt, N.; Rösner, J.; Haq, R.U.; Kann, O.; Kovács, R.; Holzhütter, H.-G.; Spies, C.; Liotta, A. Possible neurotoxicity of the anesthetic propofol: Evidence for the inhibition of complex II of the respiratory chain in area CA3 of rat hippocampal slices. *Arch. Toxicol.* **2018**, *92*, 3191–3205. [CrossRef]
49. Schindelin, J.; Rueden, C.T.; Hiner, M.C.; Eliceiri, K.W. The ImageJ ecosystem: An open platform for biomedical image analysis. *Mol. Reprod. Dev.* **2015**, *82*, 518–529. [CrossRef]
50. Schneider, C.A.; Rasband, W.S.; Eliceiri, K.W. NIH Image to ImageJ: 25 Years of image analysis. *Nat. Methods* **2012**, *9*, 671–675. [CrossRef]
51. Thevenaz, P.; Ruttimann, U.; Unser, M. A pyramid approach to subpixel registration based on intensity. *IEEE Trans. Image Process.* **1998**, *7*, 27–41. [CrossRef] [PubMed]
52. Arganda-Carreras, I.; Kaynig, V.; Rueden, C.; Eliceiri, K.W.; Schindelin, J.; Cardona, A.; Seung, H.S. Trainable Weka Segmentation: A machine learning tool for microscopy pixel classification. *Bioinformatics* **2017**, *33*, 2424–2426. [CrossRef] [PubMed]
53. Jaqaman, K.; Loerke, D.; Mettlen, M.; Kuwata, H.; Grinstein, S.; Schmid, S.L.; Danuser, G. Robust single-particle tracking in live-cell time-lapse sequences. *Nat. Methods* **2008**, *5*, 695–702. [CrossRef] [PubMed]
54. Rawls, J.; Knecht, W.; Diekert, K.; Lill, R.; Löffler, M. Requirements for the mitochondrial import and localization of dihydroorotate dehydrogenase. *Eur. J. Biochem.* **2000**, *267*, 2079–2087. [CrossRef]

Curriculum Vitae

Mein Lebenslauf wird aus datenschutzrechtlichen Gründen in der elektronischen Version meiner Arbeit nicht veröffentlicht.

Mein Lebenslauf wird aus datenschutzrechtlichen Gründen in der elektronischen Version meiner Arbeit nicht veröffentlicht.

Publication list

- **Ulshöfer R**, Bros H, Hauser AE, Niesner RA, Paul F, Malla B, Infante-Duarte C. Preventing Axonal Sodium Overload or Mitochondrial Calcium Uptake Protects Axonal Mitochondria from Oxidative Stress-Induced Alterations. Oxid Med Cell Longev. 2022 May 24. (Impact factor: 7.310)
- Malla B, Liotta A, Bros H, **Ulshöfer R**, Paul F, Hauser AE, Niesner R, Infante-Duarte C. Teriflunomide Preserves Neuronal Activity and Protects Mitochondria in Brain Slices Exposed to Oxidative Stress. Int J Mol Sci. 2022 Jan 28. (Impact factor: 5.314)
- Malla B, Cotten S, **Ulshoefer R**, Paul F, Hauser AE, Niesner R, Bros H, Infante-Duarte C. Teriflunomide preserves peripheral nerve mitochondria from oxidative stress-mediated alterations. Ther Adv Chronic Dis. 2020 Aug 11. (Impact facor: 4.970)
- **Ludwig, R**.; Malla, B.; Höhrhan, M.; Infante-Duarte, C.; Anderhalten, L. Investigating the Mitoprotective Effects of S1P Receptor Modulators Ex Vivo Using a Novel Semi-Automated Live Imaging Set-Up. Int. J. Mol. Sci. 2023 Dec 23 (Impact factor: 5.314)

Acknowledgments

"Books, Cleverness. There Are More Important Things: Friendship and bravery." (Hermoine Granger in "Harry Potter and the Philosopher's Stone")

Towards the end of my thesis, I often thought back to my first steps in the academic world, which essentially meant learning how to read. During that time, I read my first book, which has been Harry Potter. This quote reminds me of how I could never have done this work without much support from many people, most of which have turned into good friends during this journey and helped me recover my bravery again when I had lost it.

First of all, I would like to thank my primary supervisor, my mentor and role model **Prof. Dr. rer. nat. Carmen Infante-Duarte**. She supported my work in every possible way, helped me surpass any obstacles, and encouraged me to pursue this experimental work. In other words, she was the best "Doktormutter" I can possibly imagine.

Many people in my and other lab groups have my never-ending thankfulness. My gratitude encompasses **Dr. rer. nat. Bimala Malla**, who taught me most of the applied experimental methods – it was always a pleasure to exchange ideas with her. A big thank you goes to **Prof. Dr. Friedemann Paul and Dr. Sarah Staroßom** who guided and helped me with numerous suggestions to improve my work. **Prof. Dr. rer. nat. Raluca Niesner** and **Prof. Dr. vet. Med Anja Hauser** and their groups helped me with technical advice and allowed me to use their facilities, thank you for this.

The AMBIO team, especially **Dr. Jan Schmoranzer, Jutta Schüler,** and **Dr. Stefan Donat** helped me perform the microscopy in an advanced way and responded very kindly to my numerous special requests for setting up a carbogen supply in the AMBIO facility.

My **laboratory group** was my international science family throughout this time. Thanks to Natasha Asselborn, Bibiane Seeger-Schwinge, Dr. Jason Millward, Dr. Shuangqing Wang, Juliana Campo Garcia, Rafaela Vieira da Silva, Maria Schroeder Castagno, Roemel Jeusep Bueno, Maria Höhrhan, Daniel Brunotte-Strecker, Svenja Schwichtenberg, Dr. Cesar Alvarez-Gonzales, Dr. med. Anne Wisgalla, Hannah Rostalski, and Maren Salla – I will gratefully remember the time spent with you at the lab

benches, congresses, during lunch breaks, and Christmas parties. Especially, I would like to mention **Lina Carlotta Anderhalten** who did her MD/PhD at the same time in my lab group - it was amazing to have someone to be in a very similar position and working with her was truly enriching.

It takes indeed more than books and cleverness to achieve a doctoral degree and I am grateful for the support from my **family and friends**. Thank you for providing feedback on my manuscripts again and again of which you, as you told me, understood less than half and moreover thank you for shaping my life outside the lab. You have boosted my morale and helped my preserve my curiosity.

Lastly, I would like to thank **my husband Nicolas** for his endless patience with me over the course of my thesis, his loving support, his keeping me down to earth, and his calming presence. I could not have done this without you.